

NORTHWESTERN UNIVERSITY

Manipulating Exosome Signaling to Inhibit Tumor Metastasis

A DISSERTATION

SUBMITTED TO THE GRADUATE SCHOOL
IN PARTIAL FULFILLMENT OF THE REQUIREMENTS

for the degree

DOCTOR OF PHILOSOPHY

Field of Biology

By

Michael Paul Plebanek

EVANSTON, ILLINOIS

June 2018

ABSTRACT

Manipulating Exosome Signaling to Inhibit Tumor Metastasis

Michael P. Plebanek

Over the past decade significant advancements have been made across the field of cancer biology resulting in transformative new therapies. Despite these advancements, treatments for metastatic cancer remain relatively ineffective. Metastasis is coordinated by various types of “healthy” stromal cells in addition to the tumor cells themselves. This requires a means by which the tumor cells can communicate with stromal cells. Exosomes are 30-150 nm nanovesicles that function as the primary endogenous intercellular delivery vehicle. During cancer progression, cancer cells package pro-tumorigenic RNAs, proteins and DNA into exosomes and subsequently release them into circulation. After release, exosomes traffic to the sites of metastasis, prior to the arrival of circulating tumor cells, where they initiate phenotypic changes, notably immunosuppression, that support the colonization and survival of metastasis. Collectively, the microenvironment generated by these exosomes has been called the pre-metastatic niche.

In this project, we were first interested in understanding the effects of exosomes released from non-metastatic cancer cells. It is well established that exosomes from aggressive cancer cells promote metastasis, but the functions of non-aggressive cancer cell exosomes are not understood. We discovered that exosomes from non-metastatic melanoma cells drive the expansion of a Ly6C^{lo} monocyte population called patrolling monocytes (PMo). These monocytes trafficked to the metastatic sites where they cleared circulating tumor cells preventing metastasis formation in mouse models of melanoma. The expansion in the PMo population was stimulated by pigment epithelial derived factor (PEDF), a multifunctional anti-tumor protein carried in the exosomes of non-metastatic melanoma cells. Importantly, exosomes isolated from

the serum of patients with primary melanoma that did not recur had higher PEDF content compared to exosomes from patients with highly aggressive metastasis. Ultimately, this study demonstrated that exosomes from non-metastatic tumors can carry triggers like PEDF that activate innate immune responses against cancer preventing metastatic spread.

Additionally, due to the metastasis promoting functions of tumor exosomes, we were interested in developing a technology to specifically inhibit the uptake of cancer exosomes by target cells. Exosome uptake is dependent on cholesterol-rich lipid raft regions of the cell membrane. Our laboratory has developed high-density lipoprotein-like nanoparticles (HDL NP) that specifically efflux cholesterol from cells that express scavenger receptor-type B1 (SR-B1). By modulating cholesterol flux at lipid rafts, HDL NPs effectively inhibit the uptake of melanoma exosomes by multiple cell types that play important roles in the pre-metastatic niche including endothelial cells, macrophages and tumor cells themselves. This work provides a crucial step in developing a cancer therapy that functions by inhibiting the uptake of exosomes.

The development of HDL NPs led us to test their efficacy as a cancer therapeutic in a wide array of applications. We discovered that HDL NPs can function to inhibit metastasis independent of inhibiting exosome uptake, as well. Myeloid-derived suppressor cells (MDSCs) promote tumor progression by suppressing T cell mediated clearance of cancer cells. We demonstrated that HDL NPs target SR-B1 expressed by MDSCs resulting in a significant inhibition of their suppressive activity. HDL NP treatment led to increased T cell proliferation and, most importantly, significantly reduced tumor growth, metastatic tumor burden, and increased survival due to an enhanced adaptive immunity. Overall, HDL NPs have the potential to be developed into a novel multifunctional immunotherapy that can inhibit the activity of MDSCs, as well as block the uptake of exosomes in SR-B1 expressing cells.

ACKNOWLEDGEMENTS

First off, I want to say that this is the hardest section of my thesis to write. Looking back at the time I spent in graduate school, I realize how much has changed over the years and how many people helped me along the way. There truly are so many people that have helped me that it would be impossible to list everyone. To anyone that I haven't mentioned here, I want to convey my deepest gratitude for the help you have given.

Next, I would like to thank my thesis advisors, Dr. Shad Thaxton and Dr. Olga Volpert. I have been so lucky to be able to work with both of you on tremendously exciting research projects. Shad, I cannot thank you enough. You gave me the freedom to work on any idea I had and you were also always around if I needed help or had any questions, but, most importantly, your persistent excitement and optimism was contagious even when I was second-guessing my research or getting through the daily life of a graduate student. Olga, during laboratory rotations, in my first year as a graduate, you were the first person to get me truly excited about a research project. You are full of so many great ideas and you always seem one step ahead of everyone else in the field. You also taught me to slow down a bit, to think critically about my results and to understand what it takes to do important research. You have always supported me in following my dreams of starting my own research lab. Thank you again, I have truly become a better scientist and person after working with both of you.

I would also like to thank the Thaxton and Volpert Labs. Anytime I needed someone's help with an experiment or had a question, there was always someone there to ask and O ,ade some great friends along the way. Kaylin, my entire graduate school was spent in the Thaxton Lab working with you. Thank you for creating the best environment anyone could ask for. I don't know what graduate school would be like without you. Also, sorry about the mess. To Jon,

thanks for making the Thaxton Lab a great place to work. I knew I could always count on you to have a beer after a long week. Stephen, I am so grateful that you joined the lab. I know any exosome work is in good hands with you. To Nick you always kept both the Thaxton and Volpert Labs running as smoothly as possible and you helped out with the exosome project more than you realize. To Dave thank you so much for all the help on the final paper. I wouldn't have been able finish it without all your help. To Nikki from the Volpert Lab, thank you so much for all your help in Olga's Lab. You always knew exactly what to say when the day wasn't going right.

Next, I would like to thank Dr. Andrew Lipchik. When I was a 19-year old undergraduate student at Purdue University with long hair and no idea what to do with my life, you introduced me to science. You gave me a chance to work in a research lab and showed me that there was an opportunity to go to graduate school. Without the experience of working in a lab for the first time and making constant mistakes, as I learned what it took to be a scientist, I wouldn't have been able to make it through graduate school. I just want to let you know how much of an impact you have made on my life.

I couldn't write this without thanking Andrew Shum. We started graduate school together and lived together for 4 years. You have been a great friend and have kept me from going crazy even if hanging out with you might have slowed down our research a little bit and kept us at Northwestern for longer than we should have. My time as a graduate student wouldn't have been the same without you.

Next, I would like to thank my parents. Mom and Dad you taught me to always stand up for what I believe in and have instilled upon me the work ethic and the dedication that is needed to work on a project for over 6 years. But, more importantly, you have given me endless support

in everything I have done my entire life. To my brother and sisters, Daniel, Allison and Courtney, I know you will always be there for me if I need you and you can always count on me no matter where any of us are in our lives.

Most importantly, Ale. I am so lucky to be able to do this together with you. The best part about graduate school was meeting you. You always made sure to celebrate everything, even when I was feeling down on myself or not inspired by my work. Sometimes you seemed more excited about it than I did. I needed you there more times than you probably even realize. I can't wait to see what we do next with our lives. Thank you for everything. I love you.

TABLE OF CONTENTS

TABLE OF CONTENTS	7
LIST OF FIGURES	11
LIST OF TABLES	13
CHAPTER ONE	14
<i>Introduction: Understanding the Tumor Microenvironment as a Critical Mediator of Metastasis</i>	
1.1 Opening	15
1.2 The Importance of the Tumor and Metastatic Microenvironment	15
1.2.1 Metastatic Progression	15
1.2.2 The Tumor Microenvironment	17
1.2.3 The Pre-Metastatic Niche	18
1.3 The Immune System as a Gatekeeper to Metastasis	19
1.3.1 Innate Immunity and the Control of Tumor Metastasis by Patrolling Monocytes	19
1.3.2 The Adaptive Immune Response Against Cancer	22
1.3.3 Current Immunotherapies for the Treatment of Cancer	23
1.4 Biogenesis, Structure and Function of Exosomes	25
1.5 Function of Exosomes in Cancer Biology	27
1.5.1 Exosomes as Drivers of the Pre-Metastatic Niche	27
1.5.2 The Development of Exosome-Based Cancer Biomarkers	29
1.6 Roles of Exosomes in other Diseases	31
1.7 Exosome Inspired Therapeutics	33
1.7.1 Exosome Mimetics	33
1.7.2 Genetically Modified Exosomes to Deliver Specific Cargo	34
1.7.3 Exosome Vaccines	35
1.7.4 Exosomes in Regenerative Medicine	36
1.8 Scavenger Receptor type-B1(SR-B1)	37
1.8.1 SR-B1 Functions in Reverse Cholesterol Transport	37
1.8.2 Signal Transduction through SR-B1	38
1.8.3 SR-B1's Role in Cancer Biology	38
1.9 Nanomedicine: Novel Technologies for the Development of New Therapeutics	39
1.9.1 Targeted Nanotherapeutics for Cancer Therapy	39
1.9.2 High-Density Lipoprotein Nanoparticles	41
CHAPTER TWO	44
<i>Pre-metastatic Cancer Exosomes Induce Immune Surveillance by Patrolling Monocytes at the Pre-metastatic Niche</i>	
2.1 Abstract	45
2.2 Introduction	46
2.3 Results	49
2.3.1 “Non-metastatic” Exosomes (Exo ^{NM}) Prevent Lung Metastasis	49
2.3.2 Exo ^{NM} Leads to Increased Patrolling Monocytes in the Lungs	52

2.3.3 Monocytic Cells Are Necessary for anti-Metastatic Exo ^{NM} Function	56
2.3.4 Exo ^{NM} Induce Macrophage Differentiation and Phagocytic Activity	57
2.3.5 In Part, NK Cells Mediate Exo ^{NM} Induced Immune Responses	59
2.3.6 Exo ^{NM} Contain Pigment Epithelium-Derived Factor (PEDF) on the Exosomes' Surface	59
2.3.7 Exosomal PEDF Promotes Macrophage Activation and Drive Apoptosis of Neighboring Melanoma Cells	60
2.3.8 Exosomes from the Sera of Patients with non-Metastatic Melanoma Contain Significantly more PEDF	63
2.4 Discussion	65
2.5 Materials and Methods	68
2.5.1 Cell Culture	68
2.5.2 Experimental Animals	69
2.5.3 Isolation of Bone Marrow Macrophages	69
2.5.4 Exosome Collection and Characterization	70
2.5.5 Exosome Isolation from Serum	71
2.5.6 SDS-PAGE and Western Blotting	72
2.5.7 RT-PCR	72
2.5.8 Flow Cytometry	73
2.5.9 Immunohistochemistry	73
2.5.10 Transmission Electron Microscopy and Immunogold Labeling	74
2.5.11 Limited Trypsin Digestion	75
2.5.12 Phagocytosis Assay	75
2.5.13 Apoptosis Assays	76
2.5.14 Macrophage Differentiation Assay	77
2.5.15 Lung Colonization and Extravasation Assays	77
2.5.16 Clodronate Depletion of Macrophages and Monocytes	78
2.5.17 Depletion of NK Cells with anti-Asialo GM1 Antibodies	78
2.5.18 Functional Analysis of Patient Exosomes	78
2.5.19 Statistical Analysis	79
CHAPTER THREE	80
<i>Nanoparticle Targeting and Cholesterol Flux through Scavenger Receptor Type-B1 Inhibits the Cellular Uptake of Exosomes</i>	
3.1 Abstract	81
3.2 Introduction	82
3.3 Results	84
3.3.1 HDL NPs Modulate Cholesterol Flux in Melanoma Cells <i>in vitro</i>	84
3.3.2 SR-B1 Localizes to Lipid Rafts	87
3.3.3 HDL NPs Induce Clustering and Reduced Movement of SR-B1	88
3.3.4 HDL NPs Block the Uptake of Melanoma-Derived Exosomes	89
3.3.5 Targeting SR-B1 to Block Cellular Exosome Uptake	92
3.3.6 SR-B1 is Necessary for HDL NPs to Inhibit Exosome Uptake	94
3.3.7 Disrupting Exosome Uptake in Stromal Cells of the Metastatic Microenvironment	96

3.4 Discussion	97
3.5 Materials and Methods	100
3.5.1 HDL NP Synthesis	100
3.5.2 Cell Culture	100
3.5.3 Exosome Isolation and Labeling	101
3.5.4 Cell Treatment with Human HDL and HDL NP	101
3.5.5 Exosome Uptake Assays	102
3.5.6 Cholesterol and Cholesteryl Ester Quantification	103
3.5.7 Cholesterol Efflux Assays	103
3.5.8 Computer Vision Analysis of GFP-SR-B1 Domains, Intensity and Dynamics	104
3.5.9 Western Blotting	105
3.5.10 Lipid Raft Labeling	105
3.5.11 Knockdown of SR-B1	105
3.5.12 Fluorescence Microscopy	106
3.5.13 Statistical Analysis	106
CHAPTER FOUR	107
<i>Scavenger Receptor Type B1 and High-Density Lipoprotein Nanoparticles Inhibit Myeloid Derived Suppressor Cells</i>	
4.1 Abstract	108
4.2 Introduction	109
4.3 Results	113
4.3.1 MDSCs Express SR-B1 and are Targeted by HDL NPs	113
4.3.2 HDL NPs Prime the Adaptive Immune System in the Lymph Nodes	114
4.3.3 HDL NPs Relieve T Cell Suppression Caused by MDSCs	115
4.3.4 HDL NPs Reduce Metastasis and Prolong Survival in Melanoma Mouse Models	115
4.3.5 SR-B1 is Necessary for HDL NP-mediated Inhibition of Metastasis	117
4.3.6 HDL NPs Reshape the Immune Microenvironment in Melanoma Metastases	120
4.3.7 HDL NPs significantly Reduce Lewis Lung Carcinoma Growth	121
4.4 Discussion	123
4.5 Materials and Methods	128
4.5.1 Cell Culture	128
4.5.2 Experimental Animals	129
4.5.3 HDL NP Synthesis	130
4.5.4 Melanoma Lung Colonization	131
4.5.5 Isolation of Bone Marrow Cells	133
4.5.6 Isolation of Lymph Node Cells	133
4.5.7 Isolation of Spleen Cells	133
4.5.8 Isolation of Lung Cells	134
4.5.9 Orthotopic Melanoma Survival Study	134
4.5.10 Lethal Irradiation and Bone Marrow Transplant	134
4.5.11 MTS Assay	135

	10
4.5.12 Flow Cytometry	135
4.5.13 MDSC HDL NP Treatment and Toxicity Analysis	135
4.5.14 T Cell Suppression Assay	136
4.5.15 Immunohistochemistry	137
4.5.16 Lewis Lung Carcinoma Xenograft Model	138
4.5.17 RT-PCR	138
4.5.18 Statistical Analysis	138
CHAPTER FIVE	142
<i>Concluding Remarks and Future Work</i>	
REFERENCES	145
CURRICULUM VITAE	159

LIST OF FIGURES

CHAPTER 1

Figure 1.1. Metastatic Progression	16
Figure 1.2. Macrophage Polarization	19
Figure 1.3. Exosome Biogenesis	26
Figure 1.4. Exosomes Drive the Formation of the Pre-Metastatic Niche	28
Figure 1.5. Synthesis Scheme of HDL NPs	42

CHAPTER 2

Figure 2.1. Characterization of Metastatic and Non-Metastatic Melanoma Exosomes	47
Figure 2.2. Exo ^{NM} Inhibit Lung Colonization by Metastatic Melanoma	48
Figure 2.3. Schematic of Melanoma <i>In Vivo</i> Experiments in Nude Mice	50
Figure 2.4. Inhibition of Lung Extravasation by Exosomes from Naturally Occurring Metastatic and Non-Metastatic Melanoma Cells	51
Figure 2.5. Biodistribution of Melanoma Exosomes	52
Figure 2.6. Exo ^{NM} Increase PMos in the Lungs	53
Figure 2.7. Exo ^{NM} Act via the Cells of Monocytic Lineage	54
Figure 2.8. Exo ^{NM} Cause the Differentiation of RAW 264.7 Macrophages	56
Figure 2.9. NK Cells Contribute to Exosome-driven Tumor Cell Clearance	57
Figure 2.10. The Involvement of PEDF in Exosome-driven Melanoma Cell Clearance	58
Figure 2.11. Density Gradient Ultracentrifugation Characterization of Exosomal PEDF	60
Figure 2.12. In Co-cultures with Macrophages, Exo ^{NM} -dependent Apoptosis is Limited to Melanoma Cells	61
Figure 2.13. Exosomes from Sera of Patients with Non-Recurrent Melanoma Suppress Lung Metastasis	62
Figure 2.14. Characterization of Melanoma Sera Sample Exosomes	64
Figure 2.15. Schematic Representation of Immune Surveillance Events Triggered by Non-Metastatic Exosomes	67

CHAPTER 3

Figure 3.1. HDL NPs Efflux Free Cholesterol from Melanoma Cells	83
Figure 3.2. HDL NPs have no Effect on Cellular Viability	84
Figure 3.3. SR-B1 and HDL NP Distribution to Lipid Rafts	86
Figure 3.4. HDL NPs Induce Clustering of SR-B1	88
Figure 3.5. HDL NPs lead to Reduced Mobility and Dispersion of SR-B1 Containing Domains	90
Figure 3.6. HDL NPs Block the Uptake of Exosomes by A375 Melanoma cells	92
Figure 3.7. The Inhibition of Exosome Uptake is not due to Extracellular Interaction of Exosomes and HDL NP	94
Figure 3.8. Targeting SR-B1 to Induce Receptor Clustering to Inhibit Exosome Uptake	95
Figure 3.9. Expression of SR-B1 is Required for HDL NP-mediated Inhibition of Exosome Uptake	97
Figure 3.10. HDL NPs Inhibit the Uptake of Melanoma Exosomes by Endothelial Cells and Macrophages	98

Figure 3.11. Summary of the Mechanism by which HDL NPs Inhibit Exosome Uptake	102
---	-----

CHAPTER 4

Figure 4.1. SR-B1 Expression and HDL NP Targeting of Immune Cells	110
Figure 4.2. HDL NPs Display no Appreciable Cytotoxicity Towards MDSCs	111
Figure 4.3. HDL NP Treatment Modulates Systemic T Cell Distributions	112
Figure 4.4. Effect of HDL NPs on MDSC Burden in Lymph Nodes	114
Figure 4.5. T Cell Suppression by MDSCs is Inhibited by HDL NPs	116
Figure 4.6. Metastasis and Survival of Mice Pre-Treated with HDL NPs prior to Tumor Cell Administration	118
Figure 4.7. HDL NPs are not Inherently Toxic to Melanoma Cells	119
Figure 4.8. Survival of Mice with Orthotopic B16F10 Tumors after Treatment with HDL NPs	121
Figure 4.9. Effects of SR-B1 on HDL NPs Ability to Inhibit MDSC Activity	122
Figure 4.10. Effects of SR-B1 on HDL NP Efficacy	123
Figure 4.11. SR-B1 null Bone Marrow Transplant	124
Figure 4.12. Established Melanoma Metastasis Model	125
Figure 4.13. HDL NPs Reshape the Immune Microenvironment in Established Melanoma Metastasis	126
Figure 4.14. HDL NPs Inhibit Lewis Lung Carcinoma Tumor Growth	129
Figure 4.15. Summary of HDL NP Effects on MDSCs	131

LIST OF TABLES

Table 2.1. Analysis of Metastatic Melanoma Human Serum Samples	65
Table 2.2. List of Antibodies used in Chapter 2	71
Table 2.3. List of PCR Primers used in Chapter 2	74
Table 4.1. List of Antibodies used in Chapter 4	132
Table 4.2. List of PCR Primers used in Chapter 4	136

CHAPTER ONE: INTRODUCTION

Understanding the Tumor Microenvironment as a Critical Mediators of Metastasis

1.1 Opening

In 1889, over 100 years ago, Stephen Paget published the observation that different cancer-types preferentially metastasize to specific organs. It was hypothesized that the organ sites of metastasis or “soil” fostered the growth of only specific cancers or “seeds”. Paget called this new idea “The Seed and Soil Hypothesis”.¹ Over the years an extensive amount of both clinical and experimental research has confirmed that tumor cells metastasize in non-random patterns, but the events driving metastasis are much more complicated than early observers anticipated. Understanding the factors driving or preventing metastasis has been a primary goal of cancer researchers and significantly more work is needed to develop novel effective treatment for metastatic disease.

Recently, there has been a tremendous amount of research focused on understanding the importance of intercellular signaling to cancer biology.² Cancer is a heterogeneous disease and multiple cell types acting together are needed for tumor progression and subsequent metastasis.³ Therefore, efficient mechanisms of communication between tumor cells and the surrounding stromal cells have evolved. In this chapter, I will outline the role the tumor microenvironment plays in cancer biology, present exosomes as one of the premier natural delivery vehicle across biology and introduce the concept of utilizing nanotechnology to target these exosome-mediated routes of communication to inhibit metastasis.

1.2 The Importance of the Tumor and Metastatic Microenvironment

1.2.1 Metastatic Progression

Metastasis is the primary cause of death in a large majority of cancer cases.⁴ Chaffer and Weinberg state that as much as 90% of cancer associated mortality is due to tumor cell metastasis.⁵ Therefore, we need to understand this complex process in order to develop

interventions to reduce cancer associated mortality. There is a clear sequence of events leading to metastasis (**Figure 1.1**): First, as the primary tumor is developing, tumor cells must acquire an invasive phenotype. This often corresponds with undergoing epithelial to mesenchymal transition (EMT) causing the cells to become more migratory and more resistant to therapy. Then, the malignant cells must intravasate into blood or lymph circulation and localize to the sites of metastasis. Next, the tumor cells must leave the circulation or extravasate and undergo mesenchymal to epithelial transition (MET). Following extravasation, the tumor cells must then survive and proliferate at the secondary sites in order to form metastases. This step is not straightforward as there are numerous mechanisms by which metastasis are prevented or cleared by the immune system at early stages.⁶ Although these mechanisms of tumor cell clearance exist,

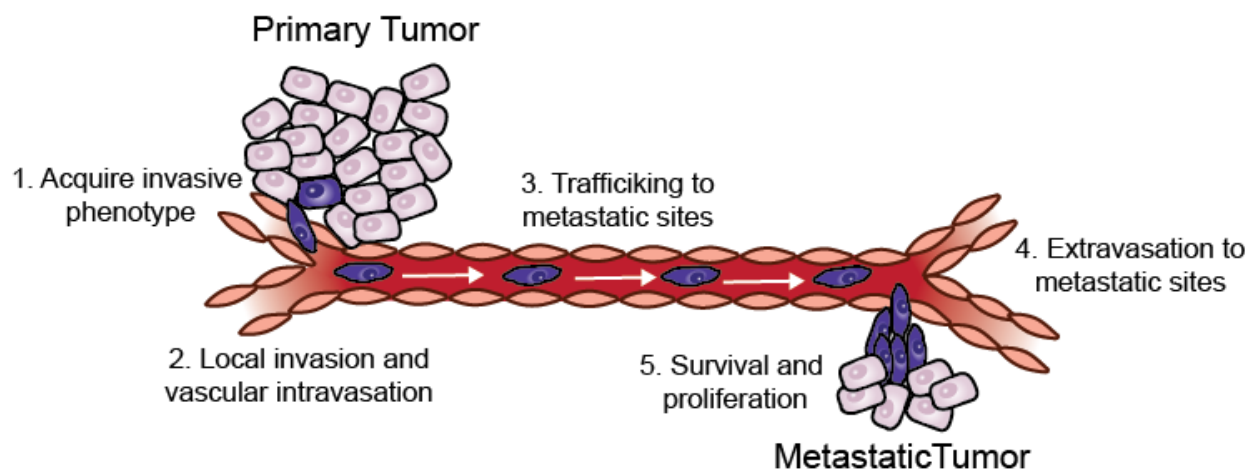


Figure 1.1: Metastatic Progression. Metastasis occurs via a step-wise process where the tumor cells: 1. Acquire an invasive phenotype. 2. Intravasate into the vasculature 3. Traffic to metastatic sites 4. Extravasate into metastatic sites and 5. Survive and proliferate to form metastasis.

metastasizing cells have developed ways to avoid clearance and encourage the formation of metastasis. One such way is through the generation of suitable microenvironments called pre-metastatic niches that form prior to the arrival of circulating tumor cells.⁷ These

microenvironments aid the survival of tumors cell and drive cell proliferation leading to the formation of stable metastasis.

1.2.2 The Tumor Microenvironment

The growth and progression of cancer is not governed simply by the tumor cells present in the malignancy. Supporting “healthy” stromal cells play a critical role that can be just as important for the developing tumor.⁸ There is a myriad of cells that make up the tumor microenvironment. For example, fibroblasts are a principal component of the tumor microenvironment.^{9,10} During tumorigenesis, through interactions with cancer cells, fibroblasts can be transformed to cancer-associated fibroblasts (CAFs) which typically express alpha-smooth muscle actin (α -SMA) amongst other markers. CAFs are a heterogeneous population of cells that accumulate in tumors and are associated with a poor prognosis.¹¹ They support tumor growth and metastasis in a number of ways including by providing growth factors like fibroblast growth factor (FGF), transforming growth factor-beta (TGF- β) and hepatocyte growth factor (HGF), which stimulate proliferation and increase chemoresistance.¹²

A large number of tumors form as carcinomas meaning that they develop from epithelial cells. Because the epithelium is not vascularized, blood vessels must develop within the tumor to provide sufficient nutrients for the increased rates of cancer cell proliferation. Moreover, as the tumor grows in size the inner most cells become nutrient starved due to the distance from a nutrient source.¹³ Therefore, endothelial cells and angiogenesis are critical for the tumor microenvironment. Angiogenesis is the process by which new blood vessels are formed and is a key process for continued tumor growth and metastasis.¹⁴ Not only does angiogenesis provide the nutrients necessary to maintain tumor proliferation, but it also provides a route for cancer cells to break away from the primary tumor enter circulation and form metastasis.¹⁵

Immune cells also compose a large ratio of the tumor stroma. These immune cells including tumor associated macrophages (TAMs), myeloid derived suppressor cells (MDSCs), neutrophils and T lymphocytes, amongst others can have both pro-tumor or anti-tumor functions, which greatly adds to the complexity of the disease. For example, depending on the cancer type TAM burden have different prognostic values.¹⁶ High TAM burden leads to a poor prognosis in breast and ovarian cancer, while holding a better prognosis in colon cancer. Also, high TAMs can lead to either a better or worse prognosis in prostate cancer. Later in this Chapter, immune cells will be discussed in significantly more detail system with regards to tumorigenesis and metastasis.

1.2.3 The Pre-Metastatic Niche

Cancer is not just a local disease; it significantly effects the patient in multiple ways and at many locations. This cannot appear more evident than is presented during metastasis. As discussed above, through interactions with stromal cells, cancer cells can generate microenvironments that support the growth and survival of the tumor.^{8,17} This does not just happen locally but occurs in distant organs, as well. Recently, these remote tumor-supporting microenvironments have been termed “the pre-metastatic niche”.¹⁷ As their name suggests, the pre-metastatic niche forms in the organs that the tumor will eventually metastasize to and its generation is a critical event during the process of metastasis. The discovery of the pre-metastatic niche also supports Paget’s 1889 observation that different cancer types preferentially form metastases in specific organs. The pre-metastatic niche forms during primary tumor development, as the cancer cells release exosomes, microvesicles and soluble factors, which traffics to the metastatic sites and causes phenotypic changes that support the eventual colonization by circulating tumor cells.¹⁷ These changes are characterized by increased

inflammation, immune suppression, vascular permeability and extracellular matrix remodeling. Additionally, there is increased recruitment of bone marrow progenitor cells that are capable of remodeling the vasculature, while also providing growth factors and survival cues to both the tumor and stromal cells. The role of exosomes in pre-metastatic niche formation is critically important will be discussed in much greater detail later in Chapter One of this thesis.

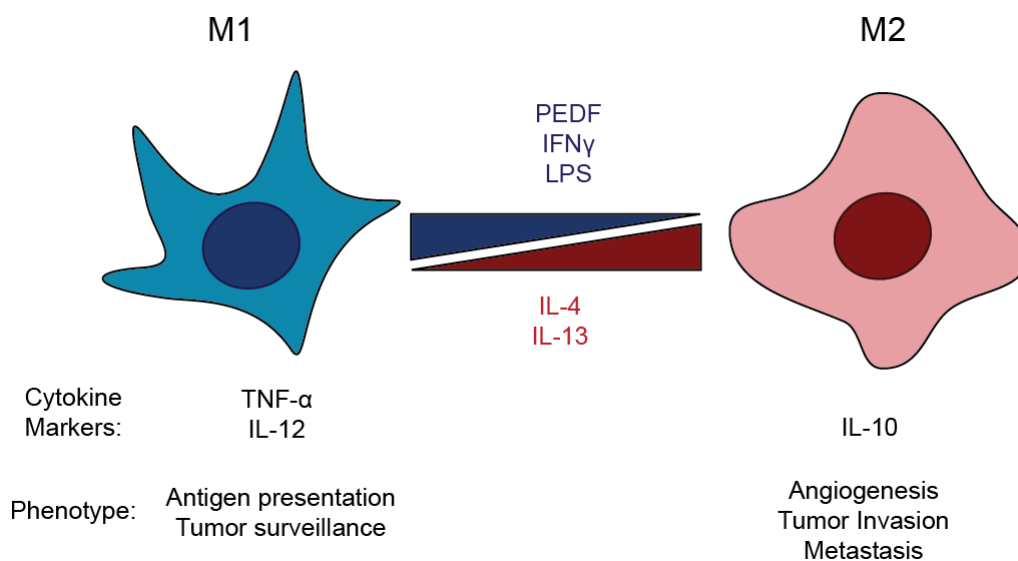


Figure 1.2: Macrophage Polarization. M1 macrophages are characterized by increased antigen presentation and tumor surveillance, while M2 macrophages support angiogenesis, tumor invasion and metastasis.

1.3 The Immune System as a Gatekeeper to Metastasis

1.3.1 Innate Immunity and the Control of Tumor Metastasis by Patrolling Monocytes

Cells of the innate immune system are important regulators of metastasis. The heterogeneity of these cell populations allows for a spectrum of functions ranging from anti-metastatic to pro-metastatic. This cannot be more evident than is demonstrated by myeloid cells. For example, macrophages can exhibit drastically different phenotypes. This phenomenon has been termed macrophage polarization. Tumor associated macrophages can be polarized to a “M1 or M2” phenotype. M1 macrophages have antimetastatic functions while M2 macrophages

support tumor growth and metastasis (**Figure 1.2**).¹⁸ Numerous signals can polarize macrophages in one towards a M1 or M2 phenotype. For examples, macrophages can be polarized to a M1 phenotype in response to pigment epithelial derived factor (PEDF) causing a reduction in metastasis.^{19,20} This function of PEDF at promoting M1 macrophages is discussed in more detail in Chapter 2 of this thesis.

Macrophages are not the only innate immune cell-type that present this dichotomy of functions. Tumor associated neutrophils can also have tumor supporting, as well as anti-tumor functions. Neutrophils are recruited to tumors and the sites of metastasis in response to danger associated molecular patterns where they contribute greatly to inflammation. Neutrophils are present in the microenvironment of many cancers including glioblastoma, melanoma, and colorectal cancer and increased numbers of neutrophils correlate with more aggressive disease. Despite these findings, the role of neutrophils in cancer is not that straightforward. As mentioned above, studies have found that neutrophils can be both beneficial and damaging during tumor progression. In cancer development, neutrophils can secrete reactive oxygen and nitrogen radicals, which can support tumorigenesis.²¹ Additionally, neutrophils can produce proteases such as matrix metalloproteinase 9 and neutrophil elastases that support angiogenesis and increase tumor cell proliferation.^{22,23} These factors also lead to significant extracellular matrix (ECM) remodeling, which contributes greatly to metastasis. Neutrophils can also function in a similar manner to granulocytic MDSCs (G-MDSCs) resulting in a suppression of antitumor immunity.²⁴ This is accomplished by the production of Arginase 1 and nitric oxide synthase resulting in the suppression of T cells. This is demonstrated by the fact that depletion of neutrophils causes increased CD8⁺ T cell activity and reduces tumor growth in mice with lung tumors.²⁵ Clearly, neutrophils play an important role in tumor progression and metastasis but the

idea of therapeutically targeting neutrophils is still in its infancy and due to the multiple functions of neutrophils, more research is needed to effectively develop these therapeutics.

While classical “inflammatory” monocytes are well established promoters of tumorigenesis and cancer metastasis, non-classical “patrolling” monocytes (PMos) function to control metastasis.^{20,26,27} PMos are a sub-population of monocytes, which develop in the bone marrow prior to being released into circulation where they patrol the vasculature. They are driven by a master regulator transcription factor Nr4a1 also called Nur77, which is required for PMo development and survival. PMos are characterized by their interactions with the vascular endothelium. This is accomplished through the expression of a complex of integrin $\beta 2$ and lymphocyte function-associated antigen 1 (LFA-1), as well as CX3CR1²⁸ where they traverse the vasculature at a speed much slower than the rolling process observed in classical monocytes neutrophils.²⁹ PMos were first discovered to function to resolve inflammation where they crawl and remove cellular debris.³⁰ Because of their role in protecting the vasculature, PMos are most notably involved in cardiovascular disease.³¹ In mouse models of myocardial infarction, monocyte depletion leads to higher mortality due to a reduction in cardiac remodeling.³² Additionally, mice lacking Nr4a1 expression in bone marrow cells have reduced wound healing compared to wild-type mice.³³ During atherosclerosis, there is a reverse correlation between the number of circulating PMos and the atherosclerotic lesion size.³⁴ Moreover, mice lacking PMos have increased atherosclerosis and the macrophages are polarized to a more inflammatory M1 phenotype.³¹ Despite the wealth of knowledge about PMo functions in cardiovascular disease, very little is known about their functions in other diseases, including cancer. Early observations have demonstrated that loss of PMos leads to increased metastasis in mouse models of breast cancer and melanoma. This is likely due to a scavenging of metastasizing tumor cells in addition

to the recruitment of NK cells to the metastatic sites.^{20,26,27} These studies are still preliminary and more work is needed to elucidate the exact role of PMos in cancer, but targeting PMos may prove to be a novel therapy for the inhibition of metastasis.

1.3.2 The Adaptive Immune Response Against Cancer

Innate immune cells drive the activation of a second branch of immunity, termed the adaptive immune response, led by B cells and T cells. These cells are extremely specific and can recognize cell types including cancer cells. The ability of T cells to infiltrate tumors and kill tumor cells has led to the development of cancer treatments called adoptive cell transfer in which T cells are manipulated and expanded *ex vivo* then reintroduced into the patient. These therapies have shown some success due to the ability of T cells to traffic to the tumors and selectively kill tumor cells.

Over the past several decades there have been numerous observations which demonstrate the importance of the adaptive immune response to preventing cancer. The most compelling of which may be the efficacy of cancer immunotherapies, specifically targeting checkpoint blockade, at inducing an immune response leading to cancer clearance. Immunotherapies will be discussed in much greater detail in the next section. Researchers have also noted various other phenomena that support the crucial role the adaptive immune response plays in suppressing malignancy. For example, in both humans and mice that are immunodeficient, either due to genetics, caused by infection (human immunodeficiency virus, Epstein Bar Virus), or due to treatment with immunosuppressive drugs after organ transplant, there is an increased cancer risk.³⁵⁻³⁷ Despite the fact that cancer cells display self-antigens, they also express many mutated “neoantigens”, as well. This provides a mechanism by which T cells can recognize cancer cells for eradication. The fact that patients with larger sets of neoantigens have greater T cell mediated

immune clearance of tumor cells overwhelmingly supports the role of T cells in controlling cancer.³⁸

1.3.3 Current Immunotherapies for the Treatment of Cancer

The role the immune system plays in the regulation of cancer progression has led to significant advances in the development of immunotherapies over the past decade.³⁹ In this section we will discuss current immunotherapies, highlight the promise these therapies hold and examine the side effects elicited by some of the most successful immunotherapies.

Recently, there has been numerous drugs developed that target the inhibitory checkpoint blockade molecules. The immune checkpoint is a series of signals on immune cells that can either stimulate or inhibit the immune system. Cancer cells take advantage of these checkpoint signals resulting in a suppression of T cell and subsequent cancer progression.⁴⁰ From a therapeutic perspective, one of the most studied checkpoint signals is cytotoxic T-lymphocyte-associated protein-4 (CTLA-4) an inhibitory receptor that can limit T cell receptor (TCR) stimulation by competing with the activating signal CD28.⁴¹ CTLA-4 is also highly expressed on regulatory T cells (T_{reg}) where it can suppress T cell effectors. After discovering the functions of CTLA-4 at blocking T cell activation, researchers began to target it as a combination therapy alongside other drugs. A monoclonal antibody for CTLA-4 called Ipilimumab was approved for treatment of metastatic melanoma in 2011.⁴² In addition to melanoma, Ipilimumab has shown efficacy in multiple tumors suggesting that preventing the immunosuppressive effects associated to CTLA-4 can result in a profound activation of anti-tumor immunity.

In addition to CTLA-4, the PD-1-PD-L1/2-axis is an important checkpoint blockade that researchers have begun to target. PD-1 is another inhibitory receptor that is expressed on T cells. The ligands for PD-1, PD-L1 and PD-L2 are expressed on antigen presenting cells and tumor

cells.⁴³ Upon activation of the PD-1 receptor, downstream T cell receptor signaling is inhibited leading to T cell exhaustion and immune suppression. T cell suppression caused by PD-L1 is associated with a poor prognosis to multiple cancer types, including melanoma.⁴⁴ Because of PD-L1's association with a poor patient outcome, the development of therapies to block PD-1 and subsequent immune suppression has produced promising results, even in patients unresponsive to conventional therapies.

<any other immunotherapies are being developed including chimeric antigen receptor (CAR) T cell therapy, which is a form of adoptive T cell transfer that allows for targeting a specific antigen by altering T cells *ex vivo* then reintroducing them back into the patient. CAR T cells express a single-chain variable antibody fragment that targets an antigen without the need for presentation by an MHC.⁴⁵ For CAR T cell therapy, it is necessary to target an antigen that is expressed by all the tumor cells in a given population and an antigen that localizes to the extracellular domain of the cell allowing it to be engaged by the CAR T receptor. Because of these requirements, initial tests of CAR T cell efficacy have targeted CD19 on B cell leukemia and lymphomas. CD19 is expressed on virtually all B cells and all B cell leukemia, therefore, developing immunity towards it can hypothetically clear all leukemia cells. Clinical trials conducted across several institutions have shown great success with complete response rates being approximately 70-90%.⁴⁶ While CAR T cell therapy has been effective at treating CD19 positive B cell leukemia, much more work is needed to develop this technology to treat other more heterogeneous tumors.

With the growing development of immunotherapies, it is crucial to understand the possibility of side effects. Clinical trials using checkpoint inhibitors have noted several immune related adverse effects. For example, anti-CTLA4 (Ipilimumab) causes immune related side

effects in 60-65% of patients.⁴⁷ While PD-1 blocking antibodies, such as nivolumab, have less frequent side effects, approximately 15% of patients experience serious adverse effects and approximately 40% experience milder immune related adverse effects.⁴⁸ The most common side effects of these therapies are rash, hypothyroidism, diarrhea and pneumonitis. Over the past decade, with the emergence of immunotherapies as a primary therapy for multiple cancers it is essential to continue to study the side effects caused by these drugs. Also, the development of immunotherapies driven by alternative mechanisms can be of tremendous significance, especially for patients that do not respond or experience these side effects.

1.4 Biogenesis, Structure and Function of Exosomes

Exosomes are 30-150 nm nanovesicles, that are released by virtually all eukaryotic cells. Exosomes primarily function as delivery vehicles due to the importance of intercellular signaling in multicellular organisms.⁴⁹ Exosomes are produced during the maturation of the endosome. After endocytosis, as the endosome is developing, reverse inward budding events leading to the endosome maturing into the late endosome and the subsequent formation of an organelle termed the multivesicular body (MVB).⁵⁰ The MVB contains an abundance of intraluminal vesicles, which will eventually be called exosomes. At this point the MVB can proceed down two routes, the MVB can merge with a lysosome, whereupon its contents are degraded, or the MVB can fuse with the plasma membrane and release the intraluminal vesicles into the extracellular space at which point they are termed exosomes (**Figure 1.3**). After release into the extracellular space, target cells can take up the exosomes both locally and at distant sites. This process, by which exosomes are generated through the late endosome and multivesicular body is the key differences that distinguishes exosomes from other extracellular vesicles including microvesicles shed from the plasma membrane. An important aspect of exosome biogenesis is the sorting of

biomolecules. The primary mechanism by which proteins are sorted into exosomes relies on the endosomal sorting complexes required for transport (ESCRT) complexes. The ESCRT complexes sort proteins into the developing intraluminal vesicles by residing at the cytoplasmic side of the endosome and recruiting ubiquitinated proteins (among others).⁵¹ Other ESCRT-independent methods of sorting to exosomes have been identified as well.

Exosomes are highly heterogeneous and their functions are determined by the state of the cell that generates them. Initially researchers thought that the main purposes of exosomes were as cellular “garbage dumps” functioning to remove unneeded cellular material, but over the past 15 years it has been established that exosomes hold essential functions as the predominant endogenous intercellular delivery vehicle.^{52,53} This critical discovery has opened the door to

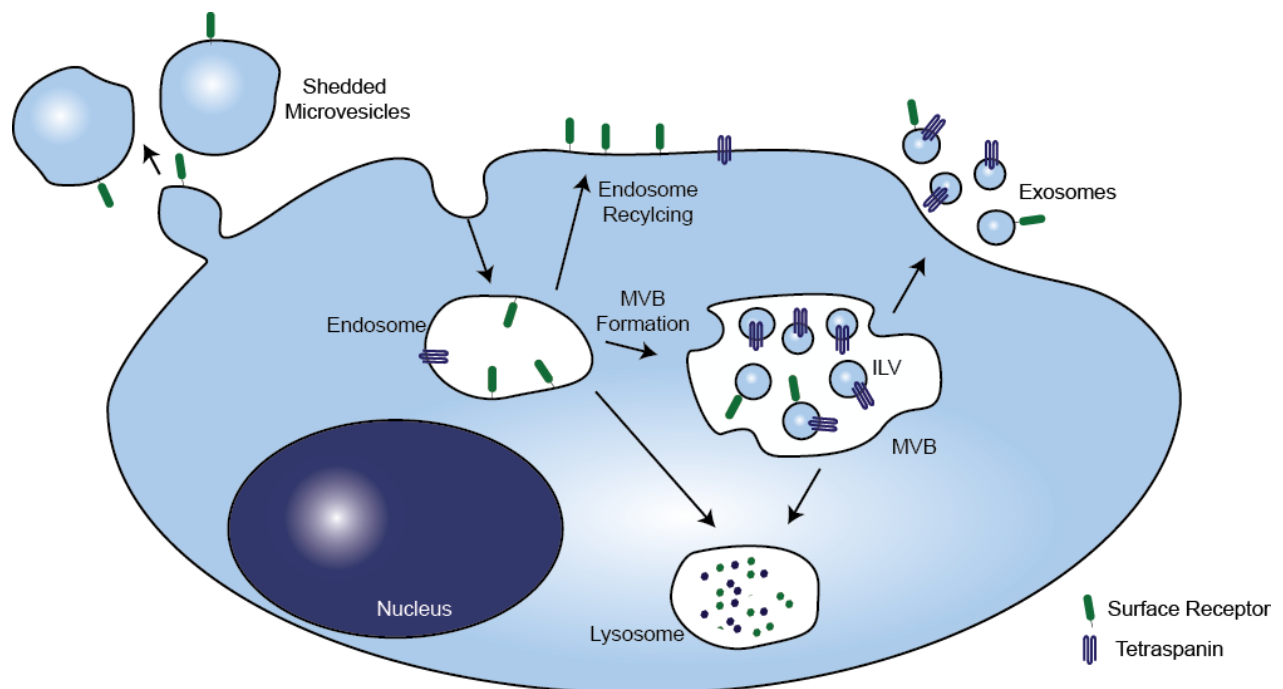


Figure 1.3: Exosome Biogenesis. Diagram showing the generation of exosomes as the endosome matures into the multivesicular body. Note that surface receptors and the exosome markers, tetraspanins, maintain their orientation from membrane to exosome allowing for recognition by ligands and receptors.

tremendous opportunities to better understand the biologic role of exosomes and to develop exosome-inspired technologies.

Because of the important role of exosomes in intercellular communication, it is crucial to understand the cargo held in exosomes, how this cargo is packaged into exosomes, and the effects of cargo after delivery to target cells, but much of this information remains largely unknown. In a landmark study, Valadi et al. demonstrated that exosomes contain RNA and are particularly enriched in small RNAs like miRNA.⁵³ Multiple researchers have gone on and demonstrated that delivery of these RNAs to recipient cells can alter gene expression.⁵⁴⁻⁵⁶ Exosomes package a wide array of functional biomolecules in addition to miRNA, including proteins and mRNA.⁵⁷ Additionally, researchers have identified double stranded DNA fragments in exosomes, as well, but the mechanisms through which DNA is packaged to exosomes and the functions of DNA upon delivery to recipient cells are still somewhat obscure.⁵⁸⁻⁶⁰

1.5 Functions of Exosomes in Cancer Biology

1.5.1 Exosomes as Drivers of the Pre-Metastatic Niche

Importantly, exosomes role is indispensable for the intercellular communication between tumor cells and the host microenvironment.⁶¹ Exosomes generated by the primary tumor promote metastasis by creating a suitable microenvironment at the target site (pre-metastatic niche), which encourages tumor cell colonization and propagation (**Figure 1.4**).⁶² They promote tumorigenesis and metastasis by delivering specific proteins and RNA to a range of cell types. For example, in 2012 Peinado et al. demonstrated that melanoma exosomes contain the receptor tyrosine kinase Met and that these exosomes can drive metastasis in part through the delivery of this oncoprotein.⁶³ In this study, mice were conditioned with melanoma exosomes. After the

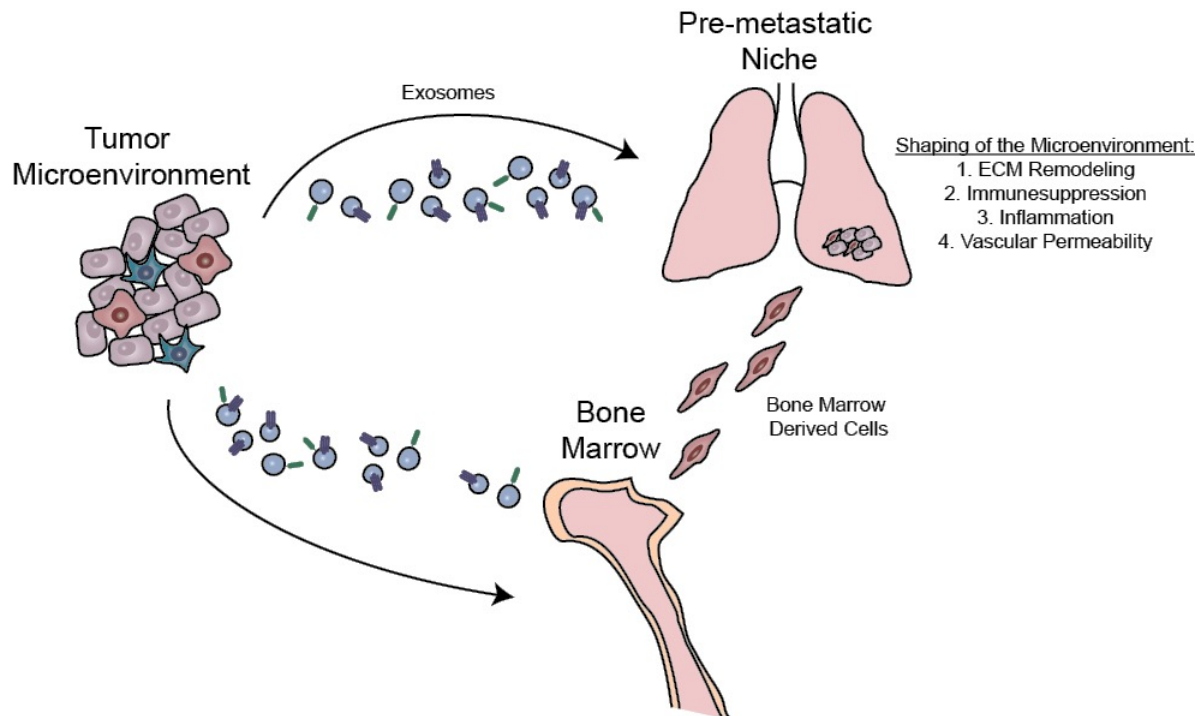


Figure 1.4: Exosomes Drive the Formation of the Pre-Metastatic Niche. Exosomes promote pre-metastatic niche formation by both directly delivering pro-tumorigenic cargo to the metastatic sites and trafficking to the bone marrow where they promote the mobilization of bone marrow derived cells, which contribute to the metastatic microenvironment.

conditioning period, mice were sacrificed and the bone marrow was transplanted to lethally irradiated mice to test the effects of exosome-educated bone marrow on metastasis. There was a significant increase of B16F10 melanoma metastasis in the mice with the exosome educated bone marrow compared to wild-type bone marrow and there were greater numbers of bone marrow cells, specifically endothelial progenitor cells, in the metastatic microenvironment. This was one of the early studies that established cancer exosomes as drivers of metastasis.

Additional studies have gone on to further cement the role of cancer exosomes in metastasis. Hood et al. showed that melanoma exosomes first traffic to the sentinel lymph node where they alter gene expression patterns resulting in increased angiogenic growth factors and a modulation of the lymph node matrix causing increased trapping of melanoma cells.⁶⁴ The

disruption of the sentinel lymph node microenvironment leads to colonization by melanoma and also facilitates future metastasis by promoting angiogenesis and immunosuppression.⁶⁵

In another recent study, Liu et al. showed that exosomes can promote metastasis through the delivery of tumor-derived miRNAs. They demonstrated that epithelial expression of toll-like receptor 3 (TLR3) promotes the formation of the lung pre-metastatic niche and subsequent metastasis. The authors go on to show that melanoma exosomes promote pre-metastatic niche formation through the recruitment of neutrophils and importantly that TLR3 is activated in lung epithelial cells by tumor exosome associated RNAs.⁶⁶ On top of the studies outlined above, multiple others have further established how exosomes promote pre-metastatic niche formation and the molecular pathways leading to metastasis.

1.5.2 The Development of Exosome-Based Cancer Biomarkers

There has been increased interest in developing novel, non-invasive biomarkers for the detection of many diseases including cancer. Exosomes provide an easily accessed source of tumor material that can be assayed for biomarkers, as a novel version of a liquid biopsy. It is estimated that there are approximately 2,000 trillion exosomes circulating in the blood of a healthy human. In cancer patients this number increases dramatically to approximately 4,000 trillion.⁶⁷ Therefore, exosomes hold tremendous potential to be used to detect circulating tumor antigens.

As was mentioned previously, exosomes have been shown to contain DNA fragments. Researchers have hypothesized that these DNA fragments may contain mutations that can be used to detect cancer. For example, in a recent publication, Thakur *et al.* demonstrate that exosomes not only carry double strand DNA but this DNA holds genetic mutations that are present in the cells from which the exosomes originated. More specifically, the *BRAF (V600E)*, a

mutation that is present in around 50% of melanoma malignancies, was detected in exosomes from all the melanoma cell lines expressing the BRAF variant.⁵⁸ Additionally, multiple mutations that are common in EGFR mutant breast cancer cell lines were found in their exosomes.⁵⁸ The discovery that exosomes contain genomic DNA is a significant discovery and can possibly be developed into a biomarker candidate for early detection of cancer or to monitor treatment responses.

For almost 10 years one of the most active areas of research with regards to exosomes has been utilizing exosomal RNA as biomarkers, most notably for cancer. Researchers suggested that due to the large increase in serum exosomes during cancer progression the miRNA cargo of the exosomes could be used as a surrogate for the tumor. For example, researchers have found multiple miRNAs in the exosomes of patients with metastatic ovarian cancer compared to benign disease.⁶⁸ These miRNAs, including miR-21, miR-200c, miR-205 and miR-214, were highly enriched in the exosomes of Stage III patients. Following this landmark study, researchers have found that many different miRNA signatures can correlate to cancer stage and have prognostic value, as well.⁶⁹

In addition to exosomal RNAs, researchers have discovered a multitude of exosomal proteins that correlate to different cancers at multiple stages.⁷⁰ Recently, Melo et al. found that circulating exosomes from early stage pancreatic cancer patients are enriched in Glypican-1.⁷¹ This is an important finding because the Glypican-1 marker could distinguish between patients suffering from pancreatitis or pancreatic cancer, a notoriously difficult cancer to detect. In melanoma, Peinado et al. found a suite of exosomal proteins that correlate with cancer stage. Stage 3 and 4 patients contained very high levels of Tyrp2, V1a4, and Hsp70 in serum exosomes compared to the exosomes from Stage 1 patients or healthy controls.⁶³ Additionally, epithelial

adhesion molecule (EpCAM) has been found in exosomes from numerous cancer types. In ovarian cancer, EpCAM-positive exosomes have been identified in early stage cancer patients.⁶⁸ While exosome biomarkers are not yet approved in the clinic for the detection of cancer, these studies demonstrate that exosomes can be easily isolated from patients and specific exosomal biomolecular cargo correlates to disease presence and progression.

1.6 Roles of Exosomes in other Diseases

Exosomes hold functions for both normal homeostasis and the pathogenesis of a myriad of diseases in addition to cancer. Here major roles of exosomes in diseases other than cancer will be discussed. In cardiovascular disease, researchers have discovered that exosomes can both ameliorate and promote the disease. For example, during the development of atherosclerotic lesions extracellular vesicles can alter endothelial homeostasis, promote cell survival and either increase or decrease inflammation.⁷² Numerous studies have shown that these vesicles can decrease nitric oxide (NO) production and recruit immune cells further exacerbating plaque formation.^{73,74} Because of the interest in exosomes during cardiovascular disease researchers have begun to assess exosome quantities after myocardial infarction as a prognostic marker, but studies have not been conclusive.⁷⁵ Here, I have outlined only negative effects of exosomes and extracellular vesicles to cardiovascular disease, studies have also been conducted exploring their uses for cardiac regenerative medicine. This will be discussed in future sections of this Thesis.

Exosomes have also been recently implicated in many neurodegenerative diseases. While the exact role of exosomes in these diseases remains controversial, early studies have found that exosomes can transmit misfolded proteins, which is a possible route of disease propagation. Misfolded proteins have been found in exosomes including alpha-synuclein in Parkinson's (PD) Disease, superoxide dismutase 1 in amyotrophic lateral sclerosis (ALS) and fragments of the

amyloid precursor protein present in Alzheimer's Disease (AD).⁷⁶⁻⁷⁹ While much remains unknown about the role of exosomes in neurodegenerative disease, the fact that these diseases are driven in large part due to the accumulation of aggregated proteins coupled to the presence of these proteins in exosomes suggests that exosomes may contribute to the propagation of the disease.

Exosomes have been quite intriguing in virology due to their similar sizes, biogenesis and cellular uptake pathways. For instance, researchers have discovered that non-enveloped viruses utilize the exosomal pathways for cell-to-cell spread. In HIV, researchers have found that exosomes can function to both promote and suppress viral infection. For example, exosomes released from many cell-types infected with HIV including macrophages, dendritic cells and T cells contain anti-viral biomolecules such as interferon-alpha, interferon-beta, and TNF-alpha.⁸⁰ On the other hand, exosomes can also contain viral proteins such as Nef and viral RNAs. It is also important to note that the functions of exosomes across virology, and biology as a whole, depends on the cell-type of origin. Therefore, exosomes released from dendritic cells are likely to function quite differently from exosomes released from T cells. Exosomes have also been observed to function in other viral infections as well. Epstein Bar Virus (EBV) infections, LMP1, EGFR and PI3K is delivered to healthy cells via exosomes, whereby they drive proliferation and promote the upregulation of cellular adhesion molecules.⁸¹ Exosomes also play an important role in the viral pathogenesis of hepatitis A (HAV) and C (HCV) viral infections. It has been discovered that full length HCV RNA is present in exosomes of infected hepatocytes and that these exosomes can transfer the RNA to recipient plasmacytoid dendritic cells or other hepatocytes.^{82,83} This is an important finding because it demonstrates that viral material can be transferred via exosomes independent of viral structural proteins. Over recent years, there is

mounting evidence of the role of exosomes to the pathogenesis of many viral infections. This coupled with the similarities viruses have to exosomes size, biogenesis and uptake pathways make understanding virology of significant importance to the study of exosomes.

1.7 Exosome Inspired Therapeutics

1.7.1 Exosome Mimetics

Researchers have attempted to create exosome-inspired therapeutics for numerous applications. The most prevalent therapeutic use of exosomes is replicating its natural functions as a targeted delivery vehicle and leveraging that to deliver specific cargos. For example, in multiple studies, researchers have developed exosomes to deliver small-molecule drugs for numerous therapeutic purposes including cancer. In one study, researchers developed “exosome mimetic nanovesicles” for the delivery of doxorubicin.⁸⁴ To do this U937 monocytes or RAW 264.7 macrophages were treated with doxorubicin. Treated whole cells were then passed through a serial extruder to generate vesicles of approximately 120 nm in diameter, roughly the same size as naturally produced exosomes. After extrusion nanovesicles were purified using density gradient ultracentrifugation and subsequently used to treat cancer cells in animal models.⁸⁴ In this study, doxorubicin-loaded nanovesicles display cytotoxicity *in vitro* to the C26 colon cancer cell line and also show a modest reduction in tumor weight and volume *in vivo*. While there was some success at slowing the growth of colon cancer cells, despite labeling their delivery vehicle as an exosome mimetic, the nanovesicles are significantly different in composition to normal exosome. In fact, while there is significant interest in developing fully synthetic exosome mimetics, this has not yet been accomplished. The appeal of developing completely synthetic exosomes is twofold; 1. It provides complete control over the contents of the exosomes. Currently, if using exosomes isolated from cell cultures, there is still uncharacterized proteins,

RNAs or DNAs that can have negative consequences. Additionally, due to exosome heterogeneity, it is difficult to know exact amounts of therapeutic cargo on a per exosome basis. This is especially important in the clinic when good manufacturing processes are necessary. 2. The number of cells needed to produce sufficient amounts of exosomes and the time-consuming nature of the exosome isolation processes (i.e. differential ultracentrifugation or size exclusion chromatography) makes acquiring enough material for treatment extremely laborious.

1.7.2 Genetically Modified Exosomes to Deliver Specific Cargo

In order to improve delivery capabilities, researchers have genetically altered cells to create exosomes that are either targeted to specific organs or contain certain cargo. For example, in one breakthrough study, Alvarez-Erviti et al demonstrated that dendritic cells can be transfected with a plasmid expressing a rabies viral glycoprotein (RVG) peptide-LAMP2b fusion protein.⁵⁵ The LAMP2b domain of the fusion protein led to localization of the fusion protein to the exosome membrane and the RVG peptide targeted the exosomes to the central nervous system. They proceeded to demonstrate exosome delivery to neurons, microglia and oligodendrocytes. Most importantly, they showed siRNA loading of exosomes and subsequent brain-specific knockdown of the gene *BACE1*, an important gene for the generation of amyloid plaques in Alzheimer's Disease. This study was a landmark first step in developing genetically modified exosomes for the targeted treatment of human disease. Several other studies have followed up and developed similar exosome-mediated siRNA technologies.^{85,86}

In Chapter 2 we discuss generating exosomes that contain the anti-tumor protein pigment epithelial derived factor (PEDF) by using lentiviral vectors to overexpress PEDF in melanoma cells.²⁰ In this study, we take a similar approach by forcing expression of PEDF, which localizes to melanoma exosomes via an unknown mechanism. PEDF can then be delivered to the cells that

are naturally targeted by melanoma exosomes. The delivery of PEDF to cells including macrophages and monocytes results in increased innate immune clearance of circulating melanoma cells. This finding will be discussed in much greater detail in this thesis in future chapters.

1.7.3 Exosome Vaccines

There has been significant interest in developing exosomes into vaccines to elicit immune responses against a variety of diseases. Researchers have used two major strategies for the development of exosome-inspired vaccines: First, as conveyors of MHCs. Second, as direct delivery vehicles of antigens. In the early 2000s, it was discovered that exosomes released by antigen presenting cells (APCs) contain major histocompatibility complexes (MHCs) (both MHC class I and MHC class II) and these MHCs maintain their orientation in the exosome membrane.⁸⁷⁻⁸⁹ Maintaining the orientation of the complex is important because it allows the MHCs to directly activate CD4⁺ or CD8⁺ T cells. Therefore, MHC-containing exosomes can illicit adaptive immune responses independent of the APC that generated the exosomes. This has opened the door to numerous studies where dendritic cells (among other APCs) were pulsed with a tumor specific antigen to present in the MHC, the exosomes were collected and used to activate cytotoxic T cells.⁹⁰

Early studies have also revealed that exosomes are carriers of antigens and can effectively deliver these to APCs. For example, researchers have found that vaccination of a mouse with tumor exosomes results in a potent CD8⁺ T cell mediated response against colon cancer cells and melanoma.⁹¹ This response functioned in both allogeneic and syngeneic models suggesting that it was not due to differences in HLA groups but due to the delivery of the tumor antigen. In addition to inducing immune responses against cancer, exosomes can also carry

pathogen antigens including the HIV Gag protein, CMV glycoprotein B and EBV latent membrane protein (LMP1). Also, many bacteria and parasites like *Toxoplasmosis Gondii* and *Mycobacterium Bovis* antigens can be loaded into dendritic cell or macrophage exosomes, respectively, resulting in protective immune responses.^{92,93} While these antigen containing exosomes have been effective in certain disease models, a successful exosome-inspired vaccine has yet to reach the clinic.

1.7.4 Exosomes in Regenerative Medicine

Exosomes have also been used as stand-alone therapies and have shown great promise in regenerative medicine. As mentioned briefly above, much of the focus of exosomes for regenerative medicine has been on cardiovascular disease. In 2005 Brill et al. first demonstrated that vesicles derived from platelets can induce angiogenesis by stimulating vascular endothelial growth factor (VEGF) resulting in revascularization and a reduction in ischemia.⁹⁴ Recently, researchers have demonstrated that bone marrow-derived mesenchymal stem cell (MSC) derived exosomes can affect cell proliferation, viability and senescence dependent upon the age of the source MSC exosomes.⁹⁵ For example, in acute kidney injury models these exosomes can increase proliferation and decrease apoptosis in proximal tubular kidney epithelial cells in a process mediated by the delivery of exosomal RNAs.⁹⁶ Additionally, in other studies researchers showed an increase in skin cell proliferation using *in vitro* models.⁹⁷ Exosomes have a clear immunomodulatory role that can also promote regeneration by recruiting immune cells leading to revascularization and preventing further tissue damage.⁹⁸ The study of exosomes in regenerative medicine is in its infancy but results show clearly that MSC exosomes can function in local tissue repair and regeneration.

1.8 Scavenger Receptor type-B1 (SR-B1)

1.8.1 SR-B1 Functions in Reverse Cholesterol Transport

SR-B1 is of great interest to our research group because it is one of the major receptors through which HDL NPs, developed in our laboratory, function.⁹⁹ In order to understand the importance of SR-B1 to cancer biology it is necessary to know its canonical functions in cardiovascular disease. SR-B1 is an integral membrane protein that is expressed in several cell types and tissues but at the highest levels in the liver and adrenal glands. SR-B1 holds critical functions in reverse cholesterol transport (RCT), the multi-step process by which cholesterol is transported by HDLs from foam cells to the liver for excretion. Briefly, during the development of atherosclerosis, circulating monocytes are recruited to the atherosclerotic sites where they mature into M2 polarized macrophages. These macrophages then begin to take up low density lipoprotein and cholesterol and become cholesterol rich foam cells. In order to resolve the huge amounts of cholesterol present in foam cells, Apolipoprotein AI containing discoidal HDLs bind to efflux receptors such as ATP-binding cassette A1 (ABCA1) or ABCG1, and free cholesterol is transported to the HDL.¹⁰⁰ Upon this transfer, free cholesterol is esterified by lecithin-cholesterol acyltransferase (LCAT) present on the HDL particle resulting in the formation of cholesteryl ester. As cholesterol is esterified it becomes more hydrophobic causing it to be packed into the HDL core. This results in the HDL shifting in size and shape from a discoidal to a spherical shape. This step is crucial because as HDL becomes more spherical it gains a higher affinity to SR-B1. Spherical HDLs are then trafficked to the liver where they bind SR-B1 and deliver cholesterol for excretion in the bile. This process is very complex and SR-B1 is a key participant, as the major receptor for cholesterol-rich spherical HDLs.¹⁰¹

1.8.2 Signal Transduction through SR-B1

There are two SR-B1 domains that are necessary for downstream signaling. The first of which is the C-terminal PDZ-interacting domain. The adapter protein PDZK1 is necessary for SR-B1 function leading to the activation of downstream signaling pathways including the PI3K/Akt pathway.¹⁰² This activation is predicted to be mediated by Src family kinases. The other critical SR-B1 domain is the C-terminal transmembrane domain. Researchers have demonstrated the importance of the C-terminal transmembrane domain to downstream signaling by creating CD36-SR-B1 chimeras. CD36 is a class B scavenger receptor that has approximately 30% sequence homology to SR-B1, although it lacks a C-terminal transmembrane domain. CD36 can bind HDL but is unable to participate in cholesterol flux and eNOS phosphorylation mediated by SR-B1 downstream signaling. Utilizing a CD36 that contains the C-terminal transmembrane domain allows for the eNOS phosphorylation caused by SR-B1.^{103,104} This data overwhelmingly demonstrates the importance of the C-terminal transmembrane domain for SR-B1 downstream signaling. It is hypothesized that the C-terminal transmembrane domain functions as a cholesterol sensor by binding free cholesterol in the plasma membrane but it is unclear the exact mechanism by which this occurs.¹⁰³

1.8.3 SR-B1's Role in Cancer Biology

The expression of SR-B1 is critical for a large number of cancers. As mentioned previously, SR-B1 functions in cholesterol metabolism but also as a mediator of cell migration, angiogenesis and proliferation. Taken together these functions can have drastic consequences during tumorigenesis and metastasis. One of the major reasons SR-B1 is of such importance is due to the dependence of cancer cells on cholesterol. In order to maintain cell membrane integrity during the increased proliferation of cancer cells, there is high SR-B1 expression.

Researchers have gone on to show this in breast cancer using siRNA mediated knockdown, as well as through the use of BLT-1 a chemical inhibitor. HDL binding to SR-B1 activates the PI3K/Akt and MAPK signaling pathways leading to cell proliferation. Both BLT-1 and siRNA targeting SR-B1 led to a decrease in breast cancer cell proliferation.¹⁰⁵ Additionally, cholesterol is a critical precursor for many steroid hormones such as androgen and SR-B1 provides some of the cholesterol necessary to produce these hormones. With this in mind, researchers have knocked down SR-B1 in castrate resistant prostate cancer models and showed that there was a decrease in the production of prostate-specific antigen.¹⁰⁶

The importance of SR-B1 to cancer proliferation and prognosis has led researchers to investigate its expression as a prognostic marker and predictor of survival. Although, SR-B1's association with cancer outcomes seems straightforward in that patients with high SR-B1 expression have poor survival outcomes (bladder cancer, breast cancer, myeloma),^{107,108} researchers have also observed the reverse correlation, patients with low SR-B1 expression can also have poor survival outcomes (ovarian cancer, lung cancer, osteosarcoma).¹⁰⁹ It is clear that the complexity of SR-B1 signaling, both in the cancer cells themselves and in the stromal cells, have functions that are not completely understood and much more work is needed to decode the roles of SR-B1 across cancer biology.

1.9 Nanomedicine: Novel Technologies for the Development of New Therapeutics

1.9.1 Targeted Nanotherapeutics for Cancer Therapy

Engineering nanoparticles as a cancer therapeutic or a diagnostic tool has been studied extensively over the past 20 years. Despite substantial advances, significant work is needed to improve tumor targeting and efficacy. Researchers have discovered that nanoparticles can target tumors using both non-specific and specific approaches. A primary route by which nanoparticles

target and accumulate in the tumor is through the enhanced permeability and retention (EPR) effect. The EPR is a negative pressure caused by poorly draining lymphatics.¹¹⁰ Nanoparticles enter the tumor through gaps in the vasculature then cannot escape due to this pressure resulting in a concentration of nanoparticles at the tumor. Some of the earliest advances in nanomaterials for cancer nanotechnology is focused on utilizing on taking advantage of the EPR effect to amass therapeutics in the tumor.¹¹⁰ Some of the early successes rely on binding a conventional chemotherapeutic to a nanoparticle. Abraxane is a conjugation of Paclitaxel to albumin approved to treat many cancers including breast cancer, lung cancer and pancreatic cancer. Another example is Doxil, which is liposome encapsulated doxorubicin used to treat late-stage ovarian cancer. In addition to improving efficacy, both these formulations have reduced side effects due to more controlled biodistribution.

One of the major problems associated with nanoparticle-based therapy is clearance by the mononuclear phagocyte system (MPS). The MPS includes organs that are rich in phagocytic cells most notably the liver or the spleen. At these organs, nanoparticles are phagocytized and subsequently cleared from circulation preventing their accumulation in the tumor. Additionally, nanoparticles can be cleared through the renal pathway, where nanoparticles less than 5 nm are excreted. Taking advantage of active targeting motifs allows for a reduction in clearance by MPS and renal pathways and enhanced targeting to the tumor.¹¹¹

While the EPR effect is useful at delivering nanoparticles to the primary tumor, smaller metastatic tumors have limited EPR making these therapies less efficient. Therefore, more active targeting mechanisms are needed, especially to treat late-stage disease. Researchers have also developed methods for actively targeting nanoparticles to the tumor. In the next section, I discuss in detail one method of active nanoparticle targeting developed in our laboratory, the use of high-

density lipoprotein nanoparticles (HDL NPs). Other laboratories have also developed innovative active targeting mechanisms. For example, early active targeting methods include utilizing antibodies conjugated to nanoparticles to specifically deliver therapy to cancer cells expressing an antibody target. A majority of these antibodies target the extracellular domain of cell surface proteins and they can be conjugated to numerous nanoparticles including AuNPs, liposomes and polymers.¹¹² Other biomolecules can also be conjugated including receptor ligands such as transferrin, folate and peptides like RGD or VEGF peptide. In addition to these targeting methods many others have been developed in an attempt to create more effective nanotherapeutics. Despite this, much work is needed to create the next generation of cancer therapies.

1.9.2 High-Density Lipoprotein Nanoparticles

High-density Lipoproteins (HDL) are natural 9-13 nm nanostructures that have multiple important functions across biology.^{100,113} They are best known for their ability to transport cholesterol, but it is becoming increasingly more evident that they have critical functions in cancer progression, immunology, and inflammation.^{114,115} As described above, the most well-established function of HDL is in reverse cholesterol transport, where cholesterol is effluxed from foam cells formed during atherosclerosis and then transported to the liver via SR-B1 where it can be excreted in bile. Throughout this process HDLs are significantly remodeled allowing for interactions with a number of different receptors. Initially, the major protein component of HDL, apolipoprotein –AI (apo-AI) is synthesized in the liver and secreted into the blood, whereby lipids and free cholesterol assemble around apo-AI forming discoidal HDL. LCAT then converts free cholesterol to cholesteryl ester a more lipophilic cholesterol analog, which is then sequestered in the hydrophobic HDL core making this reaction unidirectional. This causes a

transition from a relatively cholesterol-poor discoidal HDL to a cholesterol-rich spherical HDL. Importantly, this also allows for changes in affinities to different HDL receptors. There are multiple receptors/transporters that facilitate the transfer of cholesterol to HDL including the ATP-binding cassette transporters, ABCA1 and ABCG1, which bind and transport cholesterol to relatively cholesterol-poor HDLs and there is scavenger receptor-type B1 (SR-B1) which binds more favorably to cholesterol-rich spherical HDL. Upon HDL binding, SR-B1 mediates bidirectional cholesterol flux dependent upon the cholesterol density of the HDL and the cell. Cholesterol-rich HDLs deliver cholesterol through SR-B1; upon cholesterol delivery they shrink to a more discoidal HDL and release from SR-B1.

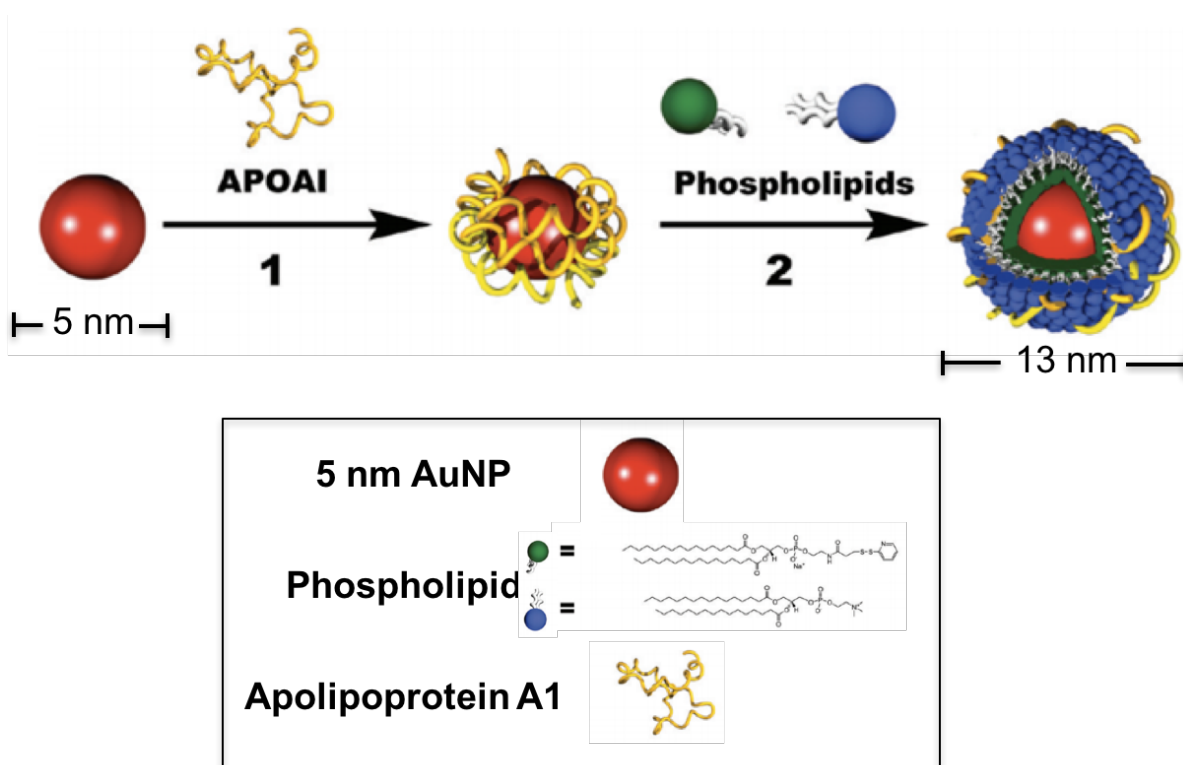


Figure 1.5: Synthesis Scheme of HDL NPs. Two-step synthesis of HDL NPs. Step 1: Apo AI is incubated with 5 nm AuNP at a 5 molar excess. Step 2: The phospholipids PDP-PE and DPPC are added and at a 250 molar excess relative to AuNP concentration.

The properties of HDL to specifically target SR-B1, ABCA1 and ABCG1 has motivated researchers to begin developing HDLs and HDL mimetics for targeted therapeutic applications.¹¹⁶⁻¹¹⁸ Because of the importance of HDL, not just as a mediator of cholesterol transport, there has been significant interest in synthesizing HDL mimetics.¹¹⁹⁻¹²¹ Over the past 10 years, our laboratory has pioneered the synthesis of HDL-like nanoparticles (HDL NPs) using a 5 nm citrate-stabilized gold nanoparticle (AuNP) core as a template. To synthesize HDL NPs, the 5 nm AuNP is incubated with apo A-I allowing for apo-AI to self-assemble around the gold core. The phospholipid PDP-PE containing a thiol head group binds tightly to the AuNP via a strong gold-thiol interaction. A second phospholipid, DPPC, interacts with AuNP bound PDP-PE through the lipophilic tails, to form a phospholipid bilayer (**Figure 1.5**, see methods Chapter 3 for a detailed instruction of HDL NP synthesis). Like natural HDL, HDL NPs are multifunctional and our laboratory has utilized them for numerous applications as a direct therapeutic and as a delivery vehicle. Initially, our laboratory applied HDL NPs to models of cardiovascular disease where like natural HDL, they would function to efflux cholesterol from atherosclerotic plaques for excretion through the liver.¹¹⁷ Additionally, we have discovered that HDL NPs induce cell death in lymphoma.¹²² In Chapter 3 of this thesis we discuss the development of HDL NPs as targeted agents to inhibit the uptake of exosomes by SR-B1-positive cells by modulating the cellular cholesterol flux of these cells. Additionally, in Chapter 4 we demonstrate that in models of melanoma HDL NPs inhibit MDSC-mediated T cell suppression causing immune clearance of tumor cells and significantly increased survival.

CHAPTER TWO

Pre-metastatic cancer exosomes induce immune surveillance by patrolling monocytes at the pre-metastatic niche

This Chapter is based on work published in:

M.P. Plebanek, N.L. Angeloni, E. Vinokour, J. Li, A. Henkin, D. Martinez-Marin, S. Filleur, R. Bhowmick, J. Henkin, S.D. Miller, I. Ifergan, Y. Lee, I. Osman, C.S. Thaxton, O.V. Volpert.
Nature Communications, 2017 Nov 6;8(1):1319.

2.1 Abstract

Metastatic cancers produce exosomes that condition pre-metastatic niches in remote microenvironments to favor metastasis. In contrast, in this chapter, we show that exosomes from poorly metastatic melanoma cells can potently inhibit metastasis to the lung. These “non-metastatic” exosomes stimulated an innate immune response through the expansion of Ly6C^{low} patrolling monocytes (PMo) in the bone marrow, which then via the recruitment of NK cells and TRAIL-dependent killing of melanoma cells by macrophages, caused cancer cells clearance at the pre-metastatic niche. These events required the induction of the Nr4a1 transcription factor and were dependent on pigment epithelium-derived factor (PEDF) carried on the exosomes outer surface. Importantly, exosomes isolated from patients with non-metastatic primary melanomas have similar ability to suppress lung metastasis. This is the first demonstration that pre-metastatic tumors produce exosomes, which elicit a broad range of PMo-reliant innate immune responses via trigger(s) of immune surveillance, causing cancer cell clearance at the pre-metastatic niche.

2.2 Introduction

Exosomes, as discussed in Chapter 1, are 30-150 nm extracellular vesicles released by virtually all cells,¹²³ are found in biological fluids and play pivotal roles in long-distance intercellular communications.^{53,124} Exosomes transfer oncogenic traits from aggressive to indolent cancer cells and, perhaps more importantly, to normal cells through the delivery of oncogenic proteins, mRNAs⁵⁴ and miRNA¹²⁵ that inhibit tumor-suppressive factors, accelerate tumorigenesis and enable tumor formation.¹²⁶ Intercellular communication via exosomes are particularly important for the formation of the pre-metastatic niche where exosomes alter the behavior of diverse cell types including the cells of immune system. Recently, it has been established that exosomes released from the primary tumor generate suitable microenvironments in secondary organs prior to the dissemination of metastases.^{61,127} Despite the clear importance of exosomes to cancer progression, mechanisms by which they promote the pre-metastatic niche are extremely complex and not fully understood.

Monocytes and macrophages are essential constituents of the metastatic microenvironments,^{128,129} where they play either tumor-promoting or tumor-suppressive roles, depending on their activation state (polarization).¹³⁰ Non-classical or patrolling Ly6C^{low} monocytes (PMos) (CD14^{dim} in humans) were initially identified for their ability to remove damaged cells/tissues and resolve the vascular inflammatory response.^{30,131} For their survival, PMos require the orphan nuclear receptor Nr4a1 (Nur77). Recently, Nr4a1-positive PMos have been shown to scavenge tumor cells and leading to reduced metastasis in the lungs.²⁶ However, the events that regulate the number of PMos at the metastatic niche remain unknown. Here, we show that exosomes released from non-metastatic melanoma cells (Exo^{NM}) are taken up by CD11b⁺ myeloid cells in the bone marrow (BM) and cause a Nr4a1-driven expansion of Ly6C^{low}

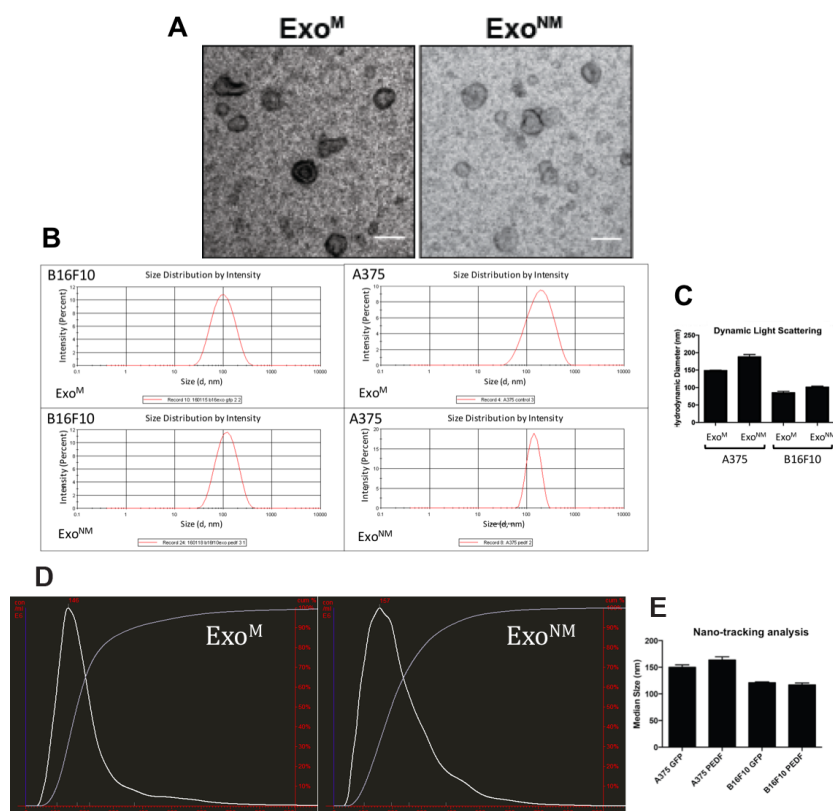


Figure 2.1: Characterization of Metastatic and Non-Metastatic Melanoma Exosomes. (A) Transmission electron microscopy (TEM) of B16F10 melanoma exosomes (Scale bar: 100 nm). (B) Dynamic light scattering analysis of exosomes from metastatic and non-metastatic A375 and B16F10 melanoma cells showing hydrodynamic diameter. (C) Quantification of average hydrodynamic diameter analyzed in B. (D) Nano-tracking analysis (Nanosight) showing size of exosomes from metastatic and non-metastatic A375 and B16F10 (E) Quantification of nano-tracking analysis (Nanosight) data acquired in D.

monocytes, which express elevated levels of integrin- β 2 (ITGB2), CX3CR1 (fractalkine receptor), and the Nr4a1 orphan nuclear receptor, which together define PMo.^{132,133}

Pigment epithelium-derived factor (PEDF) is known for its potent anti-angiogenic and anti-cancer effects.¹³⁴ In melanoma, the loss of PEDF promotes early invasive melanoma growth, amoeboid motility and metastasis.^{135,136} PEDF is also implicated in the control of inflammation and macrophage polarization;¹³⁷ however, the underlying molecular mechanisms are unknown. Here, we demonstrate that PEDF is present at high levels on the surface of exosomes from non-

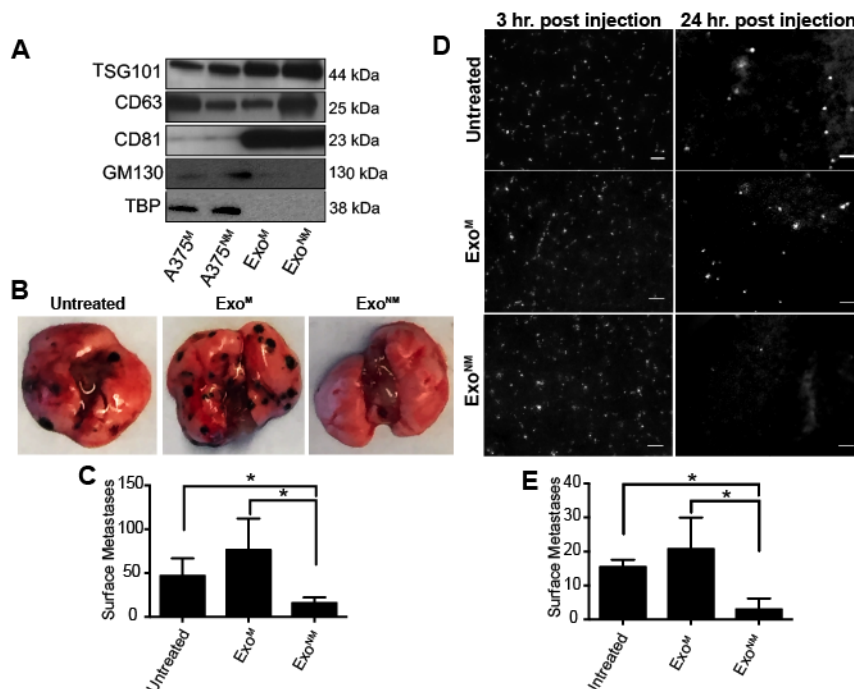


Figure 2.2: Exo^{NM} Inhibit Lung Colonization by Metastatic Melanoma. (A) Western blot of cell lysates and exosomes generated by A375^M and A375^{NM}, probed for TSG101, CD63 and CD81, to verify for enrichment in exosome preparation and GM130 and TBP to verify the lack of cellular proteins. (B) C57BL/6 mice conditioned with Exo^M or Exo^{NM} or untreated controls were inoculated i.v. with B16F10 melanoma cells. Gross images of tumor burden 2 weeks post inoculation are shown. (C) Quantification of lung colonies in B. * indicates $P < 0.05$ by two-tailed Student's *t*-test (n= 4.) (D) C57BL/6 mice conditioned with Exo^M, Exo^{NM} or untreated controls were inoculated with fluorophore-tagged B16F10 cells. Fluorescence images of lungs were taken 3 and 24 hours after inoculation to assess perfusion and extravasation, respectively. (E) Quantification of extravasated fluorescent B16F10 cells in D. (* indicates $P < 0.05$ by two-tailed *t*-test; n=5 mice per group, a minimum of 5 random images per lung were evaluated).

metastatic melanoma cells and its presence is critical for the activation of an innate immune response and the elimination of melanoma metastasis. The events triggered by exosomes involved Nr4a1 induction in bone marrow monocytes precursors, leading to PMo expansion, recruitment and differentiation of TRAIL-positive tumor-reactive macrophages, which kill and phagocytize the tumor cells. PMos, together with the recruitment of NK cells were responsible for the diminished metastasis as was demonstrated by immune cell depletion experiments. Our results suggest that pre-metastatic tumors generate triggers of innate immune response(s) such as

PEDF, which are delivered to the cells of the immune system by exosomes; the loss of these triggers enables immunosuppression and abrogates the immune clearance of cancer cells leading to metastasis.

2.3 Results

2.3.1 “Non-metastatic” Exosomes Prevent Lung Metastasis

Exosomes from metastatic melanoma cells are known to contribute to the formation of the pre-metastatic niche, which leads to metastatic colonization by circulating tumor cells.^{63,138} We sought to determine whether exosomes from non-aggressive, poorly metastatic melanomas (“non-metastatic” exosomes) could influence pre-metastatic niches by comparing exosomes from metastatic and non-metastatic variants of the mouse (B16F10) and human (A375) melanoma cell lines (Exo^M and Exo^{NM}, respectively). Metastatic and non-metastatic variants of mouse (B16) and human (A375) melanoma cell lines were generated previously, by expression of the type 2 tumor suppressor Pigment Epithelium Derived Factor¹³⁹ (see Methods). Exo^M and Exo^{NM} displayed similar size distribution, morphology and molecular composition, as was shown by transmission electron microscopy (TEM), dynamic light scattering (DLS), nano-tracking analysis (**Figure 2.1A-E**) and by Western blotting. Exo^M and Exo^{NM} contained similar amounts of exosomal markers CD63, CD81 and TSG101, while lacking markers typically not found in exosomes (golgi marker GM130 and the nuclear marker TATA binding protein, TBP) confirming the purity of isolates (**Figure 2.2A**). However, they had dramatically different effects on melanoma metastasis. C57BL/6 mice preconditioned with Exo^M from B16F10 cells and inoculated with syngeneic B16F10 pigmented melanoma cells presented with a significant increase in the metastatic burden over the baseline (no pre-treatment). In contrast, preconditioning with Exo^{NM} significantly reduced metastasis (**Figure 2.2B, C**). In agreement,

athymic nude mice preconditioned with intravenous Exo^M injections prior to the tail vein inoculation of fluorophore-tagged A375 melanoma cells presented with significant metastatic burden after 9 weeks and identical pre-treatment with Exo^{NM} decreased metastasis by ~10-fold (Figure 2.3A-C). This data demonstrated that “non-metastatic” exosomes have a capacity to inhibit lung metastasis.

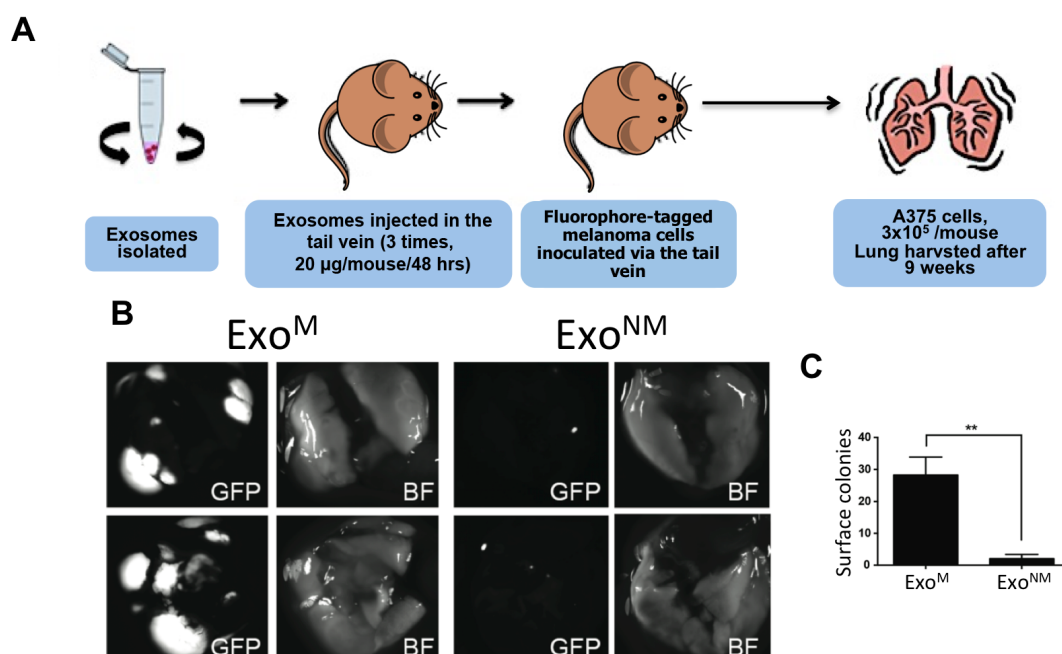


Figure 2.3: Schematic of Melanoma *In Vivo* Experiments in Nude Mice. (A) The diagram of the long-term experiments using human melanoma cells and exosomes (performed in nude mice). (B) Representative images of the lungs of mice pre-treated with exosomes and inoculated with fluorophore-tagged A375 cells. (C) Quantitative analysis of the experiment in B.

Lung colonization by metastasizing cancer cells is influenced by multiple factors, including early events (extravasation, innate immune responses) and late events (survival, proliferation, angiogenesis and adaptive immune responses).¹⁴⁰ Seeking the stage at which Exo^{NM} may interfere with metastatic dissemination, we assessed the extravasation of fluorophore (CFSE)-labeled B16F10 mouse melanoma cells in immune competent C57BL/6 mice. Two

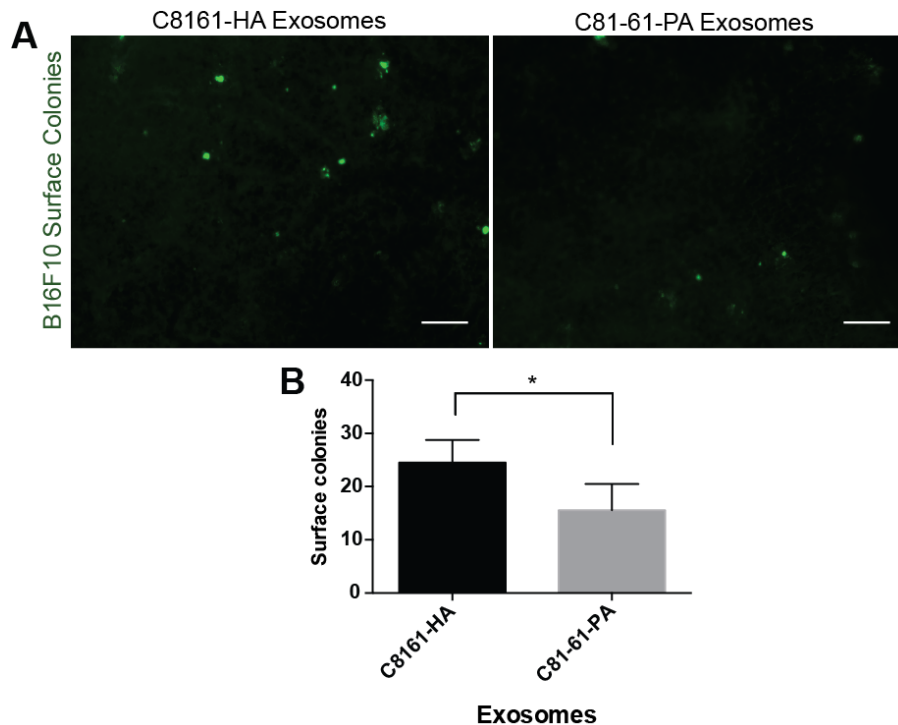


Figure 2.4: Inhibition of Lung Extravasation by Exosomes from Naturally Occurring Metastatic and Non-Metastatic Melanoma Cells. Exosomes were isolated from poorly aggressive C81-61-PA and highly aggressive C8161-HA human melanoma cells. Nude mice were injected with the indicated exosomes three times 2 days apart, followed by injection of C81-61-PA cells (10^6) via the tail vein. The lung colonies were assessed 24 hours post-injection. (A) Representative lung images. (B) Quantification of the surface colonies in the lungs of mice analyzed by fluorescence microscopy in A (n=4 animals per group, a minimum of 5 fields per animal). * indicates $P < 0.05$, assessed by two-tailed Student's *t*-test

hours after inoculation, B16F10 cells were found *en masse*, presumably in the lung vasculature regardless of pre-conditioning. After 24 h, extravasation was significantly increased in mice treated with Exo^M compared to control. In contrast, there were ~ 6-fold fewer metastatic colonies in the lungs of mice treated with Exo^{NM} than in Exo^M controls (Figure 2.2D, E). A similar effect was observed when highly aggressive human melanoma cells (C8161-HA) were injected in athymic nude mice following pre-treatment with exosomes from highly aggressive (C8161-HA) and poorly aggressive (C81-61-PA) human melanoma cell lines^{141,142} (Figure 2.4A, B). A comparable decrease of the metastatic burden in the short- and long-term models suggested that

Exo^{NM} act primarily at an early stage. Analogous responses in athymic nude mice and in immune competent mice suggested the involvement of innate, as opposed to adaptive immune response.

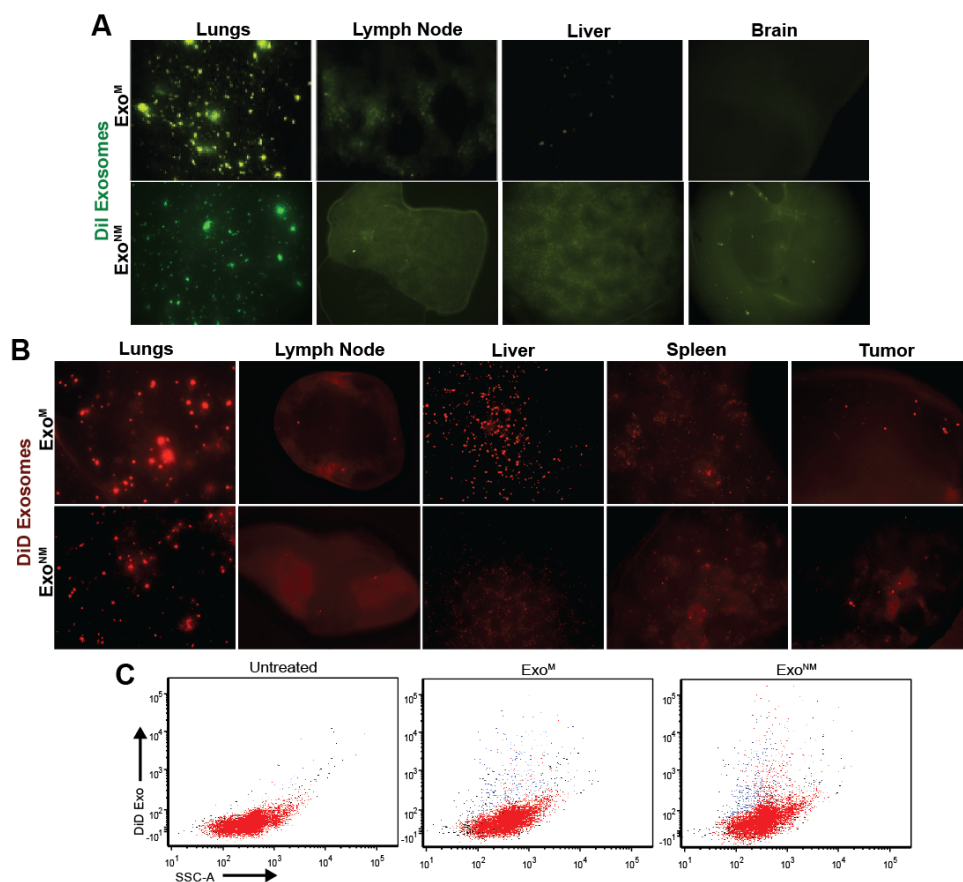


Figure 2.5: Biodistribution of Melanoma Exosomes. Mice received tail vein injections of 10 μg melanoma exosomes (Exo^M and Exo^{NM}, as indicated) labeled with the fluorescent lipophilic dye DiI (green) or DiD (red). The biodistribution of melanoma exosomes were analyzed in tumor-free mice (A) tumor-bearing mice (B) and in bone marrow isolates (C).

2.3.2 Exo^{NM} Leads to Increased Patrolling Monocytes in the Lungs

Previous studies show that exosomes home to specific metastatic niches, e.g. the lungs.^{143,144} We evaluated the biodistribution of Exo^{NM} and Exo^M labeled with fluorescent lipophilic dyes (DiI, DiD). As was observed in previous studies, exosomes homed to the lungs and select lymph nodes in tumor-free and in tumor-bearing mice; in mice bearing subcutaneous

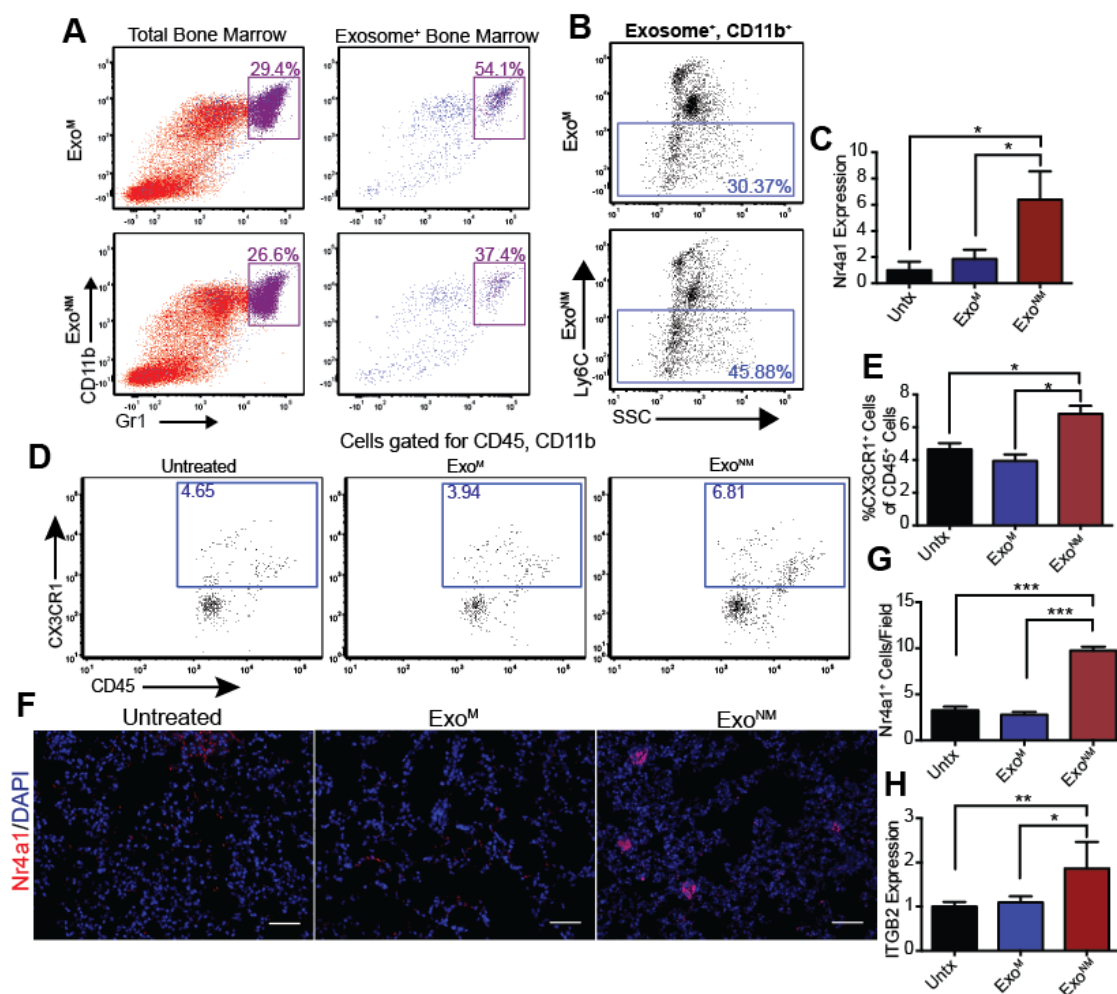


Figure 2.6: Exo^{NM} Increase PMOs in the Lungs. Tumor naïve C57BL/6 mice were treated with exosomes (Exo^M or Exo^{NM}), prior to bone marrow isolation and analysis. **(A)** Flow cytometry shows the uptake of fluorophore-tagged melanoma exosomes by the myeloid cells in the bone marrow. **Left:** Flow plots of the total CD11b⁺Gr1⁺ bone marrow populations. **Right:** Flow plots show a higher percentage of CD11b⁺Gr1⁺ cells among the bone marrow cells positive for exosome uptake. **(B)** Treatment with Exo^{NM} leads to an increase in Ly6C^{low}CD11b⁺ cells compared to Exo^M in the total BM myeloid population. **(C)** qRT-PCR measurement of mouse BM monocytes mRNA encoding Nr4a1 after treatment with the indicated exosomes (10 µg/ml, 24 hrs). **(D)** Mouse lungs stained for CD11b, CD45 and CX3CR1. FACS plots were gated for CD11b⁺CD45⁺ cells and CX3CR1⁺ cells were quantified. **(E)** Quantification of the data analysis is shown in **D**, expressed as percent CX3CR1⁺ of total CD45⁺ cells. **(F)** Immunofluorescence shows increased abundance of Nr4a1⁺ cells in the lungs of mice pre-conditioned with Exo^{NM}. **(G)** Quantification of the data analysis in **F**, expressed as number of Nr4a1⁺ cells per field. Scale bar: 50 µm (n=3 mice per group, quantification taken from 5 images per section) **(H)** qRT-PCR measurement of mouse BM monocytes mRNA encoding ITGB2 after treatment with the indicated exosomes (10 µg/ml, 24 hrs).

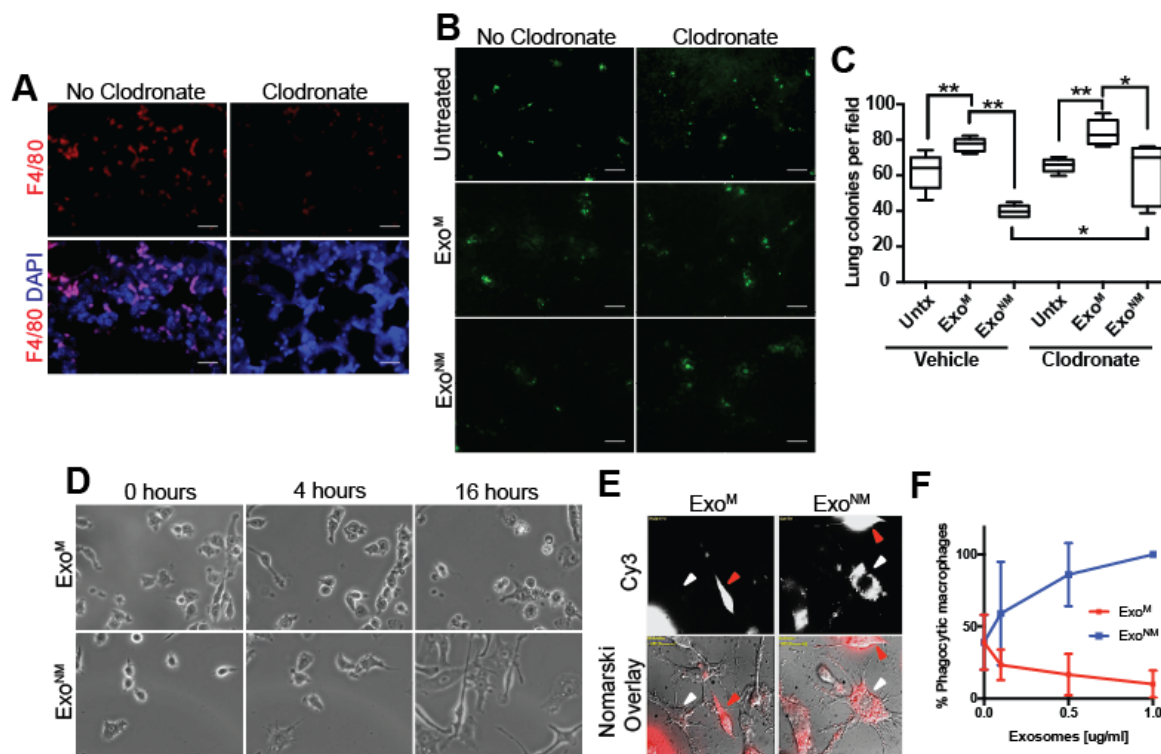


Figure 2.7: Exo^{NM} Act via the Cells of the Monocytic Lineage. (A-C) Mice were treated with control or clodronate liposomes to eliminate monocytes/macrophages, then pre-conditioned with exosomes (10µg) and used in the extravasation assay as described above. (A) Macrophage depletion was assessed by F4/80 immunofluorescence (n=3) (B, C) The inhibition of B16F10 extravasation by Exo^{NM} was reduced by monocyte depletion. Representative lung images (5x magnification) are shown in B, and quantitative analysis are shown in C. (n=5 untreated, n=6 Exo^{NM}, Exo^{NM}, 5 images per lungs) * indicates $P < 0.05$, and ** $P < 0.01$ by two-tailed t -test. Scale bar, 100 µm. (D) RAW 264.7 macrophages were treated with 10 µg/ml Exo^M or Exo^{NM} and their morphology was assessed by time-lapse microscopy. (E) Engulfment of fluorophore-tagged melanoma cells (red) by RAW264.7 macrophages after treatment with 1 µg/ml Exo^M or Exo^{NM} (Fluorescence and Nomarski image overlays). (F) Quantification of melanoma phagocytosis by RAW 264.7 macrophages after treatment with Exo^M or Exo^{NM} at indicated concentrations. ** and *** indicate $P < 0.01$ and $P < 0.001$, respectively, as calculated by Tukey's multiple comparison test with Bonferroni posttest.

B16F10 tumors, exosomes also homed to the liver (Figure 2.5A, B). Importantly, a large proportion of exosomes was found in the bone marrow (BM) (Figure 2.5C). We noted no significant differences between the distribution patterns of Exo^M and Exo^{NM}.

To identify target BM cell population(s), C57BL/6 mice were injected intravenously with DiD-labeled exosomes, and BM cells were isolated and stained for the myeloid markers CD11b and Gr1. FACS analysis showed enrichment in DiD labeled exosomes in the CD11b⁺Gr1⁺ cell population (**Figure 2.6A**). Exosome treatment resulted in a pronounced shift in the population distribution of the BM: in the total myeloid population, Exo^{NM} caused a significant increase of the Ly6C^{low} population, with a coordinate decrease in Ly6C^{high} cells (**Figure 2.6B**). Among Ly6C^{low} cells are non-classical PMos, which are critical for the resolution of inflammation and tissue damage³¹ and whose anti-metastatic function has been recently discovered.²⁶ PMos are known to rely on the orphan nuclear receptor Nr4a1 for survival.³¹ In agreement with flow cytometry data, Exo^{NM} but not Exo^M, caused about a 3-fold increase in Nr4a1 expression in cultured primary mouse bone marrow monocytes (**Figure 2.6C**) compared to the baseline levels.

Furthermore, PMos have been shown to express high levels of CX3CR1, which mediates their interactions with the vasculature^{30,133} and their anti-metastatic activity.²⁶ This led us to assess the CX3CR1 positive monocytes in the lungs of mice after pre-treatment with Exo^{NM} or Exo^M. Flow cytometry analysis revealed low numbers of CD45⁺CX3CR1⁺ cells in the lungs of mice treated with control vehicle or Exo^M. In contrast, we observed a significant increase in CX3CR1⁺CD45⁺ monocytes in the lungs of mice treated with Exo^{NM} (**Figure 2.6D, E**). The results were confirmed by immunofluorescence (IF) staining of the lung sections of mice treated with control vehicle, Ex^M or Ex^{NM} for PMo-specific marker Nr4a1 (**Figure 2.6F, G**). PMo are characterized by their ability to ‘crawl’ along the vasculature in a process which requires the LFA-1 antigen, a complex of CD11a and integrin β 2 (ITGB2). Confirming the shift towards PMo phenotype, ITGB2 was significantly upregulated in THP-1 monocytes treated with Exo^{NM} (**Figure 2.6H**).

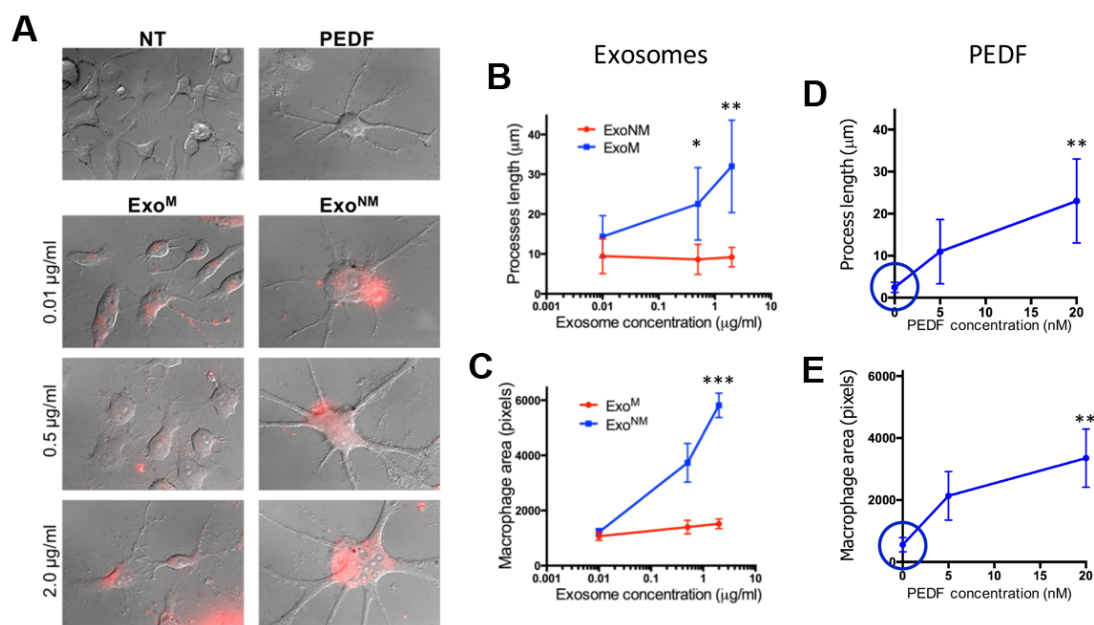


Figure 2.8: Exo^{NM} Cause the Differentiation of RAW 264.7 Macrophages. (A) RAW 264.7 macrophages were treated with 0.01, 0.5, and 2.0 µg/ml of DiI-labeled exosomes as indicated. The controls included PEDF (20 nM rPEDF) or no treatment (NT). After 24 hours the cells were analyzed by bright-field microscopy. The process length (B) and the macrophage surface area (C) were quantified to assess differentiation. (D, E) process length and surface area in RAW macrophages treated with rPEDF. Measurements were performed at 100x magnification, 20-30 randomly picked cells per data point. *, P<0.05; **, P<0.01; ***, P<0.002 by Tukey's multiple comparison test, Bopferroni post-test.

2.3.3 Monocytic Cells Are Necessary for anti-Metastatic Exo^{NM} Function

Because melanoma exosomes target cells of the monocytic lineage (Figure 2.6A, B),¹⁴⁵ we assessed the contribution of monocytes and/or macrophages to the anti-metastatic effect of Exo^{NM} by measuring tumor cell extravasation in the lungs of mice subjected to monocyte depletion using liposome-encapsulated clodronate.¹⁴⁶ The depletion was confirmed by staining of the lung tissue for the pan-macrophage marker (F4/80) (Figure 2.7A). After depletion, animals were pre-conditioned with exosomes (3 injections, 10 µg/animal) and inoculated, via the tail vein, with B16F10 melanoma cells. As observed previously, lung imaging 24 h post-inoculation showed increased lung colonization in response to Exo^M compared to the baseline and a

significant and reproducible decrease in lung colonization after pre-conditioning with Exo^{NM}. Of note, the decrease in microscopic colonies due to Exo^M was significantly relieved by the clodronate liposomes but not by control PBS liposomes (**Figure 2.7B, C**). In contrast, the increased colonization in response to Exo^M remained unaffected (**Figure 2.7B, C**). These results suggest a critical role for the cells of monocytic lineage in the anti-metastatic function of Exo^{NM}.

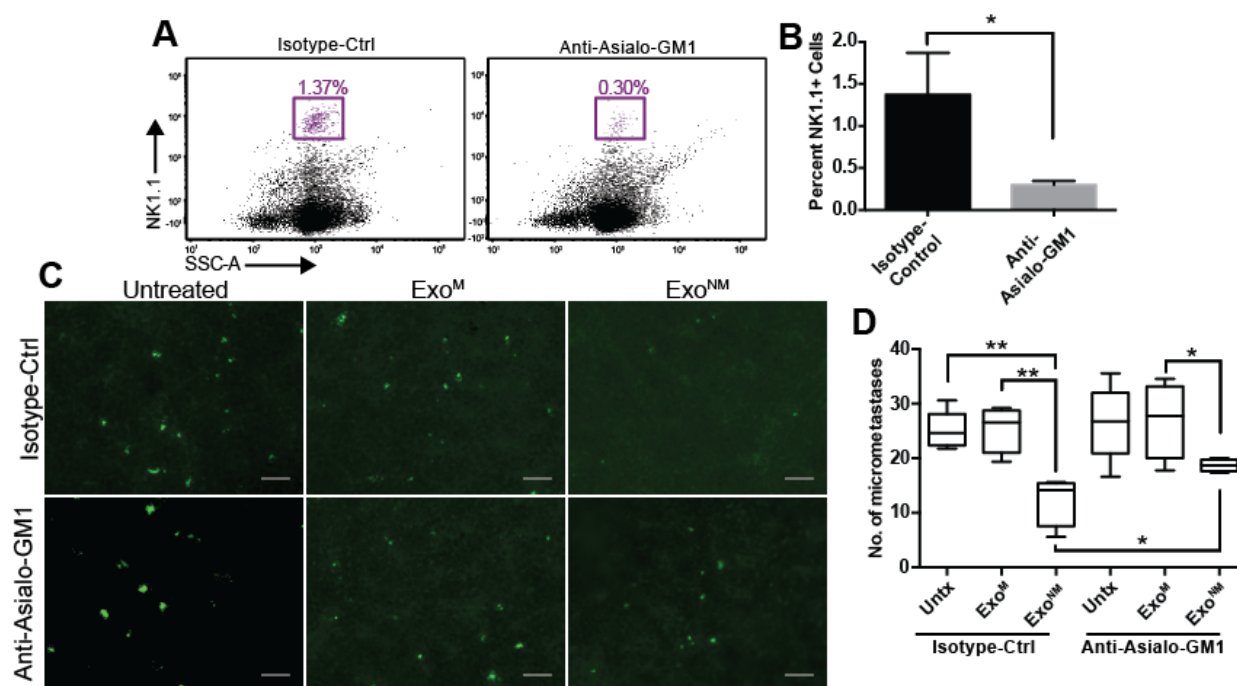


Figure 2.9: NK Cells Contribute to Exosome-driven Tumor Cell Clearance. (A, B) C57BL/6 mice were subjected to NK cell depletion with anti-asialo GM1 antibodies. (A) Flow cytometry plots showing percent NK cells in the spleens of mice 96 hours after treatment with isotype control or anti-asialo GM1 antibodies. (B) Quantification of the analysis shown in A. (n=3). (C, D) Following NK cell depletion, mice were treated with exosomes and used in an extravasation assay with CFSE-tagged B16F10 cells. (C) extravasation assessed 24 hr after melanoma cell inoculation. Scale bar: 100 μ m. (D) Quantification of experiment in C. Data are expressed as number of extravasated cells per high-powered field. (n=4, quantification, 5 images per lungs) * indicates $P < 0.05$ and ** indicates $P < 0.01$ calculated by Tukey's multiple comparison test (Bonferroni post-test).

2.3.4 Exo^{NM} Induce Macrophage Differentiation and Phagocytic Activity

Since PMos, in some cases, differentiate into phagocytic macrophages,²⁹ we tested whether Exo^{NM} are also capable of inducing macrophage differentiation and tumor cell

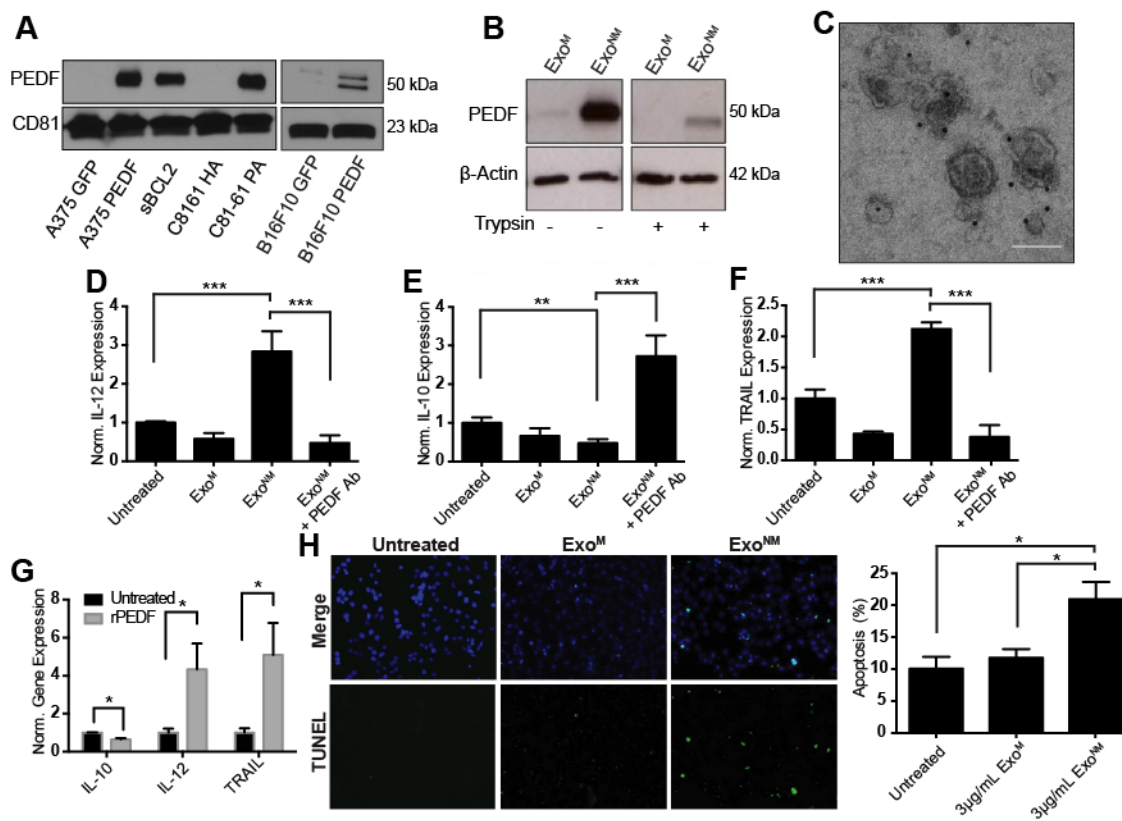


Figure 2.10: The Involvement of PEDF in Exosome-driven Melanoma Cell Clearance.

(A) Western blot shows PEDF enrichment in exosomes from non-metastatic melanoma cell lines (A375 PEDF, SBcl2, C81-61PA, B16F10 PEDF). (B) Limited trypsin digestion indicates that PEDF is tethered to the outer leaflet of exosomal membranes. (C) Immunogold staining – TEM of Exo^{NM} confirms PEDF localization to exosome surface. Scale bar: 100 nm. (D-F) RAW 264.7 macrophages were treated overnight with vehicle, Exo^M or Exo^{NM}. PEDF neutralizing antibodies were added to Exo^{NM} where indicated. IL-12, IL-10 and TRAIL mRNA were measured by qRT-PCR. (n=6). (G) RAW 264.7 macrophages were treated overnight with vehicle PBS or 20 nM recombinant PEDF (rPEDF). IL-12, IL-10 and TRAIL mRNA were measured by qRT-PCR. (n=6) (H) Co-cultures of A375 cells and RAW 264.7 macrophages treated with exosomes (3µg/ml) for 24 hrs and apoptosis measured by TUNEL. Representative images and quantitative analysis are shown. * indicates $P < 0.05$ ** indicates $P < 0.01$, and *** $P < 0.001$ as per two-tailed t -test

engulfment. Mouse macrophages (RAW 264.7) were treated with exosomes and their differentiation was assessed as the cumulative macrophage area and length of the processes. Indeed, Exo^{NM}, but not Exo^M, elicited pronounced macrophage differentiation, which was evident by cell spreading and the formation of multiple dendrite-like processes (Figure 2.7D and

Figure 2.8A-E). A recent study showed that PMos can control metastasis in part by engulfing cancer cells.²⁶ In agreement, the exposure of RAW 264.7 macrophages to Exo^{NM} but not Exo^M markedly increased their ability to engulf fluorescence-tagged melanoma cells (**Figure 2.7E, F**).

2.3.5 In Part, NK Cells Mediate Exo^{NM} Induced Immune Responses

NK cells play a critical role in preventing metastasis by recognizing tumor cell ligands resulting in the clearance of circulating tumor cells¹⁴⁷, and PMos have been previously shown to recruit NK cells to the sites of metastasis where they eliminate cancer cells by producing CCL3/4/5.²⁶ To test whether Exo^{NM} induce similar events, we depleted NK cells using an anti-Asialo-GM1 antibody prior to exosome treatment and tumor cell inoculation (**Figure 2.9A, B**). NK cell depletion significantly reduced the propensity of Exo^{NM} to inhibit lung colonization in the extravasation assay and similar to monocyte depletion experiments, the reversal of Exo^{NM} effects by NK cell depletion was incomplete, suggesting mechanisms in addition to NK recruitment are involved in metastasis prevention by Exo^{NM} (**Figure 2.9C, D**).

2.3.6 Exo^{NM} Contain Pigment Epithelium-Derived Factor (PEDF) on the Exosomes' Surface

In previous studies by our laboratory as well as other groups, it was established that pigment epithelium-derived factor (PEDF) renders melanoma cells non-metastatic.^{136,139} Importantly, PEDF is also expressed by most non-metastatic cell lines and its expression in patient samples inversely correlate with metastatic dissemination.^{135,139,148} To determine if PEDF also plays a role in the exosome-mediated inhibition of metastasis, we assessed the PEDF levels in exosomes harvested from melanoma lines with forced (A375-PEDF, B16F10-PEDF) or endogenous (sBCL2, C81-61-PA) PEDF expression¹³⁹ and from their metastatic counterparts (A375, B16F10, C8161-HA). Of note, all Exo^{NM} in our study displayed high PEDF content, while Exo^M contained little or no PEDF (**Figure 2.10A**). Since PEDF acts via cell surface

receptors, its localization within exosomes was critically important. To address the possibility of surface localization, we used limited trypsin digestion, which eliminated most of the exosomal PEDF but not β -actin, which is localized in the exosome lumen (**Figure 2.10B**), suggesting that PEDF is tethered to the outer leaflet of exosomal membrane. To corroborate this finding, immunogold labeling/ EM was used to directly visualize PEDF localization to exosomes (**Figure 2.10C**). To further confirm that PEDF localizes to exosomes, we isolated exosomes from PEDF expressing A375 melanoma cells using sucrose gradient ultracentrifugation. PEDF was present at densities from 1.08 g/ml to 1.17 g/ml, corresponding to the density of exosomes, and was present in the fractions containing the exosome marker CD81 (**Figure 2.11**).

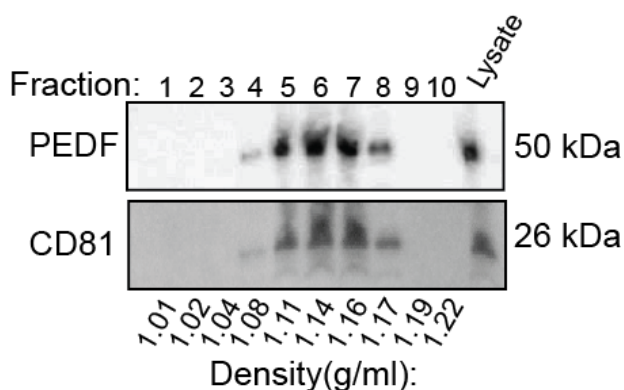


Figure 2.11: Density Gradient Ultracentrifugation Characterization of Exosomal PEDF. Exosomes were isolated by gradient centrifugation and PEDF assessed in the fractions. Note that exosome-positive (CD81) fractions contain PEDF, as shown by Western blotting.

2.3.7 Exosomal PEDF Promotes Macrophage Activation and Drive Apoptosis of Neighboring Melanoma Cells

Tumor-associated macrophages receive cues from the microenvironment, which determine their tumor-promoting or tumor-suppressive state (polarization).¹²⁸ Tumor-promoting macrophages express higher IL-10 levels, while tumor-reactive macrophages produce predominantly IL-12. We have discovered that Exo^{NM} dramatically increased IL-12 mRNA

levels in cultured macrophages; in contrast IL-12 mRNA was decreased by Exo^M (**Figure 2.10D**). In agreement, Exo^{NM} reduced IL-10 mRNA production by macrophages (**Figure 2.10E**). Importantly, a PEDF neutralizing antibody reversed the effects of Exo^{NM}, while there was no change observed in Exo^M function (**Figure 2.10D, E**). Similar to Exo^{NM}, recombinant human PEDF was also sufficient to promote macrophage differentiation observed previously (**Figure 2.8A-E**).

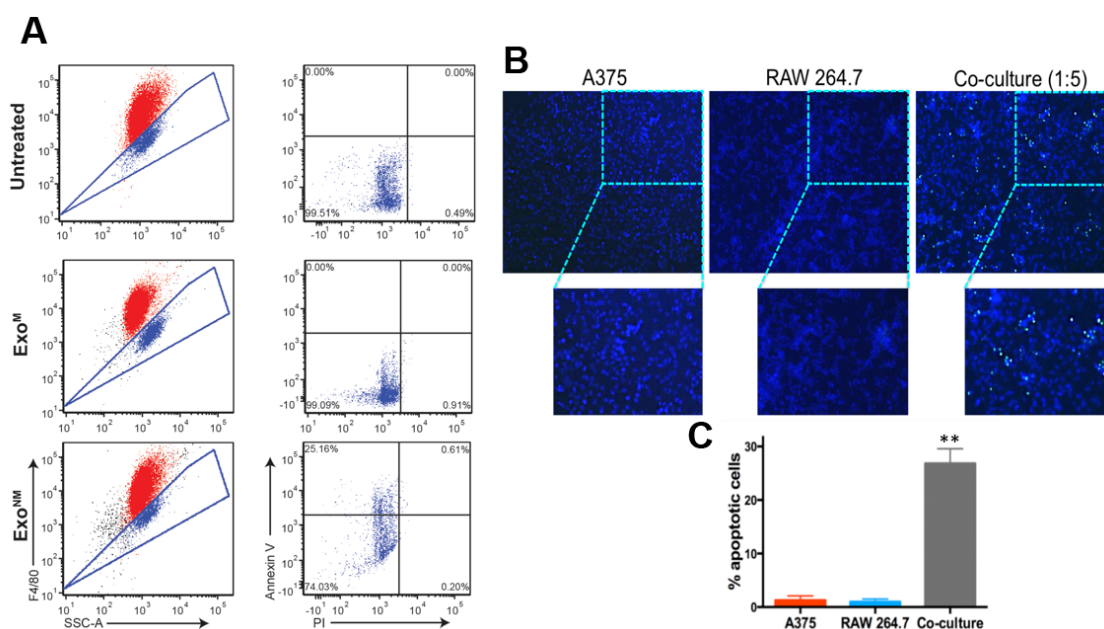


Figure 2.12: In Co-cultures with Macrophages, Exo^{NM}-dependent Apoptosis is Limited to Melanoma Cells. RAW 264.7 macrophages were grown in co-culture with A375 melanoma cells at a 5:1 ratio and treated with either Exo^M or Exo^{NM} (3 μ g/ml for 24 hours). (A) Cells were stained for F4/80 to detect macrophages and apoptotic cells were detected with annexin V using flow cytometry (B, C) or by in situ TUNEL for evaluation by fluorescence microscopy coupled with Nikon Elements software

PEDF is also known to upregulate tumor necrosis factor-related apoptosis inducing ligand (TRAIL).¹³⁷ In agreement, macrophage exposure to Exo^{NM} but not to Exo^M caused a significant increase of TRAIL mRNA expression, which was abolished by PEDF neutralizing antibody and therefore PEDF-dependent (**Figure 2.10F**). In agreement, purified recombinant

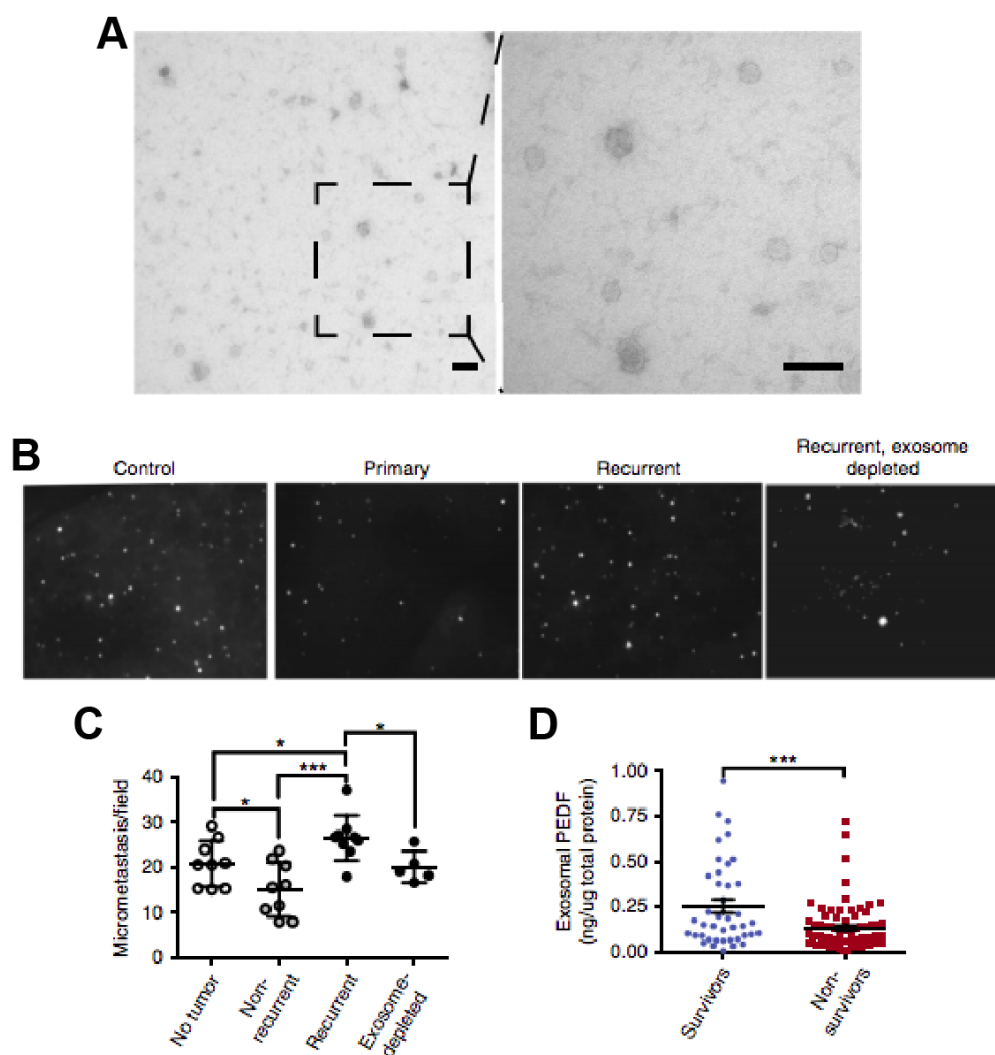


Figure 2.13: Exosomes from Sera of Patients with Non-Recurrent Melanoma Suppress Lung Metastasis (A) Representative TEM of exosomes isolated from the sera of melanoma patients. Scale bar: 100 nm (B) Exosomes from the sera of healthy control donors and of patients with primary and recurrent melanoma were injected into athymic nude mice. Exosome-depleted serum from recurrent patients was used as a control. Nude mice were injected i.v. three times, with 10 μ g exosomes, 48 hours apart followed by injection of CFSE-labeled A375 melanoma cells. The extravasated melanoma cells were counted in the lungs 24 hours later. (C) Analysis of the data presented in B. * indicates $P < 0.05$, ** indicates $P < 0.01$, and *** indicates $P < 0.001$ calculated by Tukey's multiple comparison test; (n=9 for tumor-free, non-recurrent and recurrent groups and n=5 for the group treated with exosome-depleted serum n=5 mice for recurrent exosome deplete group; five random images per animal were analyzed). (D) Patients were separated into cohorts according to survival (death from melanoma over > 5-year follow-up). Exosomal PEDF was measured by ELISA and normalized to total protein content. Statistical significance was determined by two-tailed t-test. *, $P < 0.0003$.

human PEDF caused changes similar to those elicited by Exo^{NM} in IL-10, IL-12 and TRAIL expression in RAW 264.7 macrophages. Overnight treatment with 20 nM rPEDF led to increases in TRAIL and IL-12 expression and a decrease in IL-10 expression as was evidenced by the mRNA expression levels (**Figure 2.10G**). Moreover, in co-cultures of RAW 264.7 macrophages with A375 melanoma cells, Exo^{NM} potently induced apoptosis of the melanoma cells, but not of the macrophages as was ascertained by TUNEL and Annexin V staining (**Figure 2.10H** and **Figure 2.12A**). In agreement, Exo^{NM} induced apoptosis only in co-cultures of A375 and RAW 264.7 macrophages but not in respective monocultures (**Figure 2.12B, C**). Together, our results indicate that exosomal PEDF can promote PMo differentiation to macrophages, as well as macrophage M1 polarization associated with killing and subsequent phagocytosis of melanoma cells.

2.3.8 Exosomes from the Sera of Patients with non-Metastatic Melanoma Contain Significantly more PEDF

The experiments above demonstrate that exosomes from non-metastatic melanoma cell lines block metastasis by activating PMos. However, it was unclear whether exosomes from patients have similar propensities. To determine if exosomes produced by non-metastatic primary melanoma curtail metastatic spread, we used archival serum samples collected at the time of surgery from patients with primary melanoma. The patients were subsequently stratified on the basis of recurrence after 5-year follow-ups (recurrent/metastatic and non-recurrent/non-metastatic). Exosomes were isolated from sera by precipitation followed by affinity spin columns to ensure purity and the preparation quality was assessed by TEM (**Figure 2.13A**) followed by western blotting for exosomal markers (**Figure 2.14**).

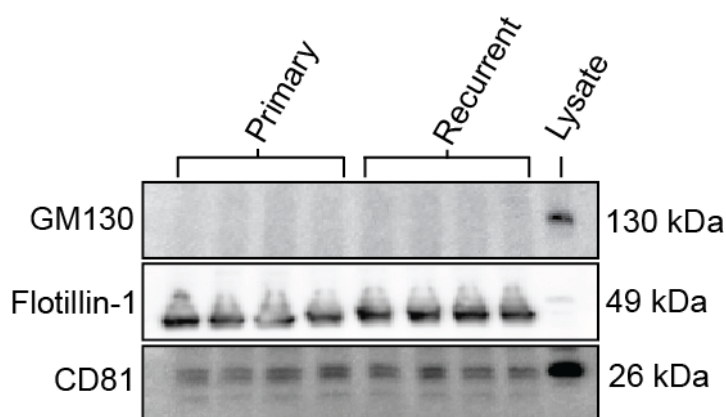


Figure 2.14: Characterization of Melanoma Sera Sample Exosomes. Exosomes were isolated from the sera of melanoma patients with recurrent metastatic disease and disease that did not spread from the primary site and analyzed for exosome markers CD81 and Flotillin-1. In contrast, exosome patient samples did not contain the golgi marker GM130, which was present in the lysate of A375 melanoma cells.

To test the effect of the patients' exosomes on lung metastasis, nude mice were pre-treated with human exosomes as described above and subsequently received tail vein injections of CFSE-labeled A375 melanoma cells. Of note, serum exosomes from recurrent patients caused a significant increase in the number of lung colonies compared to the "neutral" exosomes from healthy volunteers or exosome-depleted patient serum (**Figure 2.13B, C** and **Table 2.1**). More importantly, exosomes from the patients with non-recurring tumors caused a statistically significant decrease in lung colonization compared to control exosomes, suggesting that our findings using Exo^{NM} from cultured melanoma cell lines reflect the properties of exosomes generated by human melanoma. Of note, we have compared exosomal PEDF contents between the recurrent and non-recurrent cohorts of melanoma patients (n=141 and 42, respectively) with recurrence established in a 5-year follow-up. Although significant variability in PEDF contents was observed, exosomes from recurrent patients presented with lower PEDF contents and the difference was statistically significant (**Figure 2.13D**). These results indicate that exosomes from

the sera of non-metastatic melanoma patients can suppress metastatic colonization and the effect is associated to higher PEDF content in serum exosomes.

Patient Type	ID	Age at Diagnosis	Gender	Histological Type	Thickness (mm)	Ulceration	mitotic index	Disease Stage	Tumor stage	PEDF ng/ μ g exosomal protein
Primary	07-004	68.9	F	SUPERFICIAL SPREADING MELANOMA	0.45	ABSENT	NONE	Stage I	T1A	0.053323
Primary	07-079	56.1	M	NODULAR MELANOMA	5.5	PRESENT	MANY	Stage II	T4B	0.096080
Primary	07-243	28.4	F	SUPERFICIAL SPREADING MELANOMA	0.35	ABSENT	NONE	Stage I	T1A	0.012370
Recurrent	06-042	44.3	F	NODULAR MELANOMA	2.8	ABSENT	MANY	Stage III	T3A	0.053022
Recurrent	07-127	69.5	F	SUPERFICIAL SPREADING MELANOMA	1.75	ABSENT	MODERATE	Stage IV	T2A	0.239748
Recurrent	07-250	59.6	M	SUPERFICIAL SPREADING MELANOMA	1.1	ABSENT	NONE	Stage IV	T2A	0.189861
Tumor-free	C10106	N/A	M	N/A	N/A	N/A	N/A	N/A	N/A	0.005209
Tumor-free	C11065	N/A	F	N/A	N/A	N/A	N/A	N/A	N/A	0.013202
Tumor-free	C10125	N/A	F	N/A	N/A	N/A	N/A	N/A	N/A	0.034803

Table 2.1. Melanoma Sera Sample Exosome Additional Information.

2.4 Discussion

Over the past few years, there has been an explosion of research focused on exosomes, which led to the discovery that exosomes released from tumor cells interact with a wide array of cell types in distant organ environments allowing for the formation of tumor-promoting pre-metastatic niches.^{61,127} Given the importance of exosomes to the interaction between cancer cells and the cells of the microenvironment, we reasoned that exosomes from melanoma cells with varying propensities to metastasize would have contrasting effects on pre-metastatic niche formation. Indeed, while previous data established that exosomes from highly aggressive melanoma cells promote metastasis, in this study, we provide data that demonstrates the anti-metastatic functions of exosomes released from non-metastatic melanoma cells. Moreover, these findings likely reproduce the processes that take place in patients with non-recurrent melanoma

and possibly other cancers, because exosomes from archival serum samples taken at the time of surgery from melanoma patients whose tumor did not recur, retained the ability to suppress lung colonization in mouse model.

In a recent study, Hanna *et al* discovered the key role of non-classical patrolling monocytes (PMos) in the clearance of cancer cells at the site of metastasis, whereby they recruit cytotoxic NK cells leading to eradication of metastasizing cancer cells.²⁶ We have independently discovered that the clearance of metastasizing cancer cells driven by the “non-metastatic” exosomes stemmed from the expansion of the Ly6C^{low} PMo population. We have traced these exosomes to the CD11b⁺Gr-1⁺ cells in the bone marrow of recipient animals and demonstrated that they induced the Nr4a1 nuclear receptor in bone marrow monocytes causing PMo population expansion and their increased presence at the pre-metastatic niche. In agreement with findings by Hanna *et al*, cytotoxic NK cells were in part responsible clearance of metastasis after recruitment by PMos. In addition, we observed that non-metastatic exosomes also promote the differentiation and polarization of macrophages, which then engage in tumor cell killing and phagocytosis (**Figure 2.15**).

In earlier studies, others and we have demonstrated that in melanoma, the switch to a highly aggressive and invasive metastatic state is associated with the loss of PEDF, a type 2 tumor suppressor.^{135,136,139,149,150} Importantly, we were able to link the anti-metastatic, pro-immune properties of melanoma exosomes with PEDF, whereby tumor cells that lost PEDF expression no longer produced exosomes that maintain cancer surveillance by the innate immune system. This is the first study, which implicates cancer-derived exosomes in the induction of cancer immune surveillance and clearance.

Importantly, our results support the opposing roles of classical and non-classical

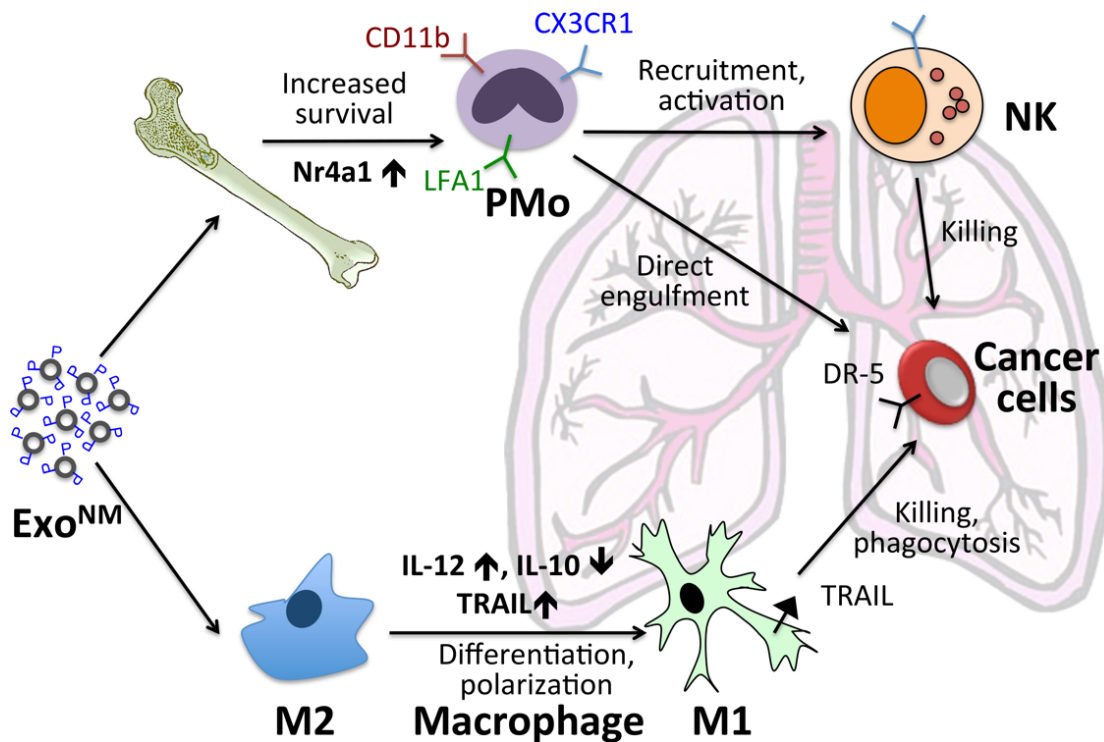


Figure 2.15: Schematic Representation of Immune Surveillance Events Triggered by Non-Metastatic Exosomes. Non-metastatic exosomes (Exo^{NM}) home to the bone marrow and to the lung. In the bone marrow, they target CD11b positive myeloid cells and increase the expression of the Nr4a1 receptor, thus increasing survival and overall numbers of patrolling monocytes (PMos), which eradicate cancer cells through recruitment of the natural killer (NK) cells and by direct engulfment of the cancer cells. In the lung, Exo^{NM} home to macrophages and cause macrophage differentiation, manifested by decreased expression of M2 marker, IL-10, and increased production of M1 marker, IL-12. In addition, macrophages undergo profound morphological changes, with multiple dendrite-like processes, and increased expression of death ligand TRAIL, leading to the melanoma cell killing and phagocytosis. These events are dependent on PEDF, which is displayed on the exosomes outer surface.

(patrolling) monocytes in cancer. On one hand, classical (inflammatory) CCR2⁺CX3CR⁻Ly6C^{high} monocytes (IMo) play a key role in the development of metastasis whereby they differentiate into inflammatory macrophages, which populate the pre-metastatic niche and support extravasation, survival and proliferation of metastatic cancer cells.¹⁵¹ Conversely, CCR2⁻CX3CR⁺Ly6C^{low} PMOs are enriched in the microvasculature of tumor-challenged lung and

reduce tumor metastasis.²⁶ In contrast to classical monocytes (IMo), PMos scour microvessels for the cell debris and particles.³⁰ In the presence of tumor cells, their patrolling behavior is disrupted and replaced by accumulation at the tumor site. Hanna *et al* show that PMo recruitment to the tumor site is mediated by CX3CR1, which interacts with endothelial-derived CX3Cl1. However, the same study underscores the low abundance of PMos in the lung. Our study provides a new mechanism underlying the increased PMo presence at the sites of metastasis, which is particular for pre-metastatic tumors. We discovered that early-stage, pre-metastatic melanoma express trigger(s) of immune clearance, which are loaded onto exosome surface and delivered, to the monocyte progenitors in the bone marrow of the host causing the expansion of CX3CR⁺, Ly6C^{low} monocyte population.

In conclusion, our study provides a completely new mechanism responsible for the increased presence of patrolling monocytes at the pre-metastatic niche and continuous elimination of circulating tumor cells in the tumor-bearing host. We for the first time demonstrate that prior to the acquisition of the metastatic capacity, tumors continuously alert host immune system by producing exosomes, which carry trigger(s) of innate immune responses and we identify one such trigger, PEDF. Furthermore, analysis of exosomes isolated from archival serum samples corroborates these findings. Taken together, our result point towards a potential new type of cancer immunotherapy based on the use of vesicular structures for delivery of such immune triggers.

2.5 Materials and Methods

2.5.1 Cell Culture

A375 melanoma cells (ATCC) were cultured in Dulbecco's Modified Eagle Medium (DMEM) containing 10% fetal bovine serum and 1% penicillin/ streptomycin. B16F10 cells

(ATCC) were cultured in DMEM containing 5% fetal bovine serum (FBS) and 1% penicillin/streptomycin. sBC12 and C8161 cells were donated by Dr. Mary J. C. Hendrix (Stanley Manne Children's Research Institute) and cultured in 50/50 DMEM/F12 containing 5% FBS, 1% penicillin/streptomycin and RPMI in 10% FBS, 15 penicillin/ streptomycin, respectively. PEDF was overexpressed in A375 and B16F10 melanoma cells as was described previously.¹³⁵ For overexpression, lentiviruses were produced by transfection into HEK 293T cells using the Lenti-XHT packaging system. Culture supernatants were collected, concentrated, titered and used for cellular transduction. Cells stably expressing the construct were selected for using puromycin, then identified and sorted for GFP expression. All cell cultures were maintained in 5% CO₂ at 37°C.

2.5.2 Experimental Animals

Mice were housed and maintained at the Northwestern University Center for Comparative Medicine according to the NIH guidelines and following protocols approved by the Northwestern University Animal Care and Use Committee. Athymic *nu/nu* mice were purchased from Harlan Laboratories and C57BL/6 mice were purchased from Jackson Laboratories.

2.5.3 Isolation of Bone Marrow Macrophages

Mouse bone marrow (BM) derived macrophages were isolated and matured as described previously.¹⁵² To isolate cells, C57BL/6 mice were sacrificed and the hind limbs were removed using aseptic technique, leaving the femur and tibia intact. The excess muscle was removed from the bones with a razor blade. The bones were then cut at the joints and the bone marrow flushed with sterile DPBS (calcium and magnesium free) using 1 ml syringe with a 27-gauge needle. The cells were then strained using a 70-micron cell strainer to remove any large pieces of tissue or bone and to form single cell suspensions. Bone marrow cells were centrifuged at 500 x g,

resuspended in 50/50 DMEM/F12 media supplemented with 10% FBS, 1% penicillin streptomycin and 20 ng/ml of M-CSF (Biolegend) and plated at 4×10^5 cells per 10 cm tissue culture dish. BM cells were incubated at 37°C, 5% CO₂ for 3 days at which point they were supplemented with additional 5 ml of cell culture media containing 20 ng/ml of M-CSF. Cells were allowed to grow for an additional 4 days whereupon they were harvested and used for further studies.

2.5.4 Exosome Collection and Characterization

Melanoma exosomes were isolated from conditioned media (CM) by differential ultracentrifugation.¹⁵³ Cells were cultured in DMEM containing 10% exosome depleted FBS (Life Technologies) and 1% penicillin streptomycin for 72 hours, the CM was collected and centrifuged at 2,000 x g to remove dead cells and debris. Next, larger vesicles and finer debris were removed by centrifugation at 10,000 x g for 30 minutes. Exosomes were then centrifuged at 100,000 x g for 70 minutes on top of a 30% sucrose cushion, and washed in PBS by another centrifugation step (100,000 x g, 70 minutes). Exosomes were re-suspended and stored in PBS. Protein content of exosomes was measured by BCA Protein assay (Thermo Scientific) and treatment doses were calculated based upon exosome protein concentration. Exosome size, morphology and number were characterized using dynamic light scattering (Malvern Zetasizer), nanoparticle tracking analysis (Nanosight) and transmission electron microscopy (FEI Spirit G2 TEM). For exosome tracking experiments, the lipophilic dye, DiI or DiD (Life Technologies), was added to exosome preparations at a concentration of 2.5 μM after the first 100,000 x g ultracentrifugation step. The labeled exosomes were then washed twice in PBS by pelleting the exosomes and discarding the supernatant.

For further purification using continuous sucrose gradient ultracentrifugation, the exosome pellet isolated after the final 100,000 x g spin outlined above was resuspended in 1 ml of 2.5 M sucrose, 20mM HEPES (pH 7.4) and loaded on the bottom of a sucrose gradient over the concentrations of 2.5 M to .25 M sucrose. Exosomes were spun for 24 hours at 100,000 x g after which 10 fractions were collected from the top, diluted in 16 ml PBS, and spun for 1 hour at 100,000 x g for one hour. The pellets were collected in 50 μ l PBS and analyzed by Western blotting.

Protein	Clone	Use	Dilution	Company
Beta-Actin	13E5	WB	1:5000	Cell Signaling Tech.
CD11b	M1/70	FC	1:100	BD Pharmingen
CD45	30-f11	FC	1:100	Biologend
CD63	TS63	WB	1:1000	Abcam
CD81	B-11	WB	1:500	Santa Cruz Biotech.
CX3CR1	Polyclonal	IHC, FC	1:100, 1:200	Novus, Biologend
F4/80	BM8	IHC	1:400	eBiosciences
Gr1	Rb6-865	FC	1:200	BD Pharmingen
NK1.1	PK136	FC	1:100	Biologend
Nurr77	EPR3209	WB	1:1000	Abcam
PEDF	Polyclonal	WB, Blocking	1:2000, 1:500	Bioproducts MD
TSG101	4A10	WB	1:2000	Abcam
Ly6C	HK1.4	FC	1:200	Biologend
Anti-Rabbit IgG	Polyclonal	WB secondary-HRP	1:5000	Jackson Immuno
Anti-Mouse IgG	Polyclonal	WB secondary-HRP	1:5000	Jackson Immuno
Anti-Rat IgG	Polyclonal	IHC secondary-Cy5	1:100	Jackson Immuno
Anti-Rabbit IgG	Polyclonal	IHC secondary-488	1:100	Jackson Immuno

Table 2.2. List of Antibodies used in Chapter 2.

2.5.5 Exosome Isolation from Serum

Due to the low volumes of sera available from patients, we isolated sera exosomes using a combination of commercial methods in order to enhance purity. Serum was first filtered using .45 μ m syringe filters and exosomes were precipitated using Exoquick (System Biosciences) (according to manufacturer's protocol). Membrane affinity spin columns (exoEasy Maxi, Qiagen) were then used to purify the exosomes further.

For PEDF analysis, exosomes were purified using CD63/CD81 conjugated Dynabeads (Invitrogen) to ensure that exosomes were free of sera components after Exoquick precipitation. The protein content was measured using BCA assay and normalized to 100 µg/ml. Exosomes were then characterized using TEM and western blotting as outlined previously.

2.5.6 SDS-PAGE and Western Blotting

For Western blots, 20 µg of total protein extract for cell lysates or 10 µg exosomal protein were resuspended in 4x Laemmli sample buffer (Biorad) and incubated at 95°C for 5 minutes. The protein samples were then resolved on Tris/Glycine/SDS pre-cast polyacrylamide gels (a 4-20% gradient, Bio-Rad, 30 minutes at 200 volts). Proteins were transferred onto polyvinylidene fluoride (PVDF) membranes (wet transfer, 2 hours, 40 volts). The membranes were blocked in 5% milk in Tris-buffered saline containing 0.1% Tween 20 (TBST) for 1 hour. The membranes were incubated with the primary antibodies (**Table 2.2**) in blocking buffer overnight at 4°C, washed 3 x 10 min in 0.1% TBST and incubated with the appropriate HRP-conjugated secondary antibody in blocking buffer for 1 hour at room temperature. The membranes were then washed in 0.1% TBST (3 x 10 min) and developed with Amersham ECL Western Blotting Detection Reagents (GE Healthcare).

2.5.7 RT-PCR

RAW 264.7, THP-1 or BM derived macrophages were treated with Exo^M or Exo^{NM} for 48 hours. mRNA was isolated using an RNeasy kit (Qiagen), and 1 µg of RNA was converted to cDNA using iScript cDNA synthesis kit (Bio-Rad). Quantitative RT-PCR was then used to amplify and measure the cDNA content using PerfeCTa SYBR Green mastermix (Quanta) on a CFX Connect RT-PCR Detection System (Bio-Rad). (For primers see **Table 2.3**).

2.5.8 Flow Cytometry

For analysis of the BM cell populations, C57BL/6 mice were treated with Exo^{NM} and Exo^M, hind limbs collected and BM cells flushed from tibias and fibulae as described above. Lymphocytes were then separated by centrifugation at 500 x g after layering on a Histopaque 1.077 g/ml density gradient. The cells at the interphase were collected and residual red blood cells lysed in ACK lysis buffer for 10 minutes at 4°C. Lymphocytes were counted and resuspended in FACS buffer (DPBS containing 1% BSA, 0.1% sodium azide) at 10⁷ cells/ml.

For analysis of lung monocytes/macrophages lungs were lavaged with DPBS, excised, and smashed in DPBS through a 70-µm-cell strainer. Red blood cells were lysed in ACK lysis and the cells washed in FACS buffer, counted and resuspended in FACS buffer (10⁷ cells/ml).

For immunostaining, 100 µl of the resuspended cells were blocked in Fc Block (BD Pharmingen) for 20 minutes at room temperature. The cells were incubated with fluorophore-conjugated antibodies (**Table 2.2**) for 1 hour at 4°C and washed in FACS buffer. Fluorescence was assessed on a BD LSR Fortessa Analyzer (Robert H. Lurie Comprehensive Cancer Center Flow Cytometry Core) and data were analyzed using FCS Express (De Novo Software).

2.5.9 Immunohistochemistry

C57BL/6 mice were sacrificed and the lungs perfused with 10% formalin, excised and allowed to fix in formalin for 24 hours. The lungs were paraffin embedded and sectioned at the Robert H. Lurie Comprehensive Cancer Center Pathology Core. Five-µm sections were deparaffinized in two changes of xylene, 10 minutes each. Sections were hydrated by sequential incubations in ethanol, 100% (2 times), 95%, 70% and 50%, 5 minutes each. Samples were then washed in deionized water and incubated with 200 µg/ml proteinase K (Abcam). For staining, sections were washed in PBS containing 0.1% tween 20 and blocked in PBS with 1% BSA, 1%

donkey serum, and 0.3% triton-x 100 and 0.01% sodium azide for 1 hour at room temperature. Primary antibodies (**Table 2.2**) were diluted in blocking buffer and incubated overnight at 4°C. Samples were washed 3 x 10 minutes in 0.1% tween 20 in PBS and incubated for 1 hour with fluorophore-conjugated secondary antibodies in blocking buffer. Slides were then washed three times in PBS with 0.1% tween 20, counterstained with DAPI and mounted in Fluoromount-G (Southern Biotech).

Gene	Primer
Actb	Fwd: 5'-aagtcagtgtagcaggaagcc-3'
	Rev: 5'-gtccccaacttgagatgtatg-3'
CX3CR1	Fwd: 5'-gaacacagtcccaagacca-3'
	Rev: 5'-tgtcctcggaacaccaca-3'
IL10	Fwd: 5'-ctccaagaccaaggtgtctac-3'
	Rev: 5'-ggagtccagcagactcaatac-3'
IL12	Fwd: 5'-gggagaagcagacccttaca-3'
	Rev: 5'-ttcaggcggagctcagatag-3'
ITGB2	Fwd: 5'-tactccattgctgcagaag-3'
	Rev: 5'-gggagctgtctgaggact-3'
Nr4a1	Fwd: 5'-cttcaggctgtctgttcgg-3'
	Rev: 5'-cgccaagtacatctgcct-3'
Tnfsf10	Fwd: 5'-cagccctaaagtaccagtaac-3'
	Rev: 5'-cacatctgtcctgaggtttctac-3'

Table 2.3. List of Primers used in Chapter 2

2.5.10 Transmission Electron Microscopy and Immunogold Labeling

Exosomes isolated as described above were stained with uranyl acetate.¹⁵³ Exosomes resuspended in 2% paraformaldehyde were allowed to adsorb onto formvar carbon-coated electron microscopy (EM) grids (Electron Microscopy Sciences) for 20 minutes. The grids were then washed in 100 µl PBS, fixed in 1% glutaraldehyde for 5 min and washed with water 7 x 2 min. To contrast the samples, each grid was transferred to a 50-µl drop of uranyl-oxalate (1:1

mix of 4% uranyl acetate and 0.15 M oxalic acid) at pH 7 for 5 min. The grids were then embedded in 2% methylcellulose, 4% uranyl acetate (9:1 v:v ratio), for 10 min on ice. Grids were removed from embedding solution with microforceps and excess fluid blotted away on Whatman no. 1 filter paper. Grids were allowed to air dry for 10 min and stored in grid boxes. Exosomes were visualized using a FEI Tecnai Spirit G2 120 kV transmission electron microscope.

For immunogold labeling, after paraformaldehyde fixation and adsorption onto EM grids, exosomes were washed 3 x 3 min in PBS and incubated for 3 min in 50 mM glycine in PBS to quench any free aldehyde groups. Next, exosomes were blocked 10 min with 5% bovine serum albumin (BSA) in PBS. PEDF antibody (BioProducts MD) was diluted in 5% BSA at 10 µg/ml and layered on the EM grids for 30 min. Grids were washed 6 x 3 min with 0.1% BSA in PBS. Protein-A gold conjugates (Ted Pella, Inc) were diluted 1:200 in blocking buffer and incubated on EM grids for 20 min. The grids were washed with PBS 8 x 2 min, followed by 5 min fixation with 1% glutaraldehyde and 8 x 2 min washes in water. Grids were then contrasted, embedded and images taken as described above.

2.5.11 Limited Trypsin Digestion

Exosomes were incubated with 0.05% trypsin for 5 minutes at room temperature to digest surface proteins only. After digestion, 4x Laemmli buffer was added to the samples, followed by gel electrophoresis and western blotting with antibodies for PEDF and β-actin (luminal marker).

2.5.12 Phagocytosis Assay

RAW 264.7 macrophages and A375 melanoma cells expressing GFP were seeded in 24-well plates at a 30:1 ratio. After 24 hours, Exo^M or Exo^{NM} were added to the cells at 0.01, 0.5 and 2.0 µg/ml. Cells were live imaged at 48 hours. Before imaging, cover glass was removed and

placed in Attoflour® Cell Chamber (Life Technologies) and filled with 1 mL of cell superfusion buffer (CSB: 0.35mM Na₂HPO₄, 110mM NaCl, 0.44mM KH₂PO₄, 5.4 mM KCl, 1mM MgSO₄, 1.3mM CaCl₃, 25mM HEPES, and the pH was adjusted to 7.4). The cell chamber was placed on the microscope platform and imaged. Nomarski/DIC images and confocal images were obtained using the Zeiss AxioVert 200 inverted fluorescence microscope, AxioCam camera, and AxioVision software. Cells were imaged using a 63x objective (N.A. 1.4; oil). The process length and the macrophage surface area were quantified using ImageJ. In separate experiments RAW 264.7 and A375 cells were plated in glass bottom dishes treated with exosomes at indicated concentrations above and cells were imaged every 15 minutes for 16 hours.

2.5.13 Apoptosis Assays

Terminal dUTP nick-end Labeling Assay (TUNEL): The cells were grown on glass coverslips coated with 0.1% gelatin (45 minutes at 37°C). RAW 264.7 macrophages were grown for 24 hours in co-culture with A375 melanoma (5:1 ratio) or as monocultures. Exosomes were then added at a concentration of 3 µg/ml. The cells were incubated for additional 24 hours, then fixed in 4% paraformaldehyde and permeabilized with 0.1% TritonX-100 for 2 min at 4°C. Apoptotic cells were detected and apoptotic cells detected using *In Situ* Cell Death Detection Kit (Roche) and visualized by fluorescence microscopy.

Annexin V staining: cells were grown as above, harvested and stained in suspension using Annexin V/propidium iodide apoptosis detection kit (Biolegend). For cell-type specific detection of cell death, the cells were co-stained with antibody for macrophage marker F4/80 (Brilliant Violet fluorophore) and analyzed by flow cytometry.

2.5.14 Macrophage Differentiation Assay

RAW 264.7 macrophages (3×10^5) were plated in a 35 mm glass-bottom dishes, allowed to adhere for 24 hours and treated with Exo^M or Exo^{NM} at a concentration of 3 $\mu\text{g/ml}$. Images were taken every 15 minutes for 16 hours in a Nikon Biostation (5% CO₂ at 37°C) focusing on the formation of dendrite-like projections. For quantification studies, the cells were seeded in 6-well dishes. NIS-Elements AR 4.00.03 (Nikon) was used for analysis following imaging. The z-stacks were merged, ROIs selected and the surface area and the multi-point function were used to measure area and length, respectively.

2.5.15 Lung Colonization and Extravasation Assays

Athymic nude mice (Harlan) were injected intravenously with 20 μg of Exo^M or Exo^{NM} 3 times 48 hours apart. After the exosome treatment, GFP-tagged A375 melanoma cells (3×10^5 cells/ mouse) were injected via the tail vein. Tumors in the lungs were allowed to develop for 9 weeks at which point the mice were sacrificed, lungs were harvested and images taken using a Nikon OV-100 imaging station (Northwestern University Center for Advanced Microscopy).

Melanoma extravasation was assessed as described previously.¹³⁵ In brief, female C57BL/6 mice were pretreated with exosomes (10 $\mu\text{g}/\text{mouse}$, two times 48 hours apart). After the second exosome treatment, the mice were inoculated with 10^6 B16F10 melanoma cells labeled with CFSE fluorescent dye. Mice were sacrificed at 3 and 24 hours after tumor cell inoculation, the lungs excised and fluorescence-labeled cells were visualized with a Nikon AZ-100 fluorescent microscope (Northwestern Center for Advanced Microscopy) or Nikon Diaphot 2000 with 3x objective. Alternatively, the extravasation of human melanoma cells was analyzed. For these experiments, exosomes were isolated from highly aggressive and poorly aggressive C8161 (C8161 HA or C81-61 PA, respectively).

2.5.16 Clodronate Depletion of Macrophages and Monocytes

C57BL/6 mice were depleted of macrophages and monocytes using clodronate containing liposomes, as described previously.¹⁴⁶ Mice were given intravenous injections of clodronate or control PBS liposomes (200 µl/mouse), 96 and 48 hours prior to exosome treatment and inoculation of CFSE-tagged melanoma cells and assessment of extravasation (see above). Six mice in each group were sacrificed and the lungs stained for F4/80 and CD11b, to ascertain the depletion of monocytic cells.

2.5.17 Depletion of NK Cells with anti-Asialo GM1 Antibodies

C57BL/6 mice were pre-treated with anti-asialo GM1 antibodies or non-specific isotype control antibodies. 20 µl anti-asialo GM1 antibodies (Wako Chemicals) were diluted 5x in PBS and were injected intraperitoneal 24 hours prior to exosome treatment and extravasation assay. Staining splenocytes with an anti-NK1.1 antibody and analyzing using flow cytometry was used to assess NK cell depletion.

2.5.18 Functional Analysis of Patient Exosomes

Exosomes from melanoma patients and healthy controls were isolated from serum collected at the New York University School of Medicine approved by the Institutional Review Board (protocol i10362) and carried out in accordance with approved guidelines. Melanoma patient serum samples were completely de-identified prior to transfer to Northwestern University. Melanoma patient serum samples were separated into three groups, healthy control, patients with primary melanoma and no recurrence, and patients with recurrence after resection of the primary melanoma. Melanoma recurrence was determined after a minimum of 5-year follow-up. Melanoma patient data was outlined in **Table 2.1**. For the depletion of exosomes from

human serum samples, recurrent melanoma patient serum was ultracentrifuged at 100,000 x g for 24 hours. After ultracentrifugation, the supernatant was removed and used for analysis.

For functional analysis of patient exosomes, to determine the function at promoting or suppressing metastasis 10 µg of exosomes (based on protein content) (isolated using protocol outlined above) was injected I.V. twice, 48 hours apart. Following the second exosome dose, 10⁶ CFSE labeled A375 human melanoma cells were inoculated I.V. Mice were sacrificed, lungs dissected and the number of melanoma lung colonies was determined by fluorescent microscopy. Exosomes from one patient were used to treat three mice.

2.5.19 Statistical Analysis

Data was expressed using \pm standard deviation of at least triplicate experiments. GraphPad Prism version 6 was used to analyze data. Microscopy and flow cytometry were analyzed using ImageJ and FCS Express, respectively. Statistics were considered significant if $P \leq 0.05$. * Denotes $P \leq 0.05$, ** $P \leq 0.01$, and *** $P \leq 0.001$.

CHAPTER THREE:

Nanoparticle Targeting and Cholesterol Flux through Scavenger Receptor Type-B1 Inhibits the Cellular Uptake of Exosomes

This Chapter is based on work published in:

M.P. Plebanek, R.K. Mutharasan, O. Volpert, A. Matov, J.C. Gatlin, C.S. Thaxton.
Scientific Reports, 2015 Oct 29; 5:15724.

3.1 Abstract

Exosomes are nanoscale vesicles that mediate intercellular communication. Cellular exosome uptake mechanisms are not well defined partly due to the lack of specific inhibitors of this complex cellular process. Exosome uptake depends on cholesterol-rich membrane microdomains called lipid rafts, and can be blocked by non-specific depletion of plasma membrane cholesterol. Scavenger receptor type B-1 (SR-B1), found in lipid rafts, is a receptor for cholesterol-rich high-density lipoproteins (HDL). We hypothesized that a synthetic nanoparticle surface mimic of HDL (HDL NP) that binds SR-B1 and removes cholesterol through would inhibit cellular exosome uptake. In cell models, our data show that HDL NPs bind SR-B1, activate cholesterol efflux, and attenuate the influx of esterified cholesterol. As a result, HDL NP treatment results in decreased dynamics and clustering of SR-B1 contained in lipid rafts and potently inhibits cellular exosome uptake. The key to this process is twofold: first HDL NPs efflux cholesterol from the cell membrane and second, HDL NPs inhibit natural HDL from delivering cholesteryl esters to the cell in a competitive manner. Thus, SR-B1 and targeted HDL NPs provide a fundamental advance in studying cholesterol-dependent cellular uptake mechanisms.

3.2 Introduction

Exosomes play a fundamental role in biology^{53,154} by transporting molecular cargo to and from cells as a means of intercellular communication.¹⁵⁵ For example, exosomes isolated from stem cells have been shown to increase tissue regeneration after injury.^{156,157} Additionally, exosomes play an important role in the immune system, through the delivery of major histocompatibility complexes (MHCs)^{158,159}. Importantly, exosomes also contribute to the pathogenesis of many diseases,^{53,76,160} including cancer.^{63,161} Cancer cells have an increased production of exosomes which function to facilitate disease progression.^{162,163} For example, exosomes produced by melanoma cells have been shown to target endothelial cells to enhance angiogenesis,¹⁶⁴ as well as macrophages and dendritic cells resulting in immune suppression.¹⁶⁵ In addition, as is evident by studies presented in Chapter 1, considerable data are accumulating showing that enhanced exosome production by cancer cells facilitates metastasis by conditioning the pre-metastatic niche through the mobilization of bone marrow cells⁸ and the delivery of pro-tumorigenic cargo to metastatic sites.⁶³

Specific receptors on target cells that exosomes utilize for uptake are relatively unknown.¹⁶⁶ Data show that target cells uptake exosomes by directly fusing with the plasma membrane,¹⁶⁷ as well as via receptor mediated endocytosis due to ligands on the surface of the exosomes.¹⁹ Because exosome-cell interactions are believed to be critical events for information transfer between the exosome and the target cell, further understanding fundamental mechanisms of these interactions may open avenues for studying intercellular communication leading to new therapies.¹⁶⁸ Key to this effort is the identification of specifically targeted agents that potentially inhibit cellular exosome uptake.¹⁶⁸ Recent data show that exosome uptake by target cells is dependent upon the integrity of plasma membrane microdomains known as lipid rafts, which are

known to be highly rich in cholesterol.¹⁶⁹ Data show that non-specific depletion of plasma membrane cholesterol alters lipid raft integrity and inhibits cellular exosome uptake.¹⁷⁰

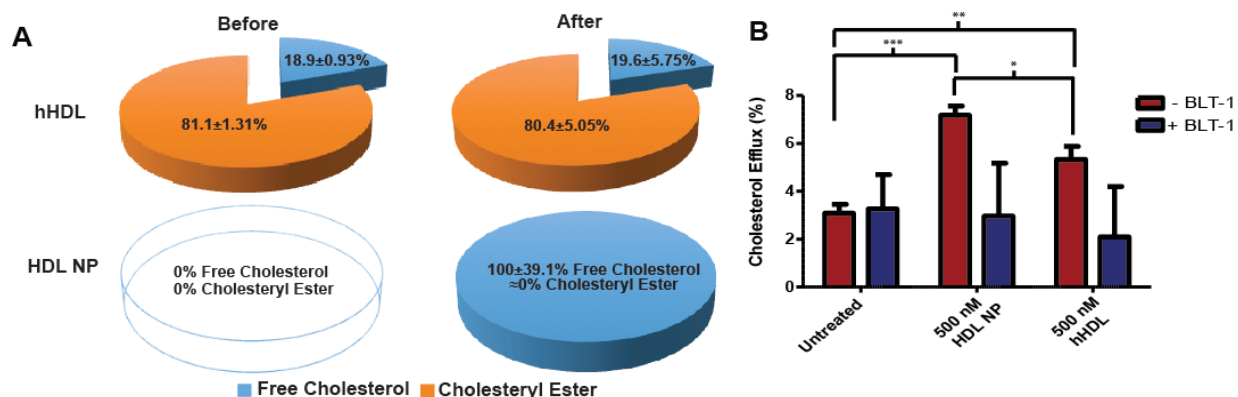


Figure 3.1: HDL NPs Efflux Free Cholesterol from Melanoma Cells. (A) Pie charts show the content, percent of total measured cholesterol, of free cholesterol and cholesteryl ester to hHDL and HDL NPs **before (left)** and **after (right)** cholesterol efflux in A375 melanoma cells. (B) Cholesterol efflux assay demonstrating SR-B1 mediated cholesterol efflux by HDL NPs and hHDL with and without the SR-B1 inhibitor BLT-1 (1 μ M).

Scavenger receptor type B-1 (SR-B1) is a high-affinity receptor for mature spherical high-density lipoproteins (HDL) that are rich in cholesterol and cholesteryl ester. Upon binding SR-B1, HDL mediates the bi-directional flux of free cholesterol between the HDL particle and the plasma membrane, and serves as a source of cholesteryl ester.^{101,171} Scavenger receptor type B-1 resides in plasma membrane lipid rafts¹⁷² where it maintains plasma membrane cholesterol balance and enables the uptake of extracellular material and cell signaling including cholesterol sensing.¹⁷³ Our group developed a synthetic, functional HDL-like nanoparticle (HDL NP)^{117,119,174} that binds SR-B1.¹⁷⁴ HDL NPs are synthesized using a gold nanoparticle (AuNP) as a core template, and then decorated with surface molecules including, phospholipids and apolipoprotein A-I (apo AI), consistent with the surface chemistry of natural, mature spherical HDLs.¹⁷⁴ HDL NPs are highly functional with regard to their ability to bind SR-B1 and efflux

free cholesterol.¹⁷⁴ Because of the core AuNP, HDL NPs are inherently devoid of cholesteryl ester. As such, HDL NPs bind SR-B1 and differentially modulate cellular cholesterol homeostasis relative to their cholesterol-rich natural HDL counterparts.^{122,174}

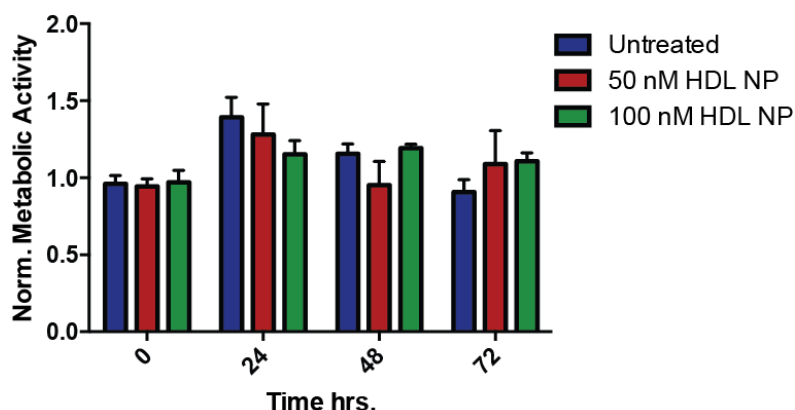


Figure 3.2: HDL NPs have no Effect on Cellular Viability. A375 melanoma cells were treated with 50 and 100 nM HDL NP and the cytotoxicity was measured using 3-(4,5-dimethylthiazol-2-yl)-5-(3-carboxymethoxyphenyl)-2-(4-sulfophenyl)-2H-tetrazolium (MTS) assay at T = 0, 24, 48, and 72 hours after HDL NP treatment.

Due to the localization of SR-B1 to lipid rafts and the dependence of exosome uptake on cholesterol balance in the plasma membrane, we hypothesized that specific targeting of SR-B1 with cholesterol binding HDL NPs^{117,119,174} would disrupt cellular exosome uptake. As a model, we explored exosomes derived from cultured melanoma cells due to the established importance of the uptake of these exosomes to cancer metastasis,^{63-65,165} and because melanoma exosomes have been shown to promote disease progression, whereby targeted inhibitors of this process may be translationally relevant.^{64,175}

3.3 Results

3.3.1 HDL NPs Modulate Cholesterol Flux in Melanoma Cells *in vitro*.

High-density lipoproteins are dynamic natural nanostructures that function to sequester, transport, and deliver cholesterol.¹⁷⁶ Many of the physical properties and functions of natural

HDLs can be mimicked by HDL NPs,¹⁷⁴ which are synthesized using a 5 nm diameter core AuNP template. The template controls final conjugate size and shape and provides a surface for the assembly of apo AI and phospholipids.¹¹⁹ Comparison of HDL NPs to spherical human HDL (hHDL) species reveals similarities with regard to size, shape, surface chemistry, and negative surface charge.^{117,174,177} Functionally, hHDLs bind SR-B1 and mediate the bi-directional flux of free cholesterol between the particle and the plasma membrane and transfer esterified cholesterol, found in the particle core, to the recipient cell.¹⁷³ HDL NPs have been shown to mediate bi-directional free cholesterol flux through SR-B1, like hHDL,^{117,119} however, the AuNP core of HDL NPs occupies the same physical space as esterified cholesterol does in spherical hHDL rendering HDL NPs incapable of delivering to cells a similar payload of cholesteryl ester.^{122,174} To clearly demonstrate this, we measured free and esterified cholesterol contained in hHDL and HDL NPs. Data reveal a lack of both free and esterified cholesterol in freshly synthesized HDL NPs (**Figure 3.1A**), as expected. hHDLs were found to have ~19% free and ~81% esterified cholesterol (percent of total measured cholesterol). Based on these results, we predicted that hHDLs and HDL NPs would exhibit differential effects on cholesterol flux in the A375 melanoma cells. To test this, we labeled the cellular cholesterol pool in melanoma cells using ³H-cholesterol, and then performed cholesterol efflux assays to measure the removal of ³H-cholesterol from these cells. Data show that HDL NPs induce cholesterol efflux at higher levels than hHDLs (**Figure 3.1B**). Treatment of cells with Blocks Lipid Transport 1 (BLT-1), an inhibitor of SR-B1-mediated cholesterol flux,¹⁷⁸ resulted in reduced efflux to both hHDLs and HDL NPs (**Figure 3.1A**) suggesting that cholesterol efflux is, at least in part, mediated by specific targeting of the SR-B1 receptor by hHDLs and HDL NPs. After the cholesterol efflux assay, hHDLs and HDL NPs were determined to have increased free cholesterol (percent of total

measured cholesterol); however, there still is no measurable esterified cholesterol in HDL NPs versus hHDLs.

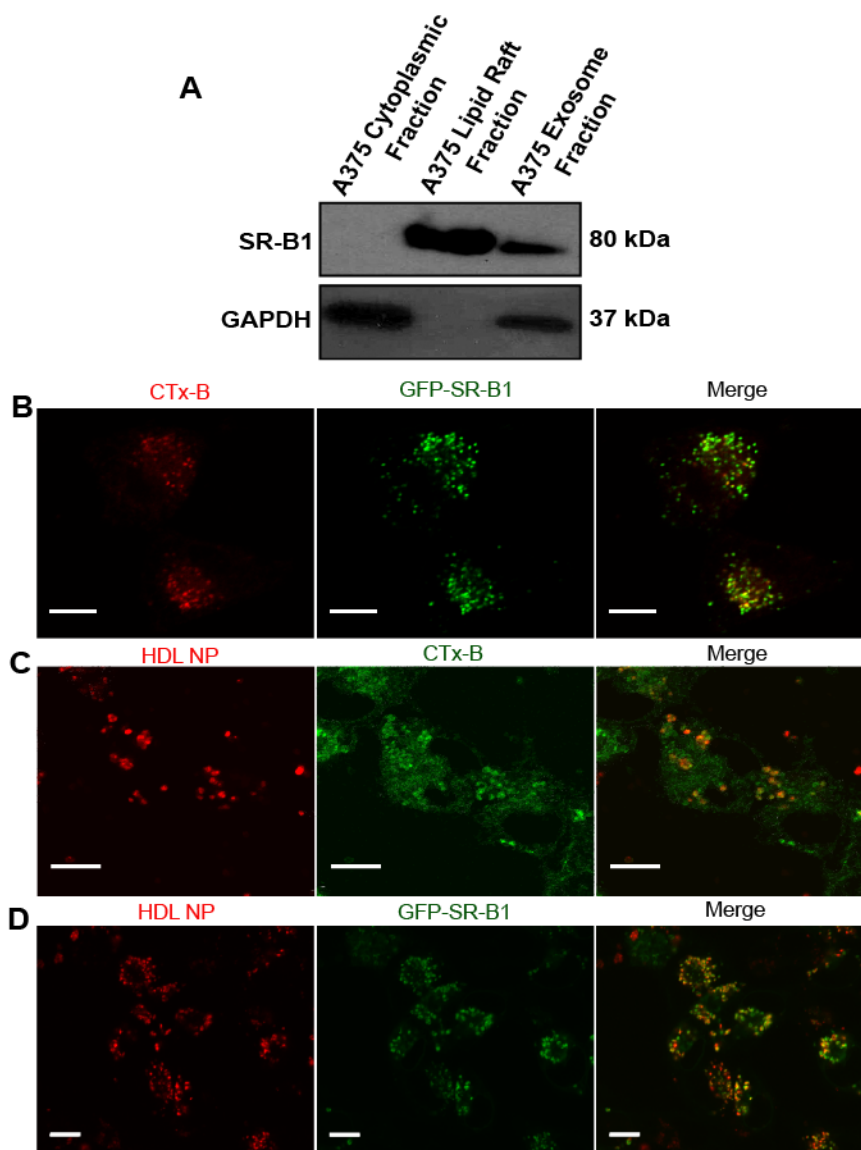


Figure 3.3: SR-B1 and HDL NP Distribution to Lipid Rafts (A) Cell compartments were fractionated and Western blot shows SR-B1 enrichment in lipid rafts, presence in exosomes, and absence in the cytoplasmic cell fraction. (B-D) Confocal fluorescence microscopy of A375 melanoma cells to assess co-localization of lipid rafts, HDL NPs, and GFP-SR-B1. (Scale bar = 10 μ m) (B) A375 cells expressing GFP-SR-B1 fusion protein (green) stained with Alexafluor-647 conjugated CTx-B (red) to label lipid rafts. (C) A375 melanoma cell lipid rafts stained with Alexafluor-488 conjugated CTx-B (green) after treatment with 20 nM DiD-labeled HDL NPs (red). (D) A375 melanoma cells expressing GFP-SR-B1 fusion protein (green) treated with DiD-labeled HDL NPs (20 nM, red).

Cell viability assays demonstrate that despite the increased cholesterol efflux induced by HDL NPs, treatment with HDL NPs at 50 and 100 nM doses does not result in reduced A375 cell viability at time points up to 72 hours (**Figure 3.2**). Thus, cholesterol and cholesteryl ester-poor HDL NPs are not inherently toxic to A375 melanoma cells, they target SR-B1, and differentially modulate cholesterol flux through this receptor. These functionally distinct properties of HDL NPs prompted us to probe biological processes, like exosome uptake, that are dependent upon cell membrane cholesterol homeostasis.

3.3.2 SR-B1 Localizes to Lipid Rafts

The mechanistic link between lipid raft integrity and the role that these cell membrane microdomains play in exosome uptake¹⁷⁰ led us to test whether SR-B1 and HDL NPs localize to lipid rafts in melanoma cells. Consistent with published results,¹⁷² analysis of lipid raft-associated proteins via western blot confirmed that SR-B1 localizes to lipid rafts in A375 melanoma cells and showed that SR-B1 is enriched in the insoluble lipid raft membrane fraction compared to the cytoplasmic fraction (**Figure 3.3A**). In complementary experiments, fluorescence confocal microscopy was used to visualize lipid rafts in A375 melanoma cells by labeling the rafts with cholera toxin subunit b (CTx-B) conjugated to Alexafluor-647. We visualized SR-B1 by stably expressing a green fluorescent protein-SR-B1 (GFP-SR-B1) fusion protein in the A375 cells.¹⁷⁹ Imaging revealed co-localization of GFP-SR-B1 with lipid rafts (**Figure 3.3B**). These data establish that lipid rafts in our model melanoma cell line are enriched in SR-B1. To determine whether HDL NPs are targeted to lipid rafts and SR-B1, we treated cells with HDL NPs labeled with a lipophilic fluorescent dye, 1,1'-dioctadecyl-3,3,3',3'-tetramethylindodicarbocyanine, 4-chlorobenzenesulfonate salt (DiD), and imaged cells to determine co-localization with lipid rafts and SR-B1. Imaging revealed that labeled HDL NPs

(red) co-localize with lipid raft CTx-B, labeled with Alexafluor-488 (**Figure 3.3C**), and with GFP-SR-B1 (**Figure 3.3D**).

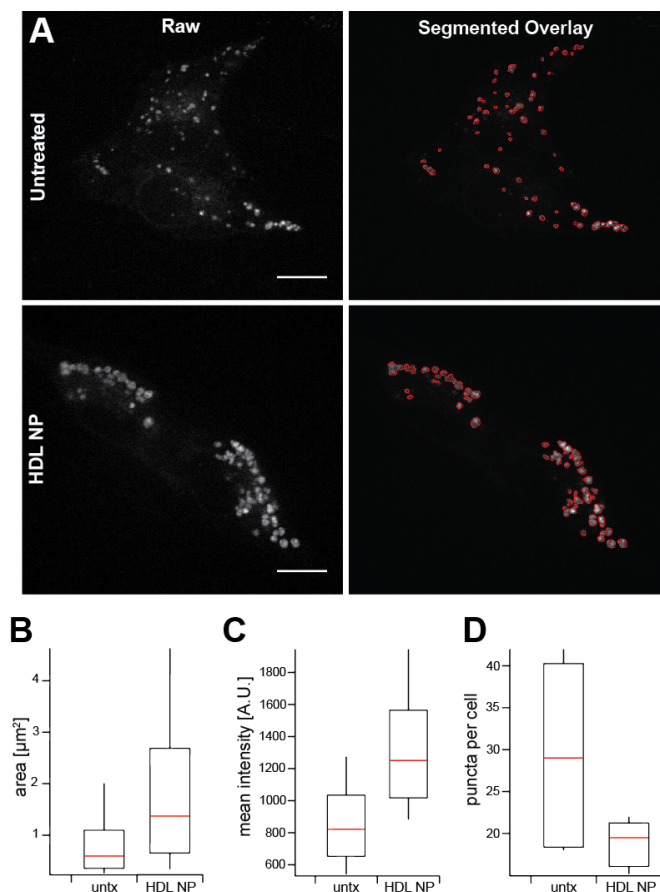


Figure 3.4: HDL NPs Induce Clustering of SR-B1. Time-lapse images of A375 melanoma cells expressing GFP-SR-B1 treated with 30 nM HDL NPs. (A) Representative confocal images of GFP-SR-B1 expressing cells under indicated experimental conditions. Raw images were segmented using a wavelet-based method to define and measure GFP-SR-B1-positive domains. For each condition, six time-lapse movies (2 min. duration, 2s lapse) were acquired with $n \geq 15$ cells/condition (scale bar: 10 μm). (B) The distribution of areas for all domains present ($*P \leq 0.05$ via permutation t-test) presented as box plots. Median, 25th and 75th percentile are shown. Whiskers extend between 10th and 90th percentile. (C) Average domain brightness per area ($*P < 0.05$ via permutation t-test). (D) Average number of GFP-SR-B1 domains per cell for the indicated conditions. ($***P < 0.00005$ via permutation t-test)

3.3.3 HDL NPs Induce Clustering and Reduced Movement of SR-B1

During co-localization experiments, intriguingly, images collected at 24 hours revealed a physical clustering of GFP-SR-B1 (**Figure 3.4A**) in a dose dependent manner, and time-lapse

microscopy revealed an apparent reduction in movement and displacement of the receptor upon the addition of HDL NPs as compared to untreated. To quantify these observations, we used automated image analysis (*Materials and Methods*)^{180,181} and data confirm an increase in the size and intensity of GFP-SR-B1 clusters, and a reduction in the number of labeled areas per cell after HDL NP treatment, respectively (**Figure 3.4A-D**). Also, we observed that GFP-SR-B1 clusters tended to remain at the cell membrane versus GFP-SR-B1 that was not clustered. This prompted us to perform tracking analysis to measure GFP-SR-B1 displacement (**Figure 3.5A**). Data revealed a significant quantitative reduction in the velocity (**Figure 3.5B**) and in the ratio of the final displacement relative to the total displacement length (*rho*) of GFP-SR-B1 clusters (**Figure 3.5C**). Collectively, these data suggest that HDL NPs bind SR-B1 in lipid rafts leading to clustering and arrested movement of GFP-SR-B1.

3.3.4 HDL NPs Block the Uptake of Melanoma-Derived Exosomes

Cellular uptake of exosomes is dependent on lipid raft-mediated endocytosis.¹⁷⁰ As HDL NPs differentially modulate cellular cholesterol homeostasis and physically modulate SR-B1 localized to lipid rafts, we tested the hypothesis that HDL NPs interfere with cellular exosome uptake. Toward this end, we isolated exosomes from A375 melanoma cells and fluorescently labeled them with 1,1'-dioctadecyl-3,3,3',3'-tetramethylindocarbocyanine perchlorate (DiI). We then treated the A375 cells with labeled exosomes in the presence or absence of HDL NPs and subsequently measured cell uptake. Confocal fluorescent microscopy revealed that HDL NP treatment decreased exosome uptake as compared to untreated control cells at 24 hours (**Figure 3.6A**). In order to quantify exosome uptake as single cells we employed flow cytometry. Data demonstrated a dose-dependent decrease in exosome uptake after HDL NP treatment (**Figure 3.6B**). At the 50 nM dose, approximately 75% of exosome uptake by the A375 cells was

blocked. Notably, the uptake of exosomes was similar in wild-type and GFP-SR-B1 expressing A375 cells, and similar reductions in exosome uptake after HDL NP treatment were observed in both cell lines (**Figure 3.7A, B**). To test if HDL NPs interact with exosome or A375 cell-associated SR-B1, cells were pre-treated with HDL NPs for 12 hours, washed free of unbound HDL NP, and then treated with DiI labeled exosomes. Reduced exosome uptake following HDL NP pre-treatment suggests that decreased uptake is not due to extracellular interaction of exosomes and HDL NPs (**Figure 3.7C, D**).

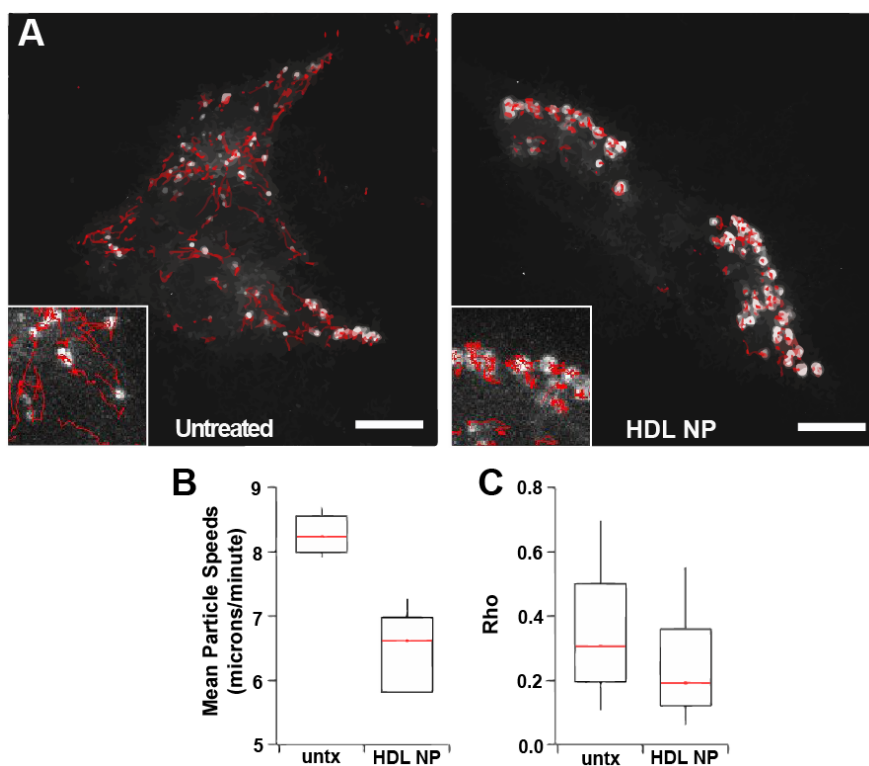


Figure 3.5: HDL NPs lead to Reduced Mobility and Dispersion of SR-B1 Containing Domains. Time-lapse confocal imaging (2s intervals) was used to visualize the SR-B1 dynamics. (A) Motion tracks from the entire duration of imaging overlaid on a single snapshot from the series. Insets provide higher magnification images of selected areas with multiple tracks (scale bar = 10 μm). (B) Average speeds per puncta for each condition ($***P < 0.00005$ via permutation t-test). (C) The ratio of net displacement (the straight-line distance from the starting point to the end point) to total track length traveled for each GFP-SR-B1 containing domain (*rho*). Values near 1 indicate directed motion.

In our cholesterol flux experiments described previously, HDL NPs and hHDL both bind to SR-B1, promoting cholesterol efflux through this receptor. To determine whether hHDL had the same effect as HDL NP on inhibiting the cellular uptake of labeled exosomes, we again used flow cytometry to test exosome uptake. Data show that hHDL treatment only minimally inhibits cellular exosome uptake (**Figure 3.7E, F**) compared to HDL NP treatment. Both hHDL and HDL NPs target SR-B1, but only the HDL NPs inhibit exosome uptake, which provided an opportunity to demonstrate that hHDL and HDL NPs compete for the same cell surface receptors involved in exosome uptake. Co-treatment of cells with HDL NP and increasing amounts of hHDL resulted in a partial concentration-dependent recovery in exosome uptake (**Figure 3.6C**) suggesting competition for SR-B1. Based on our observing only a partial recovery, we reasoned that hHDL might also reduce cellular exosome uptake at very high concentrations. To test this, A375 cells were co-treated with fluorescently labeled exosomes and hHDL at 5, 50 or 500 nM concentrations and exosome uptake was measured using flow cytometry. hHDL was unable to potently block the uptake of exosomes even at a concentration of 500 nM, which is 10-times the HDL NP concentration required for near complete inhibition of exosome uptake (**Figure 3.7E, F**). Accordingly, hHDL does not reduce cellular exosome uptake and the high concentration of hHDL needed to abrogate HDL NP-mediated inhibition of exosome uptake suggests that HDL NPs have a higher binding affinity to cell-surface SR-B1 receptors. Also, due to the ability of HDL NP to inhibit exosome uptake in comparison to hHDL, the data suggest that binding SR-B1 and differential modulation of cholesterol are both mechanistically important in inhibiting exosome uptake.

To directly test if the HDL NPs specifically target SR-B1 to inhibit exosome uptake, we treated cells with HDL NPs and a blocking antibody (Ab) to SR-B1, which has been shown to

inhibit hHDL binding to this receptor.¹⁸² Treatment of A375 cells with the blocking Ab resulted in a significant reduction in the ability of HDL NPs to inhibit exosome uptake (**Figure 3.6D**). Thus, these data support the conclusion that HDL NPs specifically block exosome uptake in melanoma cells by binding SR-B1.

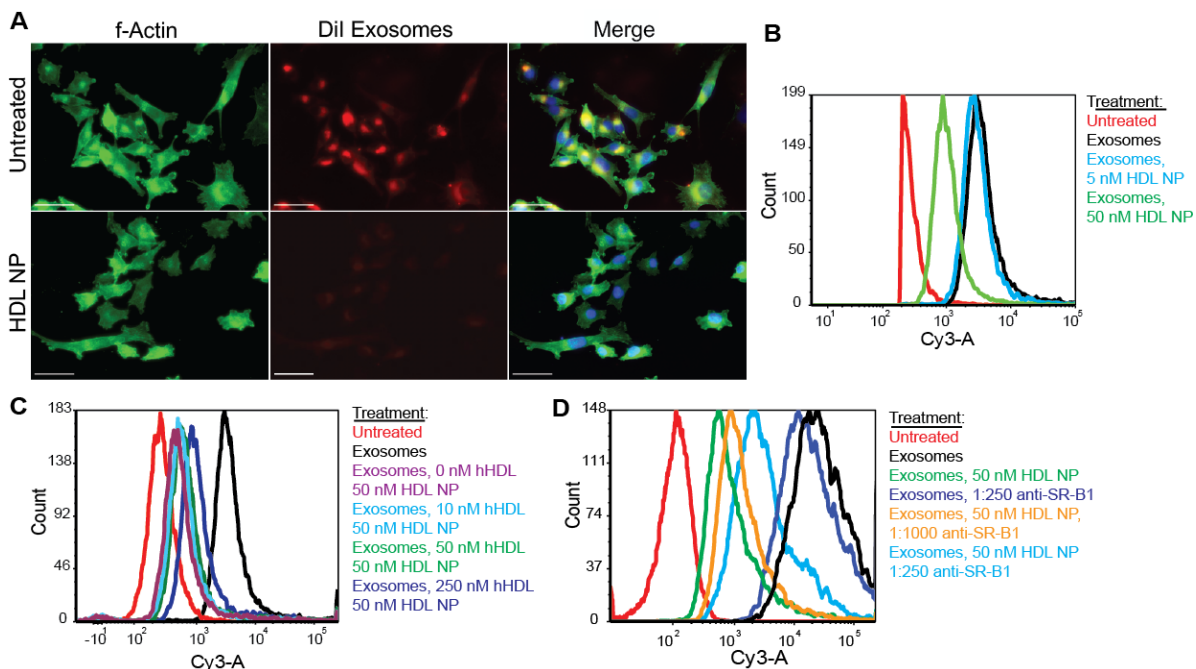


Figure 3.6: HDL NPs Block the Uptake of Exosomes by A375 Melanoma Cells. (A, B) A375 cells were treated with 1 $\mu\text{g}/\text{mL}$ of DiI-labeled exosomes (A) Exosome uptake was visualized using fluorescence microscopy after treatment with HDL NP (25 nM, 24 hrs). F-actin cytoskeleton was stained using a FITC-phalloidin conjugate and the nuclei were stained with DAPI. (Scale bar = 10 μm) (B) DiI-labeled exosome uptake by A375 cells with and without HDL NP treatment (5, 50 nM HDL NP, 24 hrs) analyzed using flow cytometry (C) Partial rescue of exosome uptake by HDL NP treated A375 cells (50 nM) using hHDL (10, 50, 250 nM). (D) Dose dependent recovery of exosome uptake in A375 cells treated with HDL NPs (50 nM, 24 hrs) by anti-SR-B1 antibody.

3.3.5 Targeting SR-B1 to Block Cellular Exosome Uptake

The pronounced effects of HDL NPs on both SR-B1 dynamics and exosome uptake led us to examine the functional importance of individual features specific to the HDL NPs. Structurally, HDL NPs comprise a 5 nm diameter gold core and have the size, shape, and surface

chemistry consistent with some hHDL species,¹¹⁷ but the inherent flexibility of NP synthesis techniques enabled generation of particles with different surface chemistry. This allowed us to measure exosome uptake and SR-B1 clustering after treating A375 cells with particles having an identical gold core, but with passive surface chemistry (polyethylene glycol nanoparticles, PEG NPs). In addition, we also probed individual, functional properties of the HDL NPs by testing if the blocking Ab targeting SR-B1;¹⁸² the small molecule inhibitor of free and esterified cholesterol flux through SR-B1, BLT-1;¹⁷⁸ siRNA targeting melanoma cell SR-B1 expression; or combining HDL NPs and hHDL with BLT-1 would modulate cellular exosome uptake. As measured using flow cytometry, HDL NPs were the only particle or SR-B1 targeted treatment capable of clustering GFP-SR-B1 and inducing potent inhibition of cellular exosome uptake (**Figure 3.8A-L**). These results suggest that HDL NPs occupy SR-B1 and modulate free and esterified cholesterol flux, and that this combination of events results in the clustering of SR-B1 and the disruption of cellular exosome uptake. Finally, these data suggest that cellular exosome uptake is, at least in part, not responsive to a reduction in cellular SR-B1 expression; however, specific binding of this receptor by HDL NPs is a potent, targeted mechanism to inhibit cellular exosome uptake.

To more conclusively support the mechanism of action of the HDL NPs, we co-treated A375 melanoma cells with hHDL and BLT-1 to simultaneously occupy SR-B1 and block free and esterified cholesterol flux through the receptor, respectively. Intriguingly, data show that combining either hHDL with BLT-1 potently inhibits exosome uptake (**Figure 3.8M, N**). However, while some clustering of SR-B1 is observed, data show that there is less than when HDL NPs are used as a single agent (**Figure 3.8O**) Therefore, as the only functional difference between treating cells with HDL NP alone versus in combination with BLT-1 is the particle's

ability to support free cholesterol flux, this function of the HDL NP is critical to clustering SR-B1. On the other hand, because exosome uptake is potently inhibited after combining hHDL with BLT-1, data support that the inhibition of exosome uptake can be attributed to SR-B1 binding and inhibition of cholesteryl ester influx.

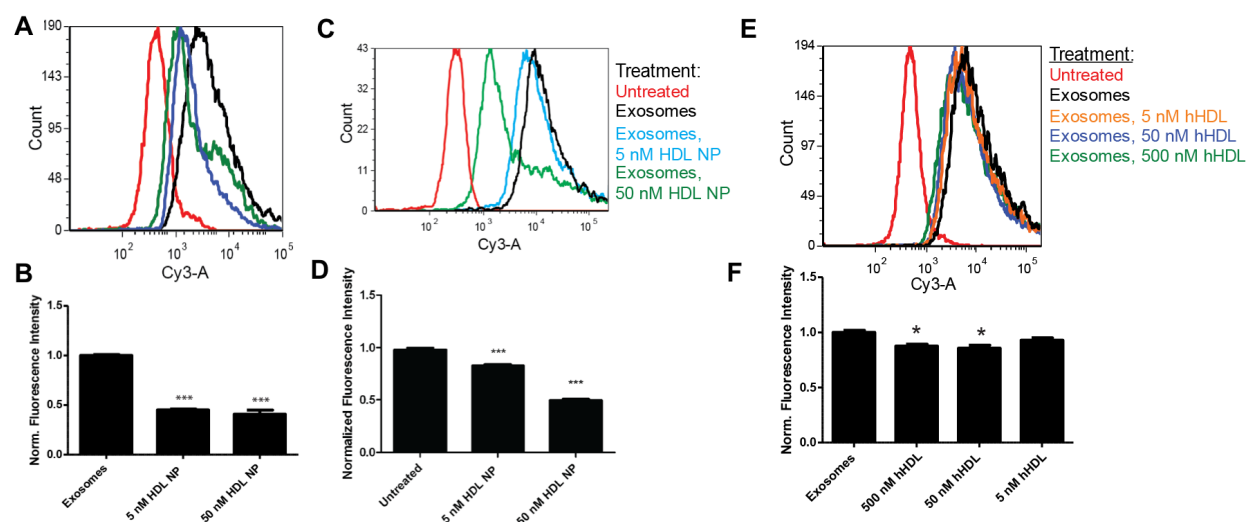
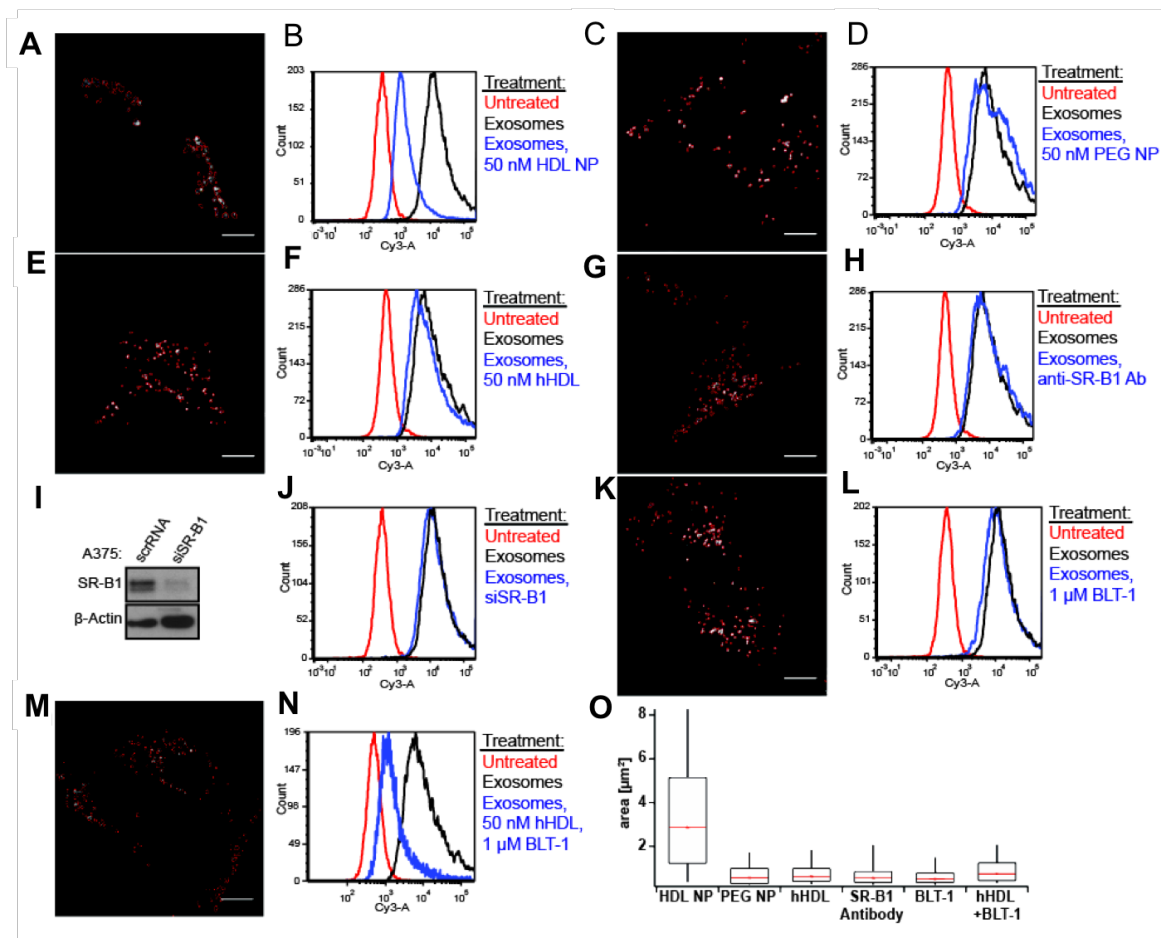


Figure 3.7: The Inhibition of Exosome Uptake is not due to Extracellular Interaction of Exosomes and HDL NP. (A) A375 cells expressing GFP-SR-B1 were treated with exosomes in the presence of 0, 5, and 50 nM HDL NPs. As was observed for the wild-type A375 cells, HDL NP treatment reduces exosome uptake in A375 cells expressing GFP-SR-B1. (B) Average fluorescence intensity of cells analyzed by flow cytometry in A. (***) represents $P < 0.001$). A375 melanoma cells were pre-treated for 12 hours with HDL NP 5 and 50 nM. Excess HDL NPs were then washed 2 times in PBS (C) Flow cytometry analysis of exosome uptake after A375 cell pre-treatment with HDL NPs. (D) Average fluorescence intensity of cells analyzed by flow cytometry in C. (***) Represents $P < 0.001$). (E) Exosomes were labeled using DiI and their uptake by A375 cells in the presence of 0, 5, 50, 500 nM hHDL was measured using flow cytometry. In contrast to HDL NP treatment, there the reduction in exosome uptake does not exceed 15%, even at 500 nM hHDL. (F) Average fluorescence intensity of cells analyzed by flow cytometry in E. (*) Represents $P < 0.05$ as compared to exosome only condition)

3.3.6 SR-B1 is Necessary for HDL NPs to Inhibit Exosome Uptake

In order to further show that HDL NPs directly target SR-B1 to inhibit exosome uptake, we knocked down SR-B1 expression with siRNA, as in the previous section, but then treated the

cells with labeled exosomes and HDL NPs. Flow cytometry data convincingly show that after SR-B1 knockdown in wild-type A375 cells (confirmed by Western blot (**Figure 3.9A**)) exosome uptake is not significantly reduced in the presence of HDL NP treatment (**Figure 3.9B**). Control experiments in wild-type A375 cells treated with scrambled siRNA reveal that HDL NP



treatment significantly reduces exosome uptake, as expected. This is important because it demonstrates that SR-B1 knockdown alone is not sufficient to inhibit exosome uptake and SR-B1 is necessary for the function of HDL NPs. These experiments further and directly implicate HDL NP targeting of SR-B1 as a mechanism to potentially reduce cellular exosome uptake.

3.3.7 Disrupting Exosome Uptake in Stromal Cells of the Metastatic Microenvironment

Data collected using melanoma cells are intriguing, but we were curious if the inhibition of exosome uptake by HDL NPs was unique to the A375 melanoma cells or effected other cells that express SR-B1. As mentioned previously, melanoma exosomes are known to target endothelial cells and macrophages, amongst others, leading to the activation of an angiogenic response,⁶⁵ inducing vascular leakiness, polarizing macrophages to a pro-tumor phenotype and the suppression of the immune system.¹⁶³ Therefore, we chose two different cell types, an endothelial cell line, human dermal microvascular endothelial cells (HMVECs) and RAW 264.7 macrophages and repeated select experiments to determine the effects of HDL NPs on exosome uptake. Like A375 cells, HMVECs were treated with DiI labeled A375 exosomes in the presence of HDL NPs, these cells exhibited a decrease in cellular fluorescence suggesting that exosome uptake is, indeed, blocked by HDL NP. In contrast, treatment with hHDL had minimal effect on exosome uptake (**Figure 3.10A**). RAW 264.7 macrophages also express SR-B1,¹⁸³ so we analyzed exosome uptake in these cells after HDL NP treatment. As was observed with HMVECs, HDL NPs decreased the uptake of exosomes, and hHDL had no effect (**Figure 3.10B**). These *ex vivo* proof-of-concept experiments not only demonstrate that HDL NPs block exosome uptake in cell types shown to be important for melanoma progression, but also suggest that HDL NP may therapeutically modulate intercellular communication events that are critical for melanoma progression.

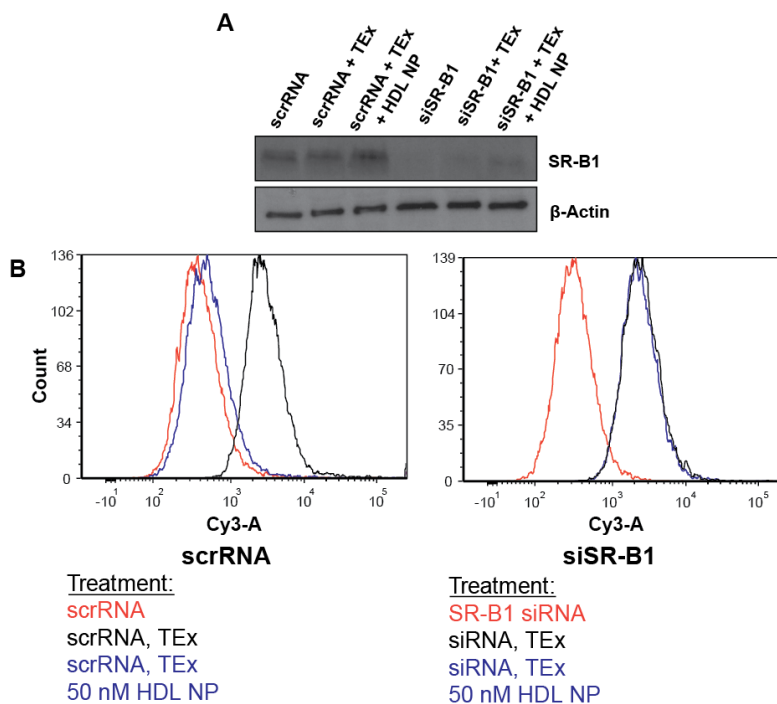


Figure 3.9: Expression of SR-B1 is Required for HDL NP-mediated Inhibition of Exosome Uptake. Wild-type A375 melanoma cells were treated with scrambled siRNA or siRNA-targeted to SR-B1. (A) Western blot reveals a reduction in SR-B1 expression in A375 cells at 48 hours after transfection with targeted siRNA. (B) Flow cytometry reveals a drastic reduction in labeled exosome uptake in the presence of HDL NPs (50 nM) in the cells treated with scrambled siRNA after 24 hours treatment. However, no significant reduction in labeled exosome uptake is observed upon HDL NP treatment in the case where siRNA expression has been reduced.

3.4 Discussion

Our data demonstrate that HDL NPs are a targeted and functional nanoconjugate that potently inhibit cellular exosome uptake in cultured melanoma, endothelial, and macrophage cells. Mechanistically, a model (Figure 3.11A, B) is proposed for HDL NPs whereby high affinity binding to SR-B1 in lipid rafts modulates free and esterified cholesterol flux through this receptor. Ultimately, HDL NP binding to SR-B1 and modulating free cholesterol flux is responsible for clustering and stagnating SR-B1 at the cell membrane. Further, HDL NP binding to SR-B1 and blocking the influx of cholesteryl ester leads to a dramatic reduction of cellular

exosome uptake. This proposed mechanism is supported by data collected using hHDL and BLT-1 whereby this combination of SR-B1 receptor occupancy and inhibition of cholesterol flux and cholesteryl ester uptake, respectively, potently inhibits cellular exosome uptake. Finally, this mechanism is specific and unique to HDL NPs, and is not shared by nanoparticles that have a gold core and altered, non-HDL-like surface chemistry; by other means of inhibiting SR-B1 using single, targeted agents (i.e. blocking Ab or BLT-1); or by knocking down the cellular expression level of SR-B1 (**Figure 3.11C**).

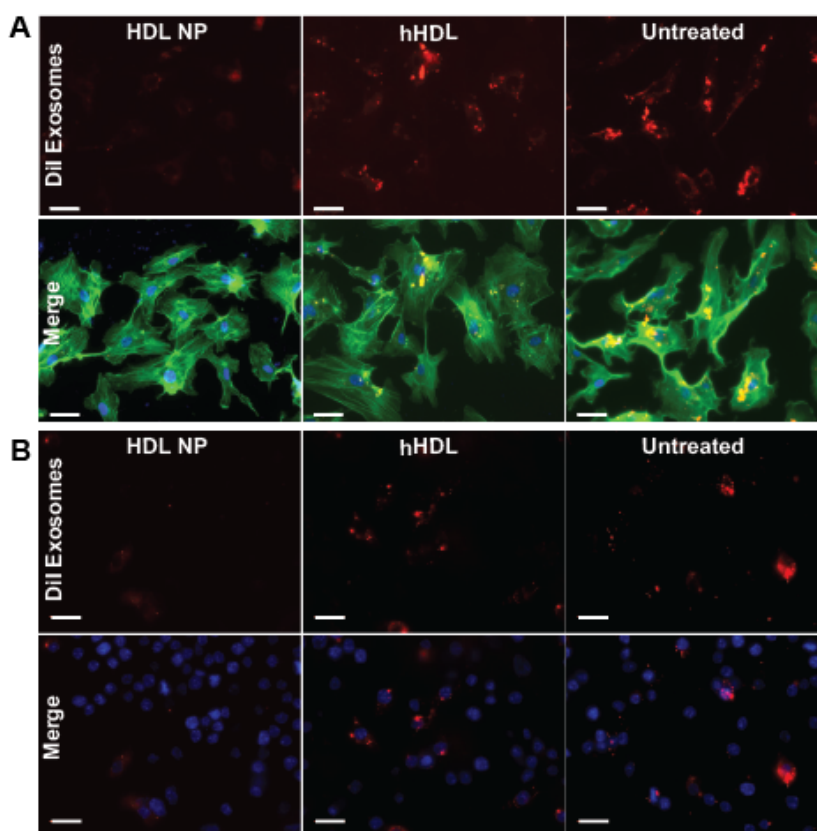


Figure 3.10: HDL NPs Inhibit the Uptake of Melanoma Exosomes by Endothelial Cells and Macrophages. (A) HMVECs were treated with 1 $\mu\text{g}/\text{mL}$ of DiI exosomes and visualized using microscopy after treatment with 25 nM HDL NP or hHDL for 24 hrs. The actin cytoskeleton was stained using a FITC-phalloidin conjugate and the nuclei were stained with DAPI. (B) RAW 264.7 macrophages were treated with 1 $\mu\text{g}/\text{mL}$ of DiI exosomes and visualized using microscopy after treatment with 25 nM HDL NP or hHDL for 4 hrs. (Scale bar: 10 μm)

The combination of HDL NPs and cellular exosome uptake provides a unique nanoparticle and phenotypic output signal that evidently uncouples targeted SR-B1 receptor binding from cholesterol flux to uncover a phenotype that is clearly impacted by local cell membrane cholesterol and cholesteryl ester flux. Further work is required to better understand downstream molecular events that occur upon functional HDL NP binding to SR-B1, especially considering the cholesterol sensing properties of SR-B1 and established signal transduction pathways. Certainly, we appreciate that HDL NPs binding to SR-B1 illicit different responses in specific cell types,^{122,184} and that cell surface and downstream second messenger signaling events may determine cell phenotype. We anticipate that different cholesterol-dependent phenotypes will be uncovered in other model systems. Finally, we are currently exploring the functional consequences of inhibiting intercellular communication events mediated by exosomes in the context of primary and metastatic melanoma models, and beyond.

In summary, our data implicate SR-B1 in the cellular uptake of exosomes in the context of targeted, functional HDL NPs that may prove to be a valuable tool to better understand cholesterol-dependent cellular uptake mechanisms of exosomes and, perhaps more broadly, other extracellular vesicles. Extension of our findings in melanoma cells to endothelial cells and macrophages suggests that the unique mechanism by which exosome uptake is inhibited by HDL NPs may be more general. Further work is focused on elucidating the functional consequences of inhibiting exosome-based information transfer between cells, and identifying cell-signaling pathways that may be altered by HDL NP binding to SR-B1 that may contribute to the observed reduction in cellular exosome uptake.

3.5 Materials and Methods

3.5.1 HDL NP Synthesis.

Biomimetic high-density lipoprotein-like nanoparticles (HDL NPs) were synthesized and characterized as previously described.^{117,119,174} For the synthesis, citrate stabilized 5 nm diameter gold nanoparticles (AuNP, Ted Pella) were used as a template for surface chemical modification. Purified human apolipoprotein AI (apoA-I) was incubated with a solution of AuNPs (80 nM) at 5-fold molar excess (400 nM) for 1 hour at room temperature (RT) with gentle stirring. Next, the phospholipids, 1-2-dipalmitoyl-sn-glycero-3-phosphocholine and 1,2-dipalmitoyl-sn-glycero-3-phosphoethanolamine-N-[3-(2-pyridyldithio)propionate] were added at 250 molar excess relative to [AuNP] in a mixture of ethanol and water (1:4), and allowed to incubate at RT for 4 hours with gentle shaking. The HDL NPs were purified and concentrated using tangential flow filtration. The HDL NP concentration and final conjugate size were determined using UV-Vis spectrophotometry ($\epsilon_{\text{AuNP}} = 9.696 \times 10^6 \text{ M}^{-1}\text{cm}^{-1}$ at $\lambda_{\text{max}} = 520 \text{ nm}$) and dynamic light scattering (DLS, Malvern Zetasizer), respectively.

3.5.2 Cell Culture

A375 melanoma cells (ATCC) and RAW 264.7 macrophages (ATCC) were cultured in Dulbecco's Modified Eagle Medium (DMEM) containing 10% fetal bovine serum and 1% penicillin/ streptomycin. Human dermal microvascular endothelial cells (HMVECs) and endothelial cell growth medium were from Promocell. Cells were incubated at 37 °C and in a humidified 5% CO₂ environment. The GFP-SR-B1 plasmid was given to us by Sirano Dhe-Paganon¹⁷⁹ of The Dana-Farber Cancer Institute was stably transfected in the A375 cells using Lipofectamine 2000 (Life Technologies) and transfectants were selected using Geneticin (Life Technologies) followed by fluorescent associated cell sorting (FACS).

3.5.3 Exosome Isolation and Labeling

A375 melanoma exosomes were isolated from conditioned media using differential ultracentrifugation.¹⁵³ As in Chapter 2, cells were cultured in exosome deficient media for 72 hours at which point the cell culture media was collected and centrifuged at 2000 x g to remove dead cells and debris. Next, larger microvesicles and cell debris were removed by centrifugation at 10,000 x g for 30 minutes. Exosomes were then pelleted by centrifugation at 100,000 x g for 70 minutes, and subsequently washed in PBS by another 100,000 x g centrifugation step for 70 minutes. Exosomes were re-suspended in PBS. Protein concentration of exosomes was analyzed by BCA Protein assay (Thermo Scientific). Exosome size and morphology was characterized using DLS and transmission electron microscopy (FEI Spirit G2 TEM). In the experiments utilizing fluorescently labeled exosomes, the lipophilic dye, DiI or DiD (Life Technologies), was added to the exosome preparation at a concentration of 2.5 μ M after the first 100,000 x g ultracentrifugation step. The fluorophore-labeled exosomes were then washed twice in PBS by pelleting the exosomes and discarding the supernatant. Notably, gold nanoparticles demonstrate distance-dependent fluorescence quenching.¹⁸⁵ In order to test if HDL NPs quenched exosome fluorescence, we incubated HDL NPs with fluorescently labeled exosomes for 4 hours and then measured the fluorescent signal.

3.5.4 Cell Treatments with Human HDL and HDL NP

For cholesterol determination assays, efflux assays, and cell treatments we used equimolar amounts of hHDL and HDL NPs based upon apo A-I concentration. The molar concentration of HDL NP was determined as discussed above, and each HDL NP has approximately three copies of apo A-I.^{117,174} Therefore, the molar concentration of apo A-I is easily calculated for the HDL NPs. Human HDL was purchased from Calbiochem. The protein

concentration of purchased hHDL was provided. From this value, the amount of apo A-I was calculated for hHDL assuming that 70% of the total protein is apo A-I,¹⁰¹ Thus, for each treatment the amount of apo A-I is equivalent for hHDL and HDL NP and, because each hHDL

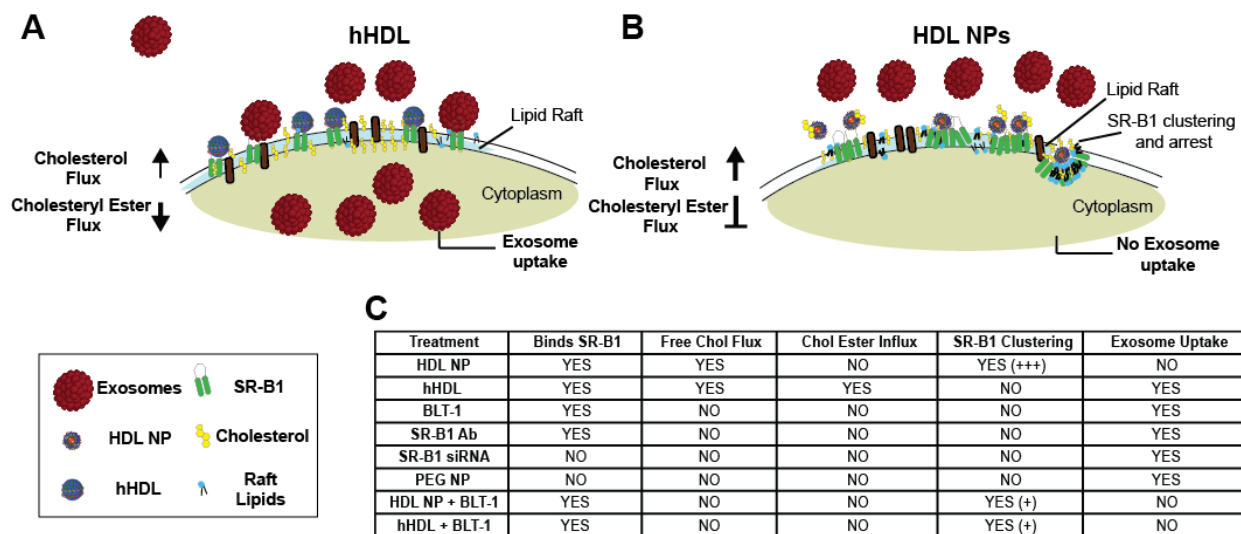


Figure 3.11: Summary of the Mechanism by which HDL NPs Inhibit Exosome Uptake. (A) In the presence of hHDL cellular exosome uptake is maintained. Through SR-B1, hHDL can remove cellular cholesterol and is a source of esterified cholesterol. (B) HDL NPs bind SR-B1 and efflux cholesterol from the cell more efficiently than hHDL and are not a source of esterified cholesterol. This leads to SR-B1 clustering and potent reduction in cellular exosome uptake. (C) Table comparing different cell treatments, their function, and the resulting phenotypic clustering and exosome uptake results.

and HDL NP has approximately three copies of apo A-I,¹⁸⁶ the dose of particles was assumed to be equivalent.

3.5.5 Exosome Uptake Assays

The cellular uptake of exosomes was measured by fluorescence microscopy and flow cytometry after cell treatments. A375 cells, HMVECs and RAW 264.7 macrophages were treated with fluorescent exosomes at a concentration of 1 $\mu\text{g/ml}$ (exosomal protein). For fluorescence microscopy experiments, cells were plated on coverslips coated with 0.1% gelatin.

Exosome uptake was measured over the course of 24 hours using a BD LSR Fortessa flow cytometer (Robert H. Lurie Comprehensive Cancer Center Flow Cytometry Core) or a Nikon A1R fluorescence microscope (Northwestern University Center for Advanced Microscopy).

3.5.6 Cholesterol and Cholesteryl Ester Quantification

The total cholesterol and cholesteryl ester content of hHDLs and HDL NPs was measured using an Amplex Red cholesterol detection assay (Life Technologies). The free cholesterol content of each sample was measured in the absence and presence of cholesterol esterase to determine the free cholesterol and total cholesterol, respectively. Cholesteryl ester quantity was determined by subtracting the free cholesterol from total cholesterol measurement. The free and esterified cholesterol content of the hHDL and HDL NP acceptors was measured after incubating with cultured A375 melanoma cells in serum free media and HDL NP (50 nM, final) or hHDL (50 nM, final) for 24 hours. After the treatment interval, the culture media was collected and centrifuged to rid the media of cells and cell debris. The total cholesterol and free cholesterol was then determined from conditioned media samples using the Amplex Red assay.

3.5.7 Cholesterol Efflux Assays

A375 cells were cultured in DMEM containing 1 $\mu\text{Ci/mL}$ [1,2,³H] cholesterol (Perkin-Elmer) overnight to label the cellular cholesterol pool. Cells were then washed in PBS and resuspended in serum free media. Human HDL or HDL NPs were added to the culture media and allowed to incubate for 6 hours. Cell culture media was then collected and subjected to liquid scintillation counting. The percentage of cholesterol efflux was determined by using the formula $\text{counts media}/(\text{counts cells} + \text{counts media}) \times 100$. Efflux of cholesterol in the absence of an acceptor was also measured and utilized as the background measurement.

3.5.8 Computer Vision Analysis of GFP-SR-B1 Domains, Intensity, and Dynamics

A semi-automated approach using ImageJ software (NIH) was employed to identify the areas of GFP-SR-B1 localization in the images. After background subtraction, an unsharp mask filter with a large radius was applied to locally enhance contrast. Manual thresholding of filtered images was then used to generate a segment mask, which could be overlaid on the original, background subtracted image to facilitate measurement of domain parameters such as area and mean intensity.

To test differences in the dynamics properties of the GFP-SR-B1 domains, we identified in automated fashion the center of mass of the spots using a wavelet-based segmentation approach¹⁸⁰ and tracked their displacement.¹⁸¹ The method used solves a global combinatorial optimization problem whose solution identifies the overall most likely links of particle trajectories throughout a movie. It allows the tracking of the heterogeneous domain motion both during phases of diffusive and linear motion. During the linking part of the algorithm, we allowed speeds of up to 42 microns/min, as we observed some very rapid motion. We did not use the gap closing option of the algorithm, as the fluorescent labeling was consistently bright and the GFP-SR-B1 motion did not result in occlusion. We included in our dynamics analysis tracks with a lifetime of over four frames.

To calculate the linearity of the motion, we introduced a parameter ρ , which is calculated as the ratio between the head-to-tail (first point to the end point) trajectory distance divided by the total distance traveled by fluorescent domains. This way, a trajectory with ρ close to 1 signifies a linearly moving spot and a trajectory with ρ close to 0 signifies randomly moving spots. For this analysis, we excluded all stationary areas by considering spots that moved a pixel per frame on average or more.

3.5.9 Western Blotting

For Western blotting, as was done for Chapter 2, 20 µg of total protein extract or 10 µg of exosomal protein were resolved on Tris/Glycine/SDS pre-cast polyacrylamide gels (a 4-20% gradient, Bio-Rad, 30 minutes at 200 volts). Proteins were transferred onto polyvinylidene fluoride (PVDF) membranes. The membranes were blocked in 5% milk in Tris-buffered saline containing 0.1% Tween 20 (TBST). The membranes were incubated with primary antibodies (diluted in blocking solution) overnight at 4 °C, was washed 3 times in 0.1% TBST (10 minutes/wash) and incubated with the appropriate HRP-conjugated secondary antibody in blocking buffer for 1 hour at room temperature. The membranes were then washed in 0.1% TBST (3 x 10 min) and developed with ECL kit (GE Healthcare). Antibodies: CD81 and GM130 (Santa Cruz Biotechnology), SR-B1 (Abcam), β-Actin (Cell Signaling Technology)

3.5.10 Lipid Raft Labeling

A375 lipid rafts were labeled using cholera toxin subunit b (CTx-B) conjugates with Alexafluor 488 or Alexafluor 647 to (Life Technologies) at a final concentration 1 µg/ml, for 30 minutes at 37 °C.¹⁷⁰ The cells were then washed in PBS and visualized using fluorescence microscopy.

3.5.11 Knockdown of SR-B1

SR-B1 was knocked down using siRNA targeted to SR-B1 (Ambion). In brief, SR-B1 siRNA and a non-targeted scrambled control were transfected into cells using RNAi Max (Life Technologies). The RNAi Max and RNA complex were allowed to incubate with the cells for 16 hrs. Cells were then washed free of the transfection reagent, fresh culture media was added, and then incubated for an additional 24 hours prior to cell treatments with exosomes and HDL NP. SR-B1 knockdown was measured using western blot.

3.5.12 Fluorescence Microscopy

Fluorescence microscopy was performed using an A1R confocal microscope with assistance from the Northwestern University Center for Advanced Microscopy. Images were analyzed using NIS Elements (Nikon) and ImageJ (NIH) software. Live cell confocal fluorescence microscopy to assess lipid raft dynamics was performed with a Nikon Eclipse T1 microscope equipped with an Andor iXon Ultra 897 camera and analyzed using Metamorph software (Molecular Devices).

3.5.13 Statistical Analysis

Data was expressed using \pm standard deviation of triplicate experiments. The unpaired two tailed student's t-test from GraphPad Prism software was used to analyze data. Statistical significance was considered for significant for $P \leq 0.05$. * Denotes $P \leq 0.05$, ** $P \leq 0.01$, and *** $P \leq 0.001$. FCS Express was used to analyze flow cytometry. Statistical analysis between the conditions (before and after HDL NP treatment) of GFP-SR-B1, integrated normalized intensity, and motion was performed using a permutation test¹⁸⁷ for means, which does not assume normality of the underlying distributions.

CHAPTER FOUR:

Scavenger Receptor Type B1 and High-Density Lipoprotein Nanoparticles Inhibit Myeloid Derived Suppressor Cells

This Chapter is based on work published in:

M.P. Plebanek, D. Bhaumik, P.J. Bryce, C.S. Thaxton
Molecular Cancer Therapeutics, 2017 Dec 27.

4.1 Abstract

Myeloid derived suppressor cells (MDSCs) are innate immune cells that potently inhibit T cells through a variety of mechanisms. In cancer, novel immunotherapies aimed to activate T cells can be rendered ineffective due to the activity of MDSCs. Thus, targeted inhibition of MDSCs may greatly enhance T cell-mediated anti-tumor immunity, but targeted mechanisms remain obscure. Here we show, for the first time, that scavenger receptor type B-1 (SR-B1), a high-affinity receptor for spherical high-density lipoprotein (HDL) and is expressed by MDSCs. Furthermore, we demonstrate that SR-B1 is specifically targeted by synthetic high-density lipoprotein-like nanoparticles (HDL NP), which inhibited MDSC activity. Using *in vitro* T cell proliferation assays, data show that HDL NPs specifically bind SR-B1 to inhibit MDSC activity. In murine cancer models, HDL NP treatment significantly reduces tumor growth, metastatic tumor burden, and increases survival due to an enhanced adaptive immune response. Flow cytometry and immunohistochemistry demonstrate that HDL NP-mediated suppression of MDSCs increased CD8⁺ T cells and reduced T_{reg} cells in the metastatic tumor microenvironment. Using transgenic mice lacking SR-B1, *in vivo* data clearly show that the HDL NPs specifically target this receptor for suppressing MDSCs. Ultimately, our data provide a new mechanism and targeted therapy, HDL NPs, to modulate a critical innate immune cell checkpoint to enhance the immune response to cancer.

4.2 Introduction

Modulating the immune system can be an effective mechanism to address numerous pathologies. In cancer, recent therapies including checkpoint blockade, cancer vaccines, and chimeric antigen receptor T cells are focused on activating the adaptive immune response.^{40,188,189} These therapies have shown some success. However, despite their promise, they are only effective in sub-sets of patients.^{190,191} As with natural immune responses, efficacy of these therapies is often drastically reduced by the action of specialized innate immune cells called myeloid derived suppressor cells (MDSCs), which potently inhibit adaptive immune cells.¹⁹²⁻¹⁹⁴ As such, novel mechanisms, targets, and therapies are needed to better harness the immune system as a cancer therapy with a specific focus on MDSCs.

The size, shape, and composition of natural high-density lipoproteins (HDL) is constantly being remodeled as the particles acquire and deliver cholesterol and cholesteryl ester to target cells.¹⁹⁵ The main protein constituent of HDLs, apolipoprotein A-I (apo A-I), mediates this dynamic biological process whereby cholesterol-poor discoidal forms of HDL become progressively more spherical upon cholesterol uptake¹⁹⁶ Cholesterol-rich, spherical HDLs containing apo A-I bind with a high affinity to scavenger receptor type B-1 (SR-B1).^{178,197,198} HDL binding SR-B1 has been studied most extensively in atherosclerosis where SR-B1 is expressed by innate myeloid cells such as macrophages and neutrophils.¹⁹⁹⁻²⁰¹ The interaction of apo A-I and HDLs with myeloid cells has critical importance in cardiovascular disease.^{202,203} Furthermore, in oncology, human apo A-I has been shown to generate an anti-tumor response in mouse models of cancer; however, the mechanisms remain obscure.^{204,205} Importantly, increased plasma apo A-I and HDL cholesterol are associated with reduced cancer risk in patients.²⁰⁶

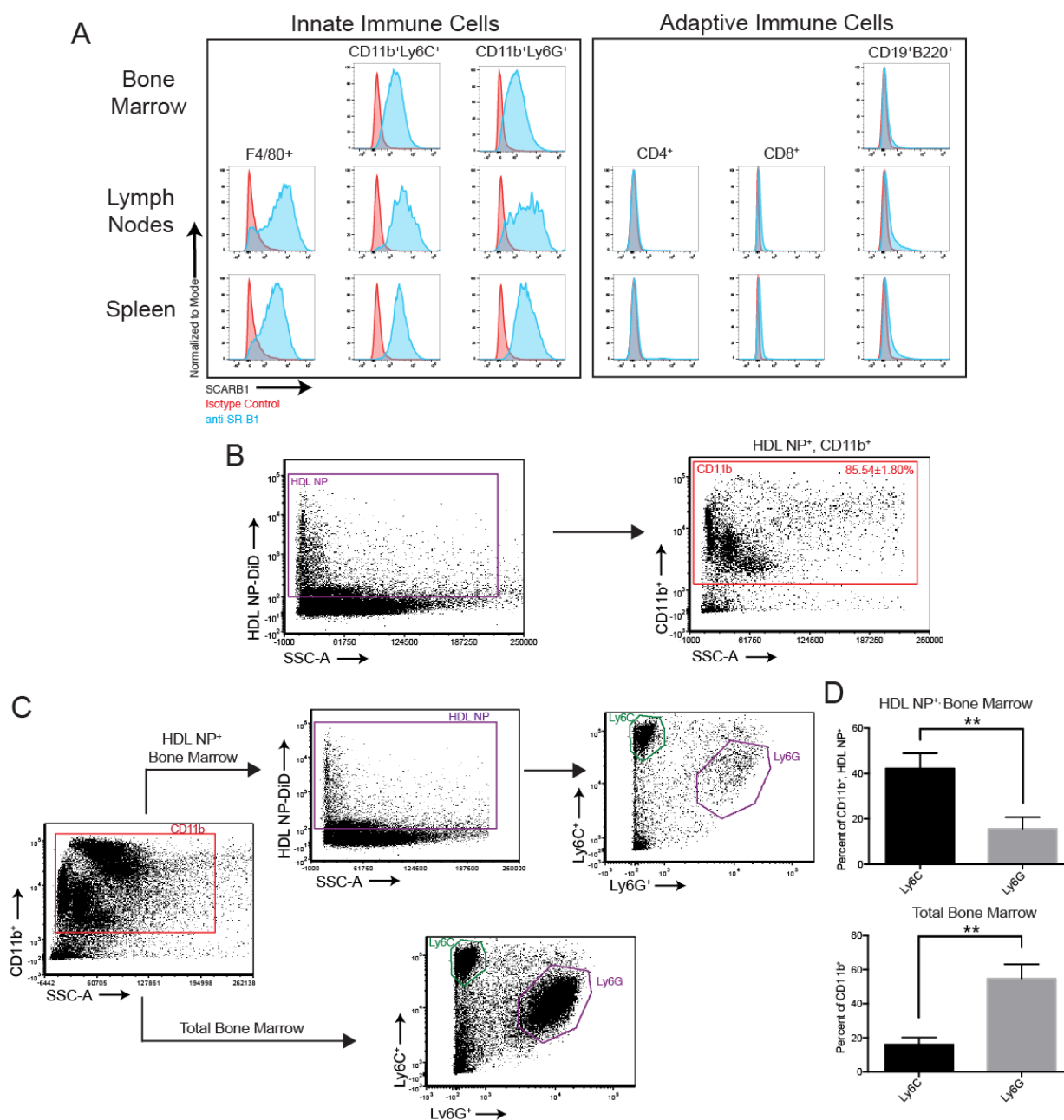


Figure 4.1: SR-B1 Expression and HDL NP Targeting of Immune Cells. (A) SR-B1 expression was quantified using flow cytometry of cells from the lymph nodes, spleen, and bone marrow of C57Bl/6 mice. (B) Flow cytometry of WT mouse bone marrow after treatment with HDL NP-DiD, first gating for HDL NP⁺ cells, to determine the percentage of HDL NP⁺ cells that are CD11b⁺. (C) HDL NPs were labeled with the DiD fluorophore and administered to C57Bl/6 mice. 24-hours later, bone marrow was isolated and the targeted immune cell distribution was determined by flow cytometry. (D) Quantification of HDL NP uptake (top) as percent of CD11b⁺, HDL NP⁺ cells that are Ly6C M-MDSCs or Ly6G PMN-MDSCs and the normal distribution of MDSC subtypes (bottom) as percent of CD11b⁺ cells that are Ly6C M-MDSCs or Ly6G PMN-MDSCs; *P* values: ***P* < 0.01 determined by two-tailed student's t-test

Given the expression of SR-B1 on myeloid cells, the role of MDSCs in bridging innate and adaptive immunity, and the involvement of apo A-I and HDL in modulating the adaptive immune response, we hypothesized that MDSCs express SR-B1 that can be targeted to reduce MDSC function and generate a potent adaptive anti-tumor immune response. To explore this hypothesis, we used spherical, functional high-density lipoprotein-like nanoparticles (HDL NPs) developed by our laboratory.^{99,207} The HDL NPs have comparable size, shape, surface charge, and surface chemistry (e.g. contain apo A-I) to natural, spherical HDLs,¹¹⁹ and more tightly bind

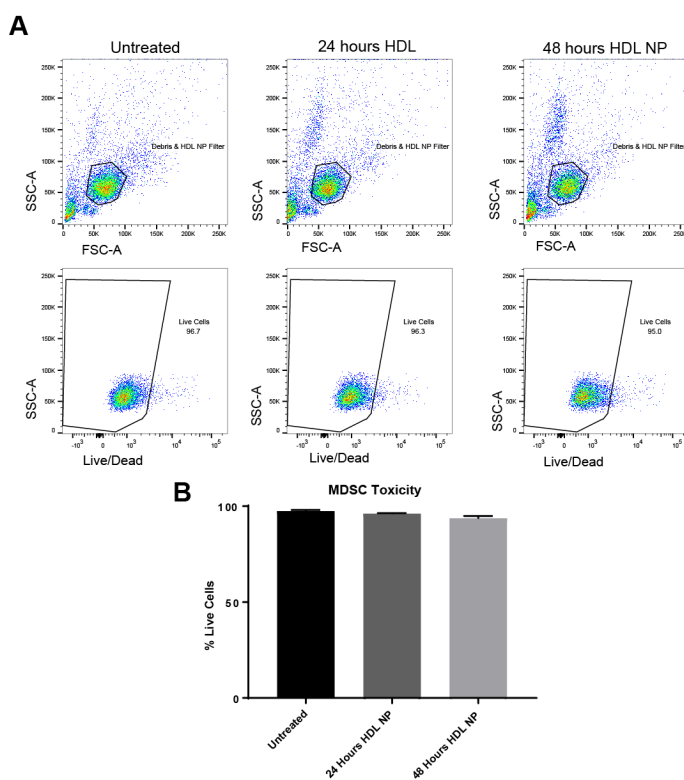


Figure 4.2: HDL NPs Display no Appreciable Cytotoxicity Towards MDSCs. Bone marrow MDSCs were isolated and placed in culture after which they were treated with PBS control or HDL NP at 50 nM for 24 or 48 hours. (A) Flow cytometry plots demonstrating the gating of MDSCs to determine live cell contents after treatment. (B) Average percent live cells for each treatment group demonstrating no substantial difference in cell death.

SR-B1 when compared to native HDL.^{122,208} Additionally, *in vivo* studies with HDL NPs have demonstrated a general lack of toxicity and a selective targeting of cells that express SR-B1.^{122,209} Data in this Chapter show that SR-B1, a high-affinity receptor for spherical HDL,^{171,210-212} is expressed by MDSCs. Targeting SR-B1 with HDL NPs reduce MDSC activity *in vitro*. In murine models of melanoma, data show that HDL NP treatment significantly reduces tumor size, metastatic tumor burden, and increases survival due to an enhanced adaptive immune response through a mechanism requiring SR-B1. Additionally, data obtained in a murine model of lung cancer confirmed that HDL NP treatment reduced tumor volume and mass. As such, HDL NPs and MDSC expression of SR-B1 enable therapeutic modulation of a critical innate immune cell checkpoint on adaptive immunity.

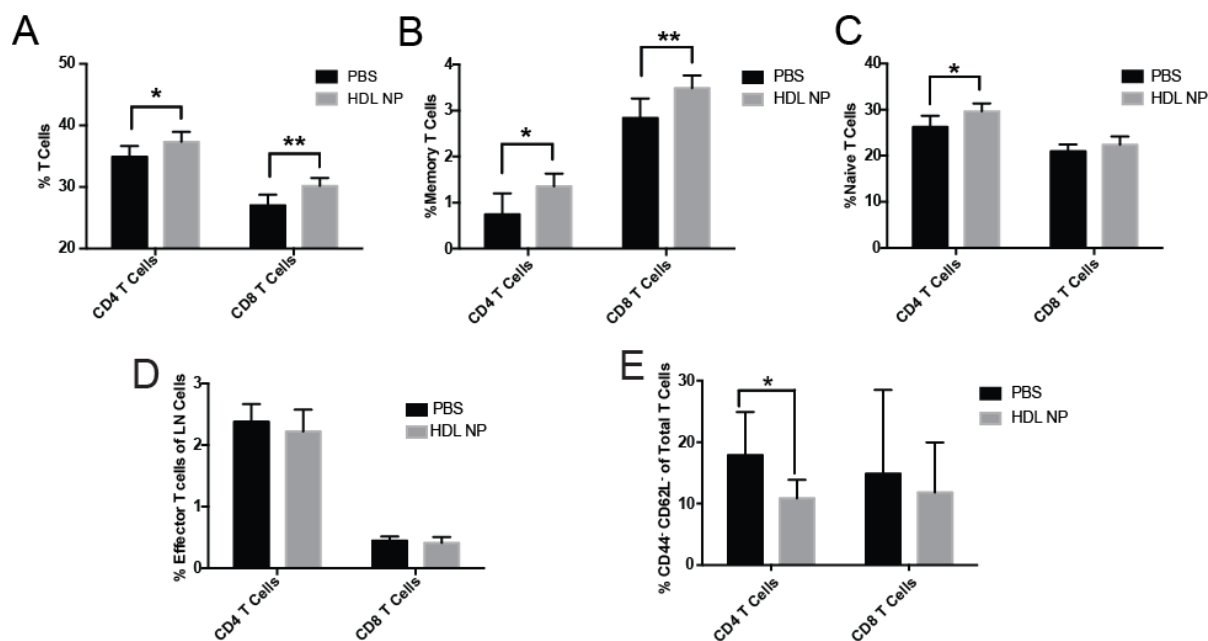


Figure 4.3: HDL NP Treatment Modulates Systemic T Cell Distributions. After treating WT mice with either PBS or HDL NP (1 μ M, 3X/ week for 1 week), immune cell distributions in lymph nodes were analyzed by flow cytometry to quantify CD4⁺ and CD8⁺ T cells with regard to T cells of each subtype, (A) Total T Cells (B) memory T cells, (C) naïve T cells, (D) effector T cells, (E) and CD44⁺CD62L⁻ naïve T cells. (To mark cleaved CD62L, impaired homing to lymphoid organs.) (A-E) *P* values: **P* < 0.05 and ***P* < 0.01 determined by two-tailed student's *t*-test.

4.3 Results

4.3.1 MDSCs Express SR-B1 and are Targeted by HDL NPs

Initially, we determined immune cell expression of SR-B1 and if, by extension, HDL NPs targeted the cells expressing SR-B1 after systemic administration. First, we isolated immune cells from the bone marrow, lymph nodes, and spleens of C57Bl/6 mice and measured SR-B1 expression. Flow cytometry revealed substantial SR-B1 expression in CD11b⁺Ly6C⁺ monocytic cells and moderate SR-B1 expression in CD11b⁺Ly6G⁺ granulocytic cells across all three immune foci (**Figure 4.1A**). With regard to adaptive immune cells, SR-B1 was not expressed by T or B cells (**Figure 4.1A**). Next, HDL NPs were labeled with fluorescent dye (DiD) and administered to C57Bl/6 mice via tail vein injection to demonstrate specific targeting to SR-B1⁺ cells. At 24 hours, data showed that HDL NPs targeted CD11b⁺ cells ($\sim 86 \pm 2\%$) in the bone marrow (**Figure 4.1B**). Furthermore, both CD11b⁺Ly6G⁺ and CD11b⁺Ly6C⁺ cells in the bone marrow were targeted, but with a high specificity toward CD11b⁺Ly6C⁺ cells (**Figure 4.1C, D**). At three and five days following injection, labeled MDSCs were no longer detected in the bone marrow. Importantly, HDL NPs have no cytotoxic effects for CD11b⁺Ly6G⁺ and CD11b⁺Ly6C⁺ cells (**Figure 4.2A, B**). These data demonstrate that CD11b⁺Ly6G⁺ and CD11b⁺Ly6C⁺ cells express SR-B1 and are targeted by HDL NPs.

4.3.2 HDL NPs Prime the Adaptive Immune System in the Lymph Nodes

In order to determine if HDL NP targeting of SR-B1 to CD11b⁺Ly6G⁺ and CD11b⁺Ly6C⁺ MDSCs impacts the adaptive immune cell balance in healthy mice, we systemically administered HDL NPs (3X/week for 1 week) to C57Bl/6 mice and then measured T cell distributions in lymph nodes. We focused on T cells because of their capacity for robust anti-tumor immune responses¹⁹² and lymph nodes to sample multiple immune foci. Data show

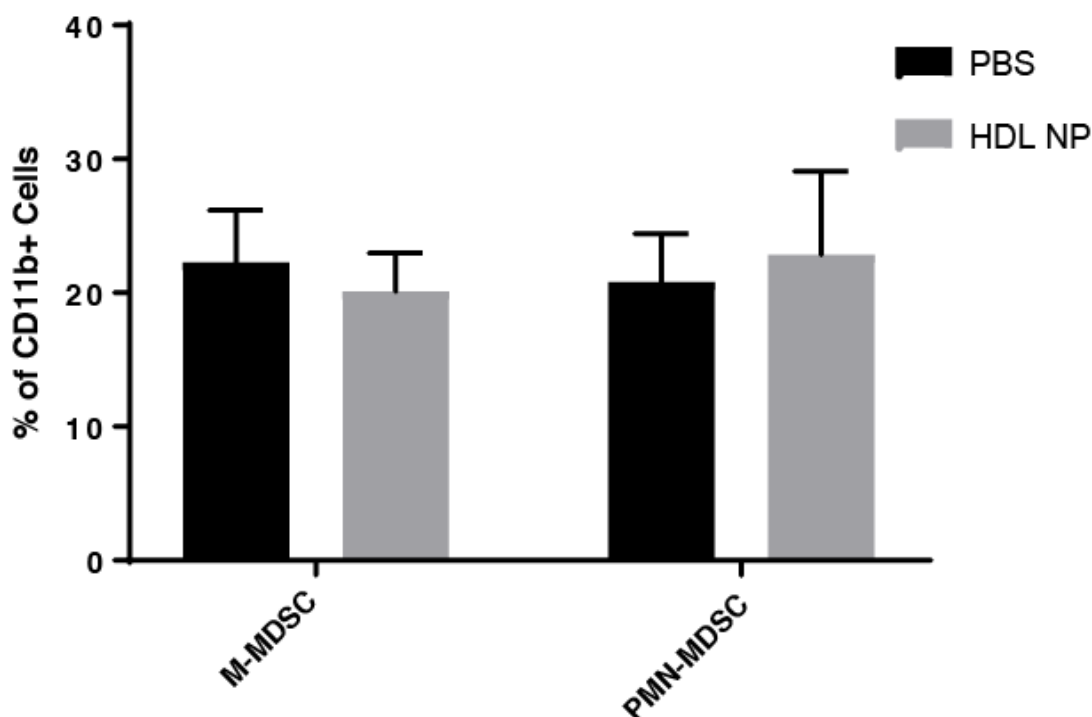


Figure 4.4: Effect of HDL NPs on MDSC Burden in Lymph Nodes. HDL NP pre-treatment and MDSC distribution in the lymph nodes. After treating WT mice with either PBS (n=7) or HDL NP (n=7) 3X/ week for 1 week, MDSC presence was analyzed in lymph node isolates by flow cytometry. Data demonstrate no significant modulation of either M-MDSCs or PMN-MDSCs in the lymph nodes.

that after systemic HDL NP administration there was a significant increase in the number of total CD4⁺ and CD8⁺ T cells in the lymph nodes compared to control mice (**Figure 4.3A**). Additionally, there were increased memory CD4⁺ and CD8⁺ T cells and a significant increase in the CD4⁺ naïve T cell population (**Figure 4.3B, C**). There was no significant change in the effector populations of either T cell subset (**Figure 4.3D**). Interestingly, the increased naïve CD4⁺ T cells results from a relative reduction in CD4⁺CD62L⁻CD44⁻ T cells after HDL NP treatment (**Figure 4.3E**). These data correlate with one of the key suppressive mechanisms of MDSCs; whereby they cleave CD62L from naïve T cells to prevent them from penetrating lymphoid organs and becoming activated.²¹³ Additionally, there was no difference in either M-

MDSC or PMN-MDSCs in the lymph nodes after HDL NP treatment (**Figure 4.4**). These data, and SR-B1 expression being limited to MDSCs, greatly suggests that HDL NPs interact directly with MDSCs to reduce their suppressive functions and systemically prime the adaptive immune response.

4.3.3 HDL NPs Relieve T Cell Suppression Caused by MDSCs

To test whether the measured differences in T cell numbers were caused by an HDL NP-mediated reduction in MDSC activity, we measured the ability of the MDSCs to suppress CFSE-labeled T cell proliferation after stimulation with anti-CD3/CD28 conjugated beads. The MDSCs were isolated from mice with well-established melanoma lung metastases. Mice were treated 3 times with either PBS or HDL NPs (every 48 hours, 100 μ l, 1 μ M) whereupon MDSCs were isolated from the bone marrow, then cultured with HDL NPs for 48 hours. CFSE-labeled T cells were stimulated with anti-CD3/CD28 conjugated beads. Data show that MDSCs only exposed to PBS considerably suppressed both CD4⁺ and CD8⁺ T cells at 4:1, and 8:1 ratios (T cells:MDSCs), and HDL NP treatment substantially relieved the inhibitive effects and restored proliferation at each of the tested ratios (**Figure 4.5A, B**). Mechanistically, at the molecular level, HDL NPs caused a reduction in the expression of genes critical for MDSC-mediated T cell suppression including *S100A9*, inducible nitric oxide synthase (*Nos2*), Arginase-1 (*Arg1*), chemokine (C-C motif) ligand 5 (*CCL5*), and tumor necrosis factor alpha (*TNF- α*) as measured by quantitative RT-PCR (**Figure 4.5C**). Ultimately, HDL NPs mediate a functional reduction in MDSC activity, which enables a potent adaptive immune cell activation.

4.3.4 HDL NPs Reduce Metastasis and Prolong Survival in Melanoma Mouse Models

After measuring functional inhibition of MDSCs *in vitro* and observing increased adaptive immune cells in healthy mice after treatment with HDL NPs, we hypothesized that pre-

treating a melanoma mouse model with HDL NPs to generate a primed adaptive immune system would reduce lung metastasis and cancer progression. Accordingly, we systemically administered HDL NPs (3X/week for 1 week) to C57Bl/6 mice prior to systemic inoculation

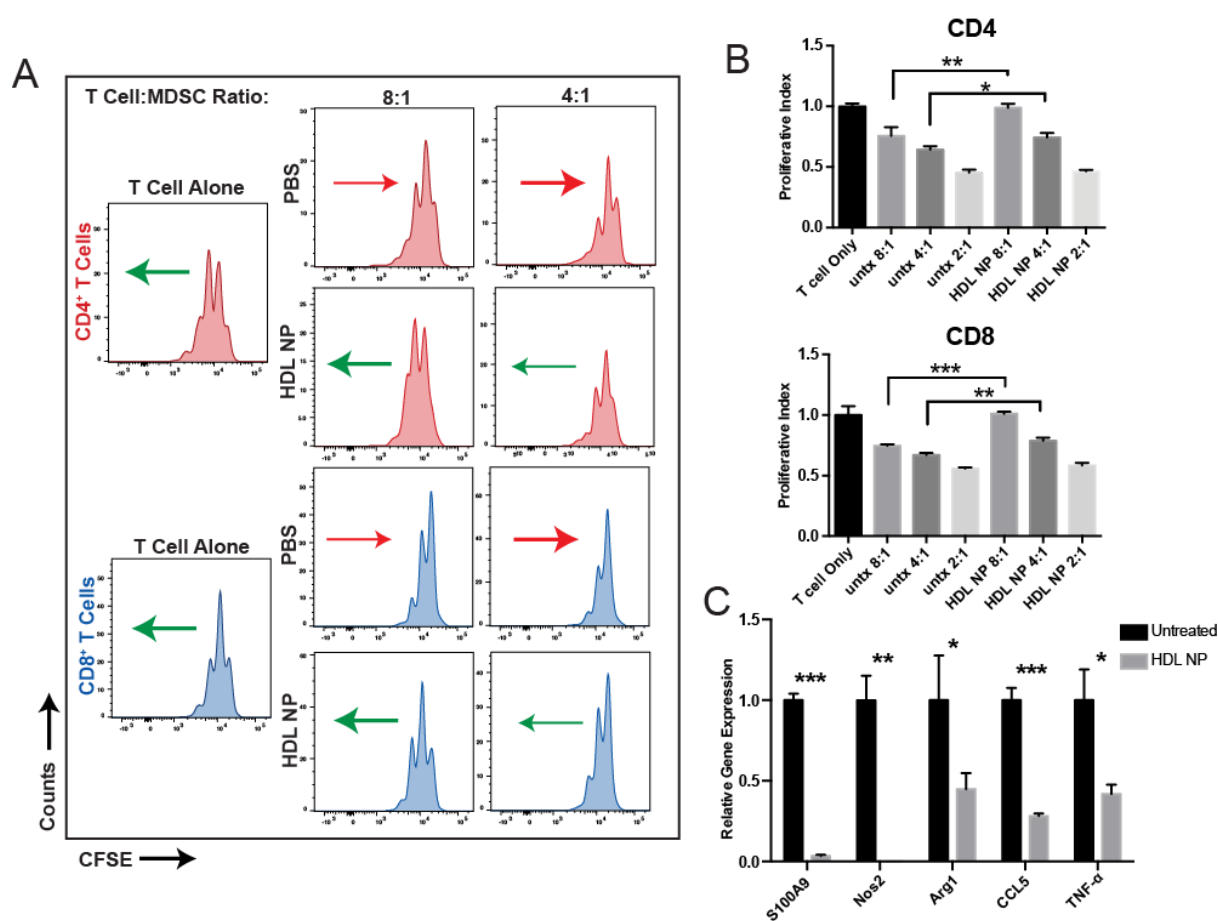


Figure 4.5: T Cell Suppression by MDSCs is Inhibited by HDL NPs. (A) After CFSE staining, T cells were stimulated using anti-CD3/CD28 conjugated beads and co-cultured for 48 hours with isolated MDSCs at 4:1 and 8:1 ratios (T cells:MDSC) from mice treated with HDL NP or PBS. Flow cytometry was used to determine CFSE labeling in CD4⁺ and CD8⁺ T cells in order to evaluate suppressive effects of MDSCs. Arrows represent the general shift (red = less proliferation and green = more proliferation) in the CFSE signal of the cell population relative to its PBS or HDL NP treated counterpart. (B) Quantification of the proliferative index, defined by the normalized number of T cell proliferations in A. (C) After treating MDSCs with HDL NPs, gene expression was quantified by RT-PCR for S100A9, NOS2, Arg1, CCL5 and TNF- α with comparison made to PBS treated control MDSCs. A-C, *P* values: **P* < 0.05, ***P* < 0.01 and ****P* < 0.001 by two-tailed student's t-test.

with B16F10 melanoma cells (**Figure 4.6A**). Two weeks after melanoma cell administration, mice were sacrificed and the metastatic burden was quantified in the lungs. Data demonstrated that HDL NP therapy drastically reduced lung metastasis with regard to the number and size of the lung lesions (**Figure 4.6B-D**). Notably, *in vitro* data demonstrate no direct cytotoxic effect of HDL or HDL NPs on B16F10 melanoma cells (**Figure 4.7**). In order to test if systemic HDL NP pre-treatment translated to an impactful survival advantage, the study was repeated with continued time points and survival was quantified. Data clearly show a significant prolonged survival advantage for mice treated with only three doses of HDL NPs prior to introduction of tumor cells (**Figure 4.6E**). Finally, we utilized an orthotopic primary tumor model of melanoma to demonstrate that HDL NPs increased mouse survival as compared to PBS control treated mice. C57Bl/6 mice received intradermal injections of B16F10 melanoma cells. When the tumors became palpable, we treated the mice with intravenous injections of HDL NP (100 μ l, 1 μ M) or PBS (100 μ l) every 48 hours. Data demonstrate a significant increase in survival of the HDL NP treated mice when compared to those treated with PBS (**Figure 4.8**). Together these data suggest that HDL NP treatment leads to reduced melanoma metastasis and significantly increased survival.

4.3.5 *SR-B1 is Necessary for HDL NP-mediated Inhibition of Metastasis*

To unequivocally implicate SR-B1 targeting by HDL NPs, the *in vitro* suppression of SR-B1^{-/-} MDSCs on T cell proliferation was measured after HDL NP treatment and compared to controls treated with PBS. SR-B1^{-/-} MDSCs inhibited T cell proliferation at T cell:MDSC ratios of (4:1 and 8:1), but, unlike MDSCs isolated from wild-type mice (**Figure 4.5A**), HDL NP treatment did not inhibit MDSC activity with a resultant increase in T cell proliferation when

compared to controls (**Figure 4.9A, B**). These data demonstrate that HDL NPs function through SR-B1 to regulate MDSC function.

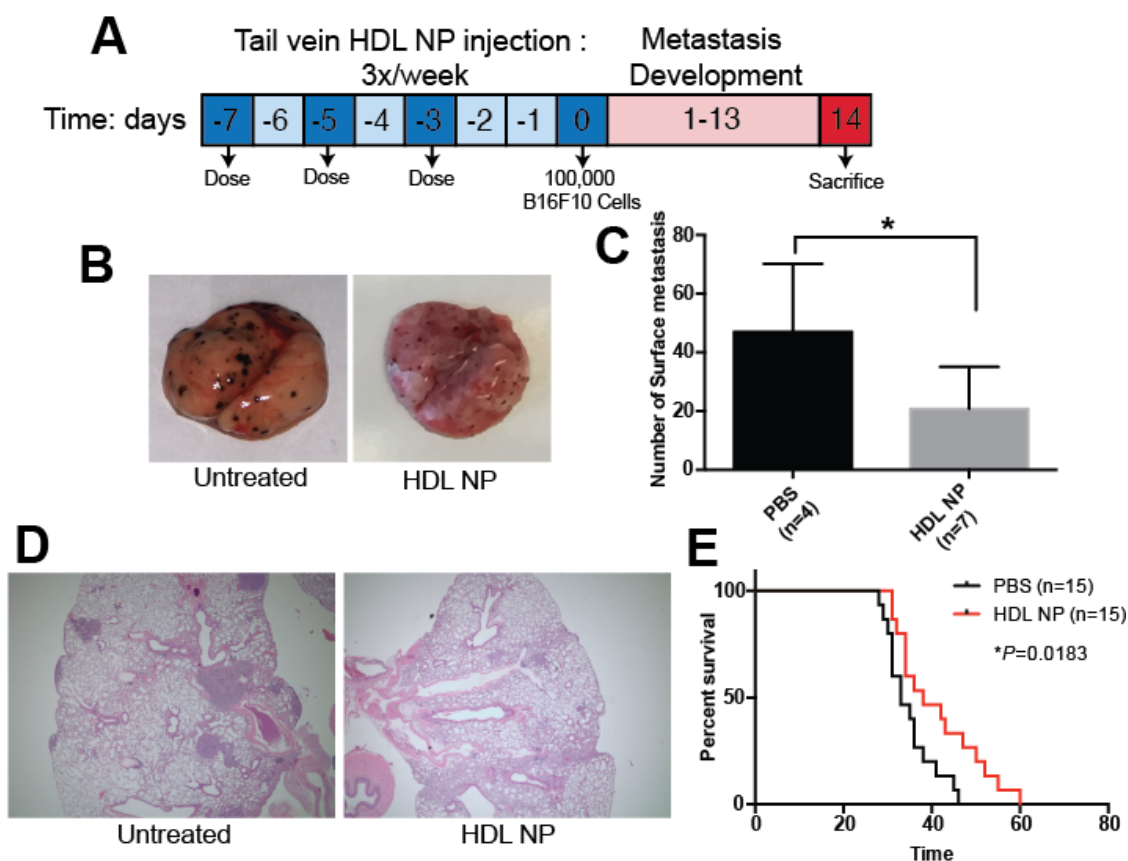


Figure 4.6: Metastasis and Survival of Mice Pre-Treated with HDL NPs prior to Tumor Cell Administration. (A) Time-line of C57Bl/6 metastatic lung colonization assay of mice treated with HDL NP (100 μ l, 1 μ M) or PBS (control) and inoculated with 1×10^5 B16F10 cells. (B) Lung colonization 2-weeks after tumor inoculation. Surface metastases appear as darkly pigmented lesions. (C) Quantification of the number of surface metastases in B. *P* values: **P* < 0.05 by two-tailed student's t-test. (D) H&E staining of lungs from mice in B. (E) Survival curve of PBS and HDL NP pre-treated mice after inoculation with B16F10 cells showing increased survival after HDL NP treatment (n=15 per group).

Furthermore, in order to demonstrate the *in vivo* function of HDL NPs on MDSC activity using SR-B1^{-/-} mice, we applied the same pre-treatment regimen and melanoma model as was employed above for wild type mice. Convincingly, data showed that HDL NPs had no effect in SR-B1^{-/-} mice at reducing lung metastasis when compared to controls (**Figure 4.10A, B**). In fact,

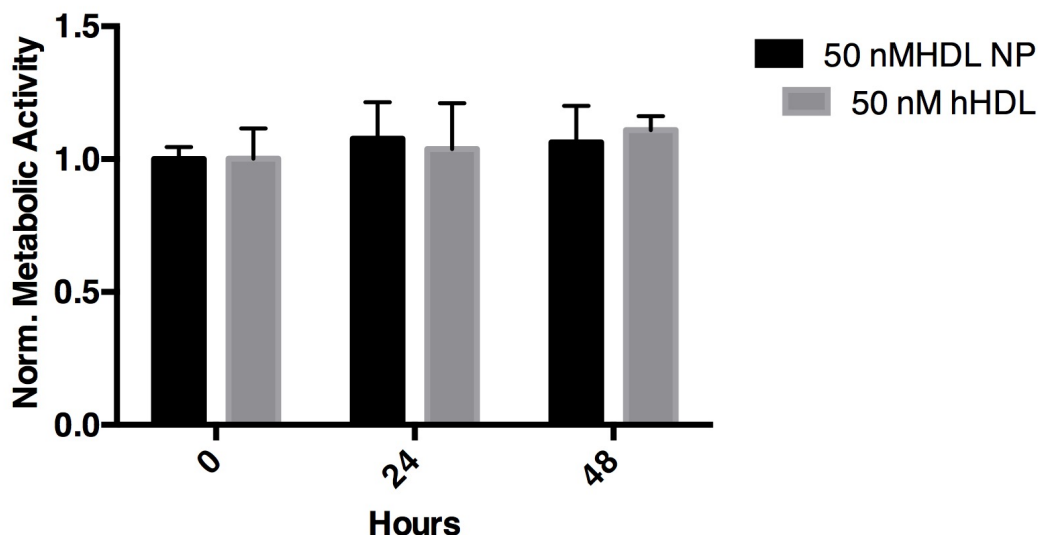


Figure 4.7: HDL NPs are Not Inherently Toxic to Melanoma Cells. B16F10 cells were incubated with HDL NPs (50 nM) or human HDL (hHDL) for up to 48 hours. MTS assay shows no reduction in viability after treatment with HDL NP or hHDL when compared to untreated (0 hour time point).

both PBS control and HDL NP-treated SR-B1^{-/-} mice demonstrated an enormous increase in metastasis compared to wild-type mice (**Figure 4.10A, B**). The finding of increased metastasis may be due to the fact that SR-B1^{-/-} mice demonstrate high circulating HDL,²¹⁴ which can bind SR-B1 expressed by the B16F10 cells and enhance metastasis and proliferation.²¹⁵ To further explore, wild-type mice were lethally irradiated and then transplanted with bone marrow obtained from SR-B^{-/-} mice. This allowed for the generation of wild-type mice with myeloid cells that do not express SR-B1 (BMT, **Figure 4.11**). Like in the SR-B1^{-/-} mice, HDL NP treatment did not reduce melanoma lung metastasis versus PBS in the BMT mice (**Figure 4.10A, B**). Also, the number of lung metastases in both the PBS and HDL NP treated BMT groups were not statistically different from the numbers measured in wild-type mice treated with PBS, but were statistically different from the reduction in metastasis observed after the wild-type mice were

treated with HDL NP (**Figure 4.10B**). Finally, transplanting the SR-B1^{-/-} bone marrow to wild-type mice reduced the number of metastases observed from the larger numbers measured in the mice with global SR-B1 knockout (**Figure 4.10B**). In short, HDL NPs clearly and selectively target SR-B1 to release an innate immune checkpoint imparted by MDSCs.

4.3.6 HDL NPs Reshape the Immune Microenvironment in Melanoma Metastases

Next, we sought to demonstrate that HDL NP therapy administered after established metastatic disease would confer a robust adaptive immune response resulting in tumor clearance. To this end, we initiated melanoma lung metastasis by systemic administration of B16F10 cells. After waiting 5 days to allow ample time for the mice to develop florid lung metastases, we started treating the mice with HDL NPs (3X/ week for two weeks) (**Figure 4.12A**). After treatment, the mice were sacrificed and the metastatic burden, as well as the immune cell populations in the tumor microenvironment, were quantified using flow cytometry and immunohistochemistry. The 18-day endpoint was chosen as it provided substantial time for metastases to develop, but was less than the 28-day mark when control treated mice began to die from disease burden (see **Figure 4.6E**). Data demonstrated reduced metastatic burden in mice treated with HDL NPs (**Figure 4.12B, C**). Furthermore, HDL NP treatment profoundly increased the number of cytotoxic CD8⁺ T cells, and decreased Ly6C⁺ cells, both globally in the lung and in the tumor microenvironment, measured by flow cytometry and IHC, respectively (**Fig. 4.12D-J**). Furthermore, HDL NP treatment led to a reduction CD4⁺ cells as measured by flow cytometry (**Fig. 4.12E**). Upon closer inspection by IHC, this was likely the result of a reduction in FOXP3⁺ T regulatory cells (**Figure 4.12H**). Additionally, in the tumor microenvironment, we measured an increase in CD3⁺ T cells and a reduction in F4/80⁺ cells (macrophages) after HDL NP treatment (**Figure 4.13A, B**). Collectively, these data demonstrate that HDL NPs potently

enhance an adaptive immune response in the tumor microenvironment of established metastases and significantly reduce disease burden.

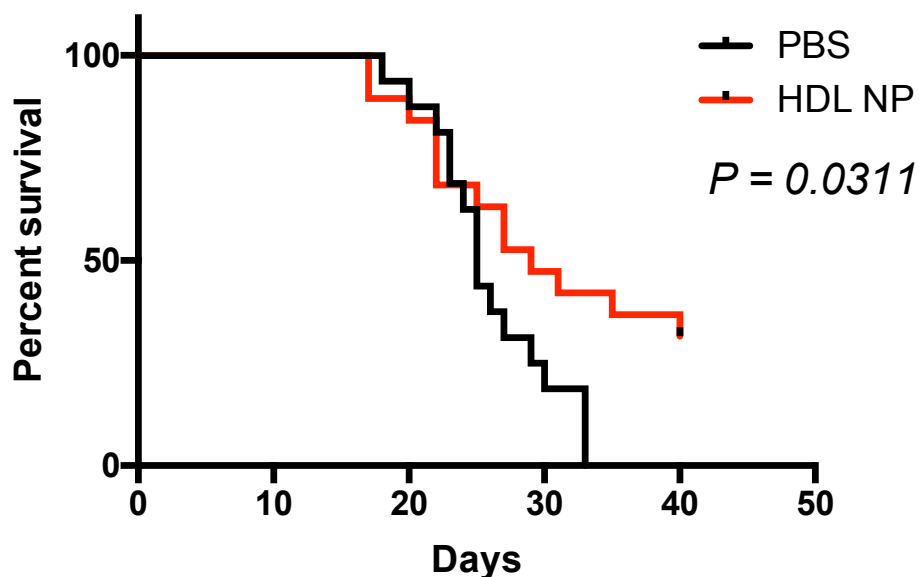


Figure 4.8: Survival of Mice with Orthotopic B16F10 Tumors after Treatment with HDL NPs. B16F10 cells were injected intradermally into C57Bl/6 mice and subsequently treated with HDL NPs via the tail-vein. HDL NP treatment led to a significant increase in survival as compared to PBS treated controls.

4.3.7 HDL NPs Significantly Reduce Lewis Lung Carcinoma Growth

In order to demonstrate that HDL NPs were effective in treating multiple cancer types, we utilized another syngeneic murine model and measured tumor response with and without HDL NP treatment. Lewis lung carcinoma (LLC) xenografts were established in C57Bl/6 mice and the ability of systemically administered HDL NPs to slow LLC progression was tested. Tumors were initiated by injecting 5×10^5 LLC cells subcutaneously into the flank of each mouse. The tumors were measured once palpable, 8 days following the initial injection, and every 48 hours thereafter. On day 9, once the tumors reached $\sim 50 \text{ mm}^3$, the mice were treated intravenously with 200 μl of 1 μM HDL NPs for a total of 5 doses over the ensuing 10 days. Data show a significant reduction in the volume and weight of the tumors after treatment with

HDL NPs upon the completion of the study (**Figure 4.14A-C**). These data are noteworthy because they demonstrate that HDL NPs can effectively slow the progression of multiple cancer types.

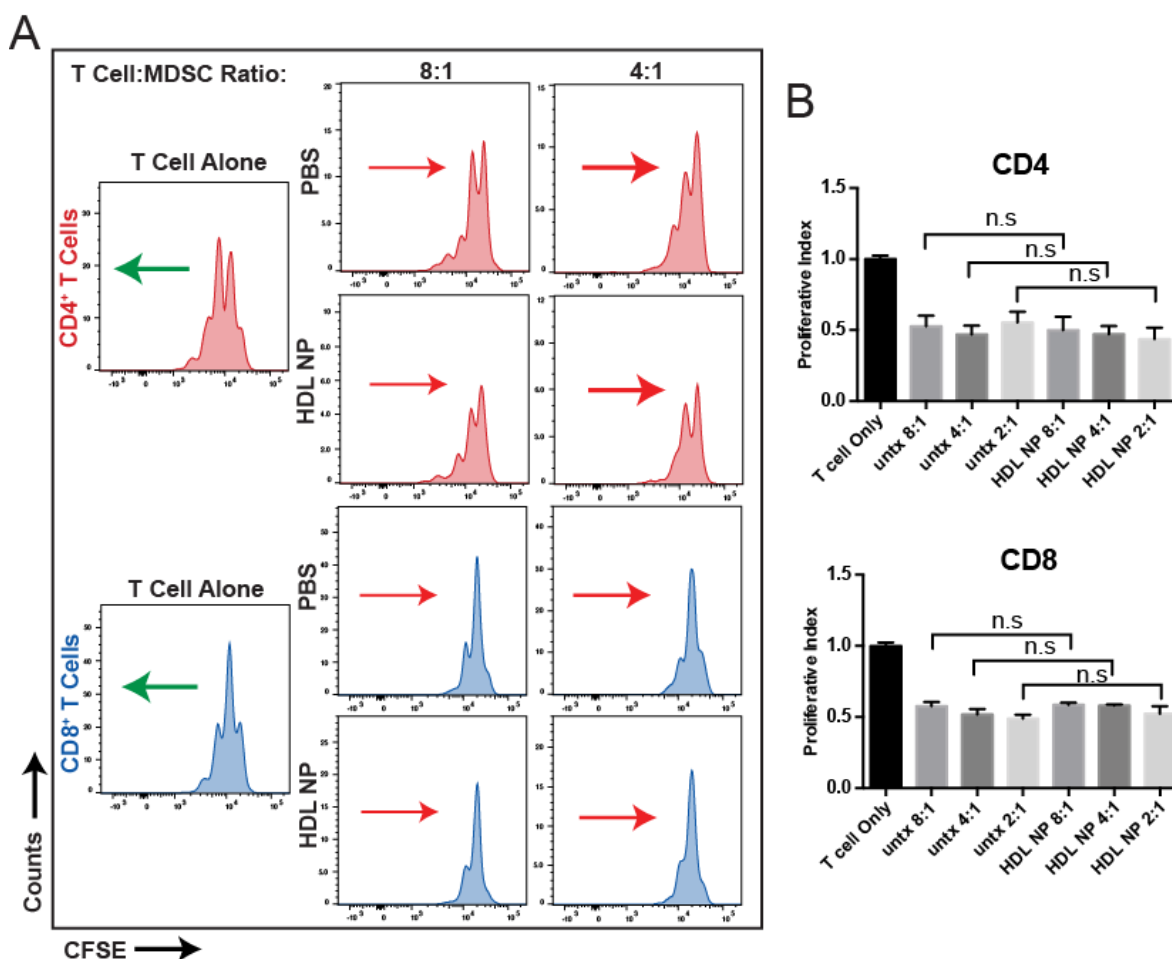


Figure 4.9: Effects of SR-B1 on HDL NPs Ability to Inhibit MDSC Activity. (A) T cells stained with CFSE and stimulated with anti-CD3/CD28 conjugated beads were co-cultured for 48 hours with MDSCs isolated from tumor bearing SR-B1^{-/-} mice at ratios of 4:1 and 8:1 (T cell:MDSC). The mice had been treated with HDL NP or PBS. Flow cytometry determined CFSE labeling in CD4⁺ and CD8⁺ T cells in order to evaluate suppressive effects of SR-B1^{-/-} MDSCs. Arrows represent the general shift (red = less proliferation and green = more proliferation) in the CFSE signal of the cell population relative to its PBS or HDL NP treated counterpart. (B) Quantification of the proliferative index, defined by the normalized number of T cell proliferations in A. *P* values: **P* < 0.01 by two-tailed *t*-test, n.s.= not significant.

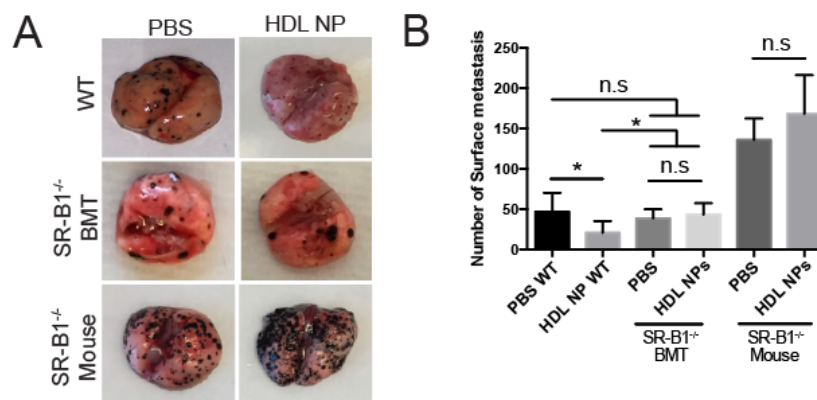


Figure 4.10: Effects of SR-B1 on HDL NP Efficacy. (A) B16F10 lung colonization in SR-B1^{-/-} mice after pre-treatment with HDL NPs compared with SR-B1^{-/-} mice treated with PBS and WT control mice. (B) Quantification of the surface metastases in A. P values: *P < 0.01 by two-tailed t- test.

4.4 Discussion

High-density lipoprotein nanoparticles are capable of therapeutically activating an adaptive immune response by targeting SR-B1 expressed by MDSCs. Using HDL NPs, our data are the first to implicate SR-B1 expression by MDSCs as a target for therapy. Data in healthy mice reveal that HDL NP targeting of MDSCs may modulate the balance of the immune system to reduce immune suppression and activate T cell-mediated immunity. Furthermore, *in vitro* data using MDSCs obtained from mice with existing melanoma lung metastases support that HDL NP targeting of SR-B1 reduces MDSC-mediated suppression and enhances CD8⁺ and CD4⁺ T cell proliferation, with a more pronounced effect on the CD8⁺ T cells.²¹⁶ *In vivo* data collected in murine models of cancer clearly show that HDL NP binding to SR-B1 reduces the ability of MDSCs to inhibit T cell mediated immune responses to cancer through molecular mechanisms, summarized in **Figure 4.15**, which include reduced MDSC expression of *ARG1*, *NOS2*, and *CCL5*. SR-B1 targeting data were confirmed using MDSCs isolated from SR-B1^{-/-} mice using both *in vitro* and *in vivo* model systems. Ultimately, from a therapeutic standpoint, HDL NP

treatment significantly reduced tumor growth, metastatic tumor burden, and increased survival by enhancing adaptive immunity.

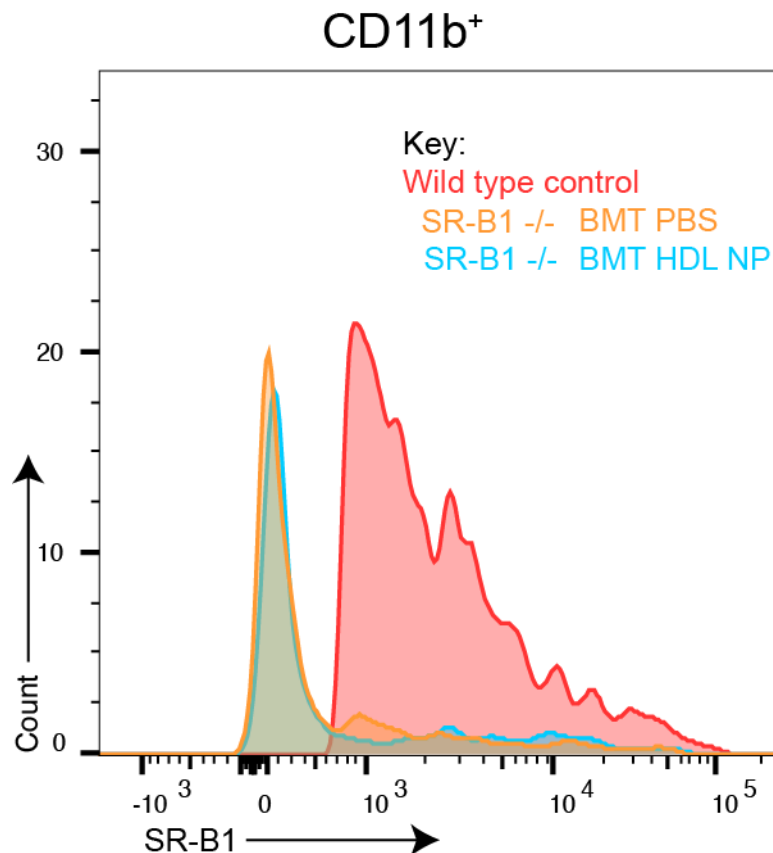


Figure 4.11: SR-B1 null Bone Marrow Transplant. SR-B1 expression in CD11b⁺ myeloid cells obtained from wild-type mice after lethal irradiation and transplant of bone marrow harvested from SR-B1^{-/-} donor mice. Flow cytometry data demonstrate the lack of SR-B1 expression in CD11b⁺ cells obtained from the bone marrow of wild-type mice following bone marrow transplant (BMT) using cells from SR-B1^{-/-} mice. Bone marrow from PBS and HDL NP treated BMT mice are included.

With regard to HDL metabolism, our data are consistent with other studies that employed apoA-I knockout mice demonstrating that these mice were much more prone to tumor growth and metastasis. In this model, apo A-I infusions led to reduced metastasis and tumor burden.^{204,205} However, the mechanism through which apo A-I achieved this response was not identified. Additional studies implicate the other two known transporters of cholesterol to HDLs, ATP binding cassette transporters A1 and G1 (ABCA1 and ABCG1), in the proliferative abilities

of hematopoietic stem cells with an emphasis on myeloid progenitor cells.²⁰² Data showed that proliferation of these cells was increased in mice lacking both ABCA1/ABCG1, and reduced myeloid progenitor cell proliferation was achieved by infusing HDL, but not apo A-I. Finally, data from humans suggest that serum levels of HDLs and apo A-I correlate with a reduced incidence of cancer, metastasis, and cancer-associated mortality.²⁰⁶ Collectively, these findings substantiate our data demonstrating that HDL NPs target SR-B1 expressed by MDSCs, reduce their function, and enhance anti-tumor immunity.

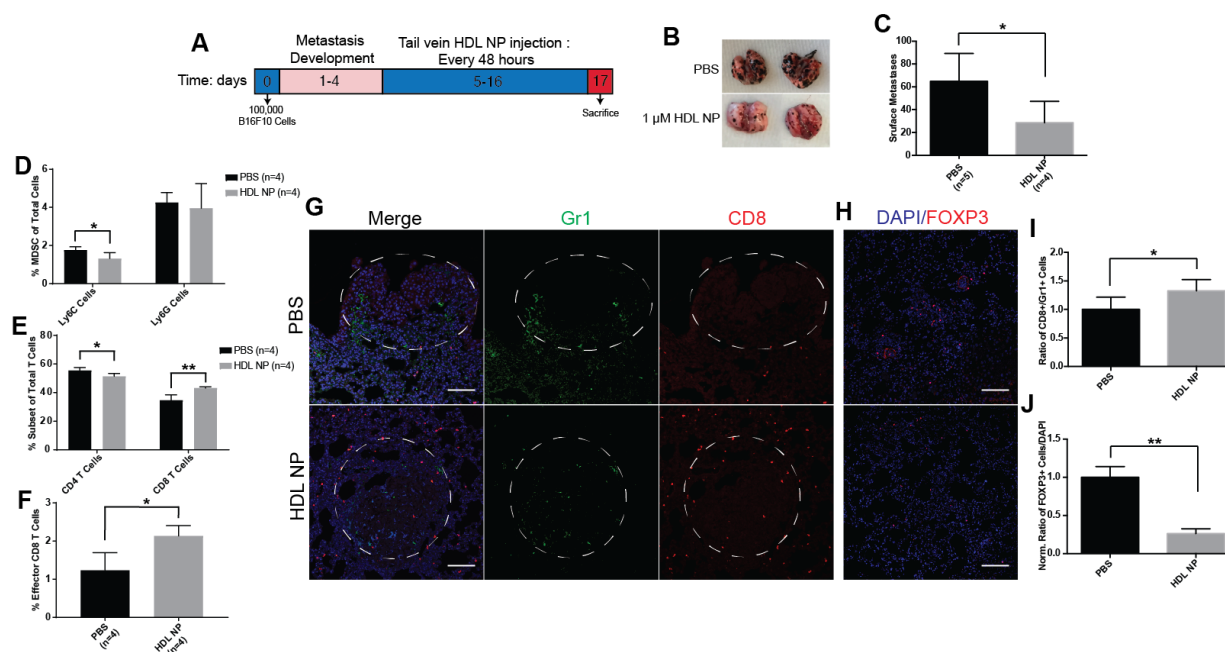


Figure 4.12: Established Melanoma Metastasis Model. B16F10 lung metastases were established for 5 days and then treatment was initiated with HDL NPs for two weeks. (A) HDL NP treatment timeline. (B) Representative images showing metastatic lung burden after HDL NP treatment. (C) Quantification of lung metastases in B. (D-F) Flow cytometry analysis of digested lungs of mice with B16F10 metastasis after HDL NP treatment (D) Total percent PMN- and M-MDSCs. (E) CD4 and CD8 T cell population subsets. (F) Total effector T cell percentage. (G) IHC of lungs for CD8⁺ T cell (red) and Gr-1 (green) tumor infiltration after HDL NP treatment in mice with metastases. (H) IHC of T regulatory cells in the lungs of B16F10 metastasis bearing mice after HDL NP treatment. (I) Quantification of CD8⁺:GR1⁺ cells infiltrating the metastatic tumor in H. (J) Quantification of the number of T regulatory cells in H. (A-J) *P* values: **P* < 0.05 and ***P* < 0.01 by two-tailed t-test.

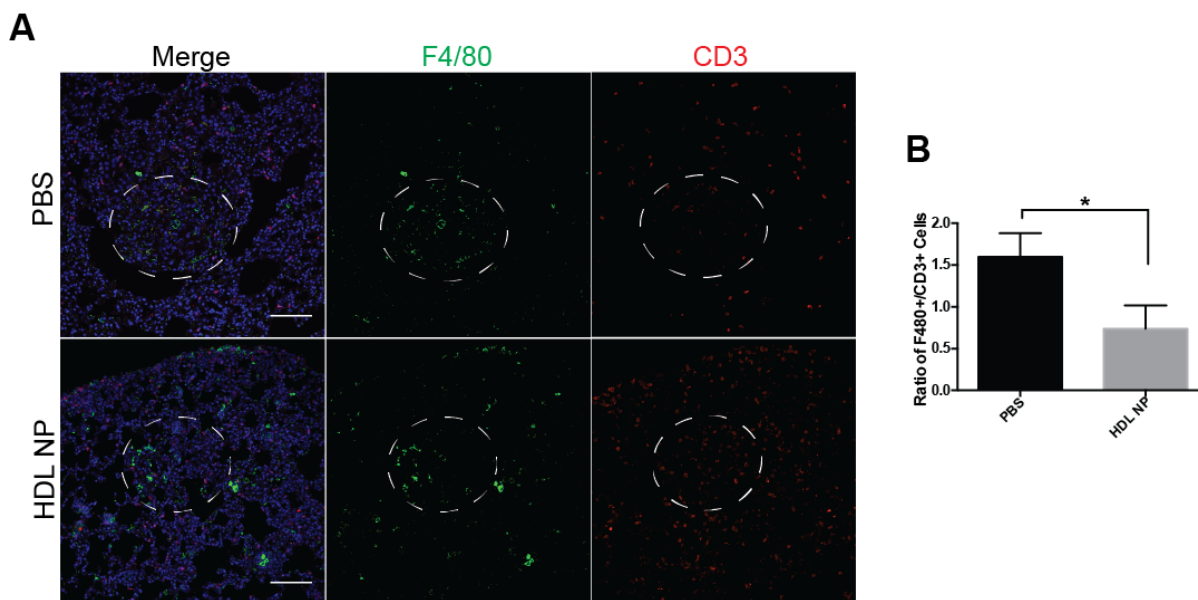


Figure 4.13: HDL NPs Reshape the Immune Microenvironment in Established Melanoma Metastasis. 1×10^5 B16F10 melanoma cells were injected I.V. into C57Bl/6 mice and allowed to develop for 5 days, at which point mice were treated with HDL NPs according to the dosing scheme in **Figure 4.12A** or treated with control PBS. **(A)** Lungs were dissected and macrophages (F4/80) and T cells (CD3) were analyzed by IHC. Metastatic tumor outline in dotted white line. Scale bar 100 μ m **(B)** The ratio of tumor associated macrophages to tumor infiltrating T cells from **A** was quantified (n=5). *P* values: **P* < 0.05 by two-tailed student's t-test.

High-density lipoproteins function to transport cholesterol, and cholesterol metabolism is known to play a critical role in the proliferation of myeloid cells.²¹⁷ For instance, patients receiving HMG-CoA reductase inhibitors (i.e. “statins”), which inhibit the rate-limiting step in *de novo* cholesterol synthesis, have reduced neutrophil and monocyte counts, further demonstrating the importance of cholesterol metabolism to myeloid cell homeostasis.²¹⁸ Utilizing the HDL NP, a mimic of mature spherical HDL that binds SR-B1, enabled us to identify and implicate this receptor on MDSCs. The potency of the HDL NPs at reducing multiple MDSC functions is attributed to tight binding of SR-B1 imparted by the gold nanoparticle core that stabilizes the HDL NP size and shape, and has been shown to potently

reduce cellular cholesterol.^{99,122} Therefore, specifically reducing cellular cholesterol by targeting SR-B1 with HDL NPs has great potential to suppress the function of MDSCs.

Our data (**Figure 4.1A**), and work by others,²¹⁹ demonstrate that, in addition to MDSCs, macrophages also express SR-B1. In the tumor microenvironment macrophages can be polarized to an M1, tumor inhibitive, or M2, tumor promoting, phenotype.¹⁸ The current work does not address differences in macrophage polarization in the tumor microenvironment due to HDL NP treatment. However, data obtained using the established melanoma tumor model show that HDL NP treatment reduced the F4/80⁺:CD3 cell ratio in the tumor microenvironment, and did not appear to change the number of F4/80⁺ cells in the tumor microenvironment (**Figure 4.13A, B**). Further studies of HDL NP effects on macrophages and macrophage polarization are currently underway in our laboratory.

Targeting MDSCs can be an extremely effective cancer treatment especially in combination with other drugs.²²⁰ Recently, researchers have shown that suppressing MDSCs with non-specific DNA methyltransferase and histone deacetylase inhibitors can eradicate tumors resistant to conventional checkpoint blockade.²²¹ There has also been significant discussion focused on preventing the recruitment of MDSCs to the tumor site by targeting the chemokine receptors CXCR2 and CXCR4 and colony stimulating factor 1 receptor (CSF1R).²²² Ultimately, targeting MDSCs and inhibiting their suppressive functions is a promising treatment, especially alongside other immune activators, to treat cancer. Certainly, exquisite targeting of SR-B1 by HDL NPs provides a new strategy to reduce MDSC activity and enhance antitumor immunity and combining HDL NPs with other immunotherapies may prove to be an even more effective therapeutic.

In summary, work presented in this Chapter conclusively demonstrate that SR-B1 is expressed by MDSCs. Engaging this receptor by HDL NPs inhibits MDSC function and activates an adaptive immune response to cancer. Interestingly, our data also point to the importance of cholesterol metabolism to MDSC biology. From a therapeutic standpoint, HDL NPs may augment the efficacy of existing immunotherapies whose function is drastically reduced by MDSCs. Therefore, combination therapies using HDL NPs with conventional checkpoint inhibitors or cell therapies, may provide significant therapeutic benefit. In short, SR-B1-targeted HDL NP therapy may be effective for multiple diseases, like cancer, potentiated by MDSCs.

4.5 Materials and Methods

4.5.1 Cell Culture

B16F10 and Lewis Lung Carcinoma (LLC) cells were purchased from American Type Culture Collection (ATCC), and cultured in DMEM containing 10% fetal bovine serum (FBS) and 1% penicillin/streptomycin (Life Technologies). Cells were passaged every 48-72 hours. B16F10 cells were purchased ~2 years ago, frozen at passage 3, and used for experiments prior to passage 8. The LLC cell line was purchased ~3 years ago, frozen at passage 3, and experiments were conducted prior to passage 8. Both of the cell lines are murine and were not authenticated. Mycoplasma testing was conducted using Plasmotest Mycoplasma Detection Kit (Invivogen), and the cells were found to be negative (10/01/2017). Mouse T cells isolated for MDSC suppression assays were cultured in RPMI-1640 containing 10% FBS, 2.5% HEPES, 1% penicillin/streptomycin, 1% sodium pyruvate, 1% non-essential amino acids, and 0.1% 2-mercaptoethanol. Mouse MDSCs were grown in RPMI containing 10% FBS, 1%

penicillin/streptomycin, IL-6 (10 ng/ml, Biolegend) and GM-CSF (20 ng/ml, Biolegend) for maturation. Cell cultures were maintained in 5% CO₂ at 37°C.

4.5.2 Experimental Animals

Mice were housed and cared for at the Northwestern University Center for Comparative Medicine according to the NIH guidelines and following protocols approved by the Northwestern University Animal Care and Use Committee. C57Bl/6 mice at 6-8 weeks old were purchased from Jackson Laboratories. All animals were used soon after purchase. For SR-B1 knockout experiments, male and female heterozygous SCARB1^{Tm1Kri} (SR-B1^{-/-}) were purchased

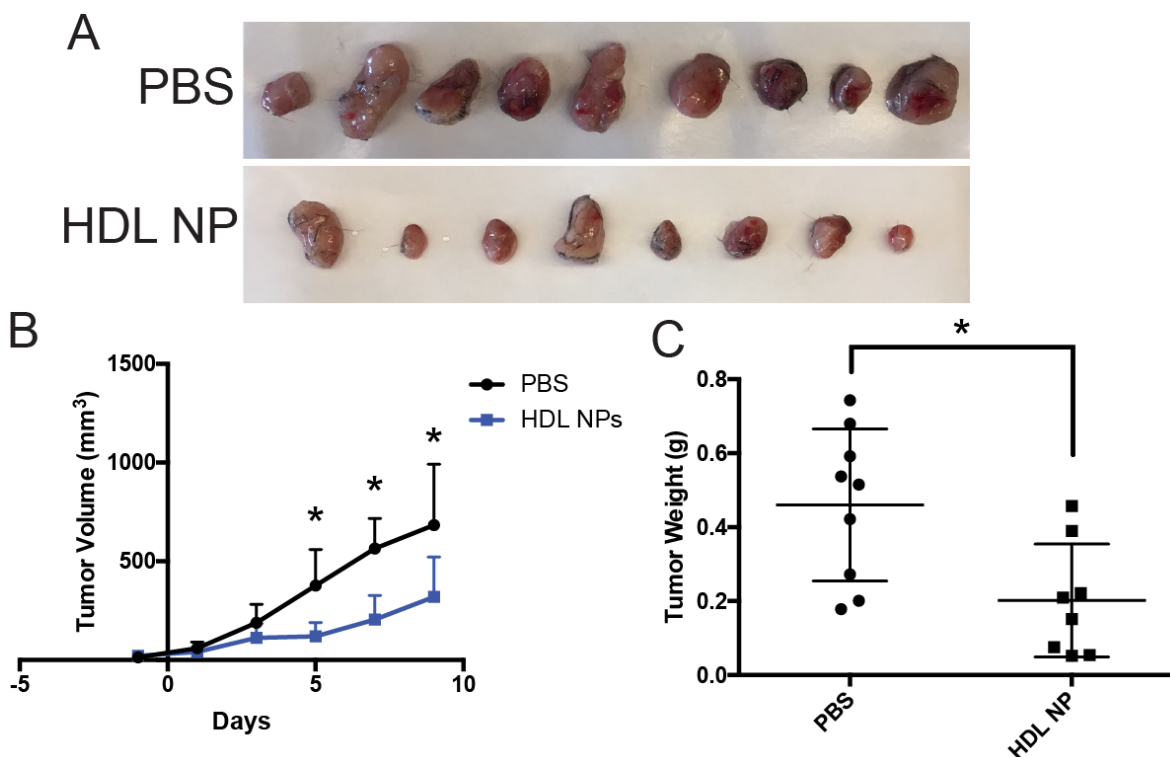


Figure 4.14: HDL NPs Inhibit Lewis Lung Carcinoma Tumor Growth. (A-C) LLC tumor xenograft study in C57Bl/6 mice. (A) LLC tumors excised from C57Bl/6 mice following treatment with phosphate buffered saline (PBS) or HDL NPs. (B) LLC growth curve as measured by volume (mm³) over the HDL NP treatment course. (C) The weight (g) of the LLC tumors shown in A. *P* values: **P* < 0.05 by two-tailed student's t-test.

from Jackson Laboratory and bred to generate homozygous null mice. Female SR-B1^{-/-} are sterile. Animals were weaned at 21 days of age and genotyped. At 6 weeks of age mice were utilized for experiments, as appropriate. Mice were randomized for all experiments and researchers were blinded during analysis.

4.5.3 HDL NP Synthesis

High-density lipoprotein-like nanoparticles (HDL NPs) were synthesized and characterized as previously described in the methods section of Chapter 3.⁹⁹ Briefly, citrate stabilized 5 nm diameter gold nanoparticles (AuNP, Ted Pella) were used as a template for surface chemical modification. Purified human apolipoprotein AI (apoA-I, MyBioSource) was incubated with a solution of AuNPs (80 nM) at 5-fold molar excess (400 nM, final) overnight at room temperature (RT) with gentle stirring. Next, the phospholipids, 1-2-dipalmitoyl-sn-glycero-3-phosphocholine (DPPC) and 1,2-dipalmitoyl-sn-glycero-3-phosphoethanolamine-N-[3-(2-pyridyldithio)propionate] (PDP-PE) were added at 250 molar excess relative to [AuNP] in a mixture of ethanol and water (1:4), and allowed to incubate at RT for 4 hours with gentle stirring. The HDL NPs were then purified and concentrated using tangential flow filtration. The HDL NP concentration and final conjugate size were determined using UV-Vis spectrophotometry ($\epsilon_{\text{AuNP}} = 9.696 \times 10^6 \text{ M}^{-1}\text{cm}^{-1}$ at $\lambda_{\text{max}} = 520 \text{ nm}$) and dynamic light scattering (DLS, Malvern Zetasizer), respectively.

For fluorescence-tagged HDL NPs, the lipophilic fluorophore dialkylcarbocyanine (DiD, Life Technologies) was added to 1 ml of 1 μM HDL NPs at a 2.5 molar excess (2.5 μM) and incubated at 37 °C for 1 hour with mild shaking. Non-conjugated dye was washed from the particles by centrifugation at 14,000 x g for 1 hour, decanting of the supernatant, and then the particle pellet was re-suspended in water followed by an additional wash step.

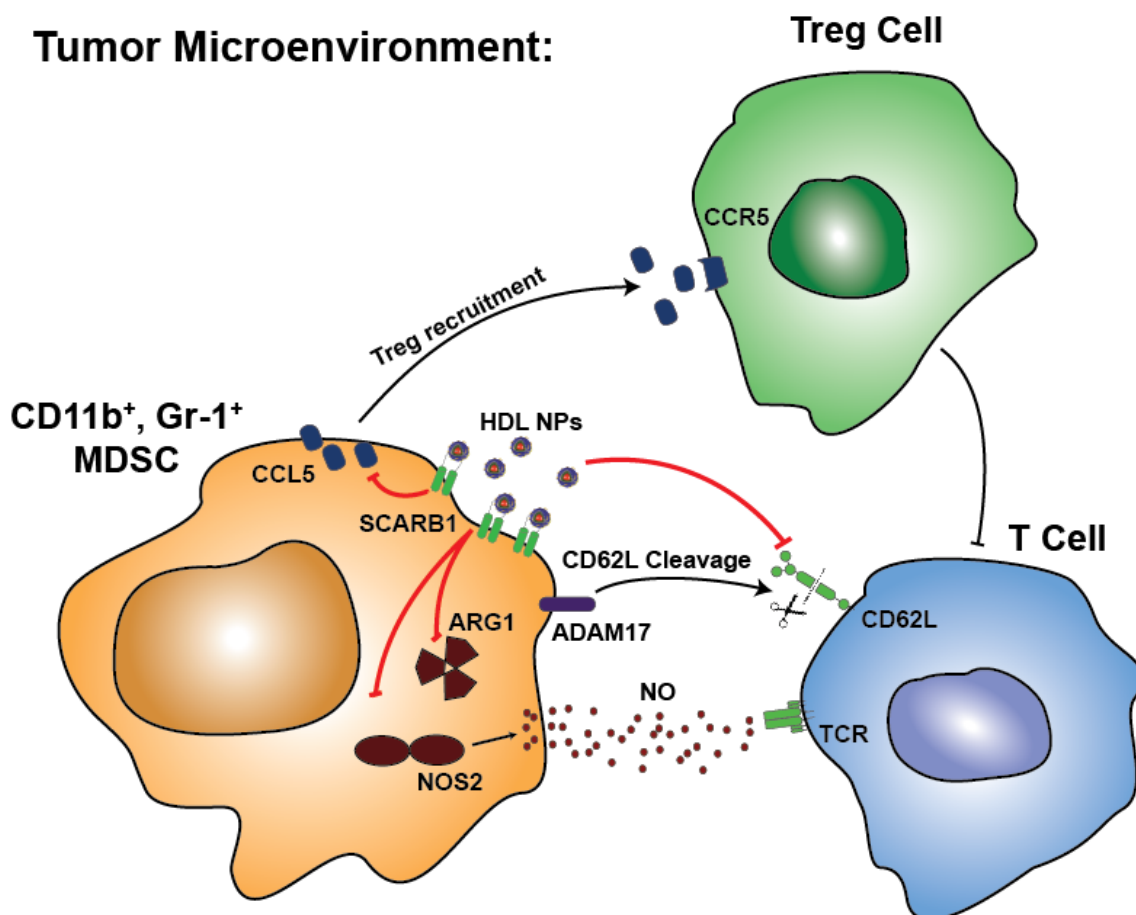


Figure 4.15: Summary of HDL NP Effects on MDSCs. HDL NPs reduce the functions of MDSCs by multiple mechanisms through SR-B1. HDL NPs inhibit the production of NO by downregulating NOS2 and ARG1. Additionally, HDL NPs inhibit CCL5 production blocking the recruitment of T regulatory cells and prevent the cleavage of CD62L allowing for T cell recruitment to lymphatic tissues.

4.5.4 Melanoma Lung Colonization

HDL NP pre-treatment studies: C57Bl/6 mice were treated via the tail vein with 100 μ l HDL NPs at a concentration of 1 μ M every 48 hours for a total of 3 doses. 72 hours following the final dose, mice were inoculated with 1×10^5 B16F10 melanoma cells and metastatic tumors were allowed to form over the course of 2 weeks at which point mice were sacrificed, lungs dissected and the metastatic tumors were counted (pigmentation allowed for easy visualization). Lungs

were then fixed and processed for IHC, see below. For the survival study, mice were treated as outlined above but removed from the study upon reaching the survival endpoint. Outlined in our accepted IACUC protocol.

SR-B1	NB400-104A	FC	3:100	Novus
CD11b	M1/70	FC	1:100	BD Pharmingen
F4/80	BM8	FC, IHC	1:100, 1:400	Biologend, eBiosciences
Ly6C	HK1.4	FC	1:200	Biologend
Ly6G	1A8	FC	1:100	Biologend
CD3	145-2 C11, 17A2, SP7	FC, IHC	1:100, 1:500	Biologend, Abcam
CD4	RM4-4,	FC	1:100	
CD8	53-6.7, Polyclonal	FC, IHC	1:100, 1:400	Biologend, Abcam
CD19	eBio1D3	FC	1:100	eBiosciences
B220	RA3-6B2	FC	1:100	Biologend
CD44	IM7	FC	1:100	Biologend
CD62L	MEL-14	FC	1:100	BD Biosciences
Gr-1	RB6-865	IHC	1:100	R&D Systems
FOXP3	Polyclonal	IHC	1:200	Abcam
Anti-Rat IgG	Polyclonal	IHC secondary-488	1:100	Jackson ImmunoResearch
Anti-Rabbit IgG	Polyclonal	FC, IHC secondary-Cy5	1:100	Novus, Jackson ImmunoResearch

Table 4.1: List of Antibodies used in Chapter 4

Established melanoma metastasis models: C57Bl/6 mice were inoculated with 1×10^5 B16F10 melanoma cells via the tail vein and the metastatic tumors were allowed to form over the course of 5 days prior to HDL NP dosing. At day 5, mice were treated with HDL NPs at a concentration of 1 μ M (200 μ L) every 48 hours for 2 weeks. Mice were then sacrificed, lungs and lymph nodes were dissected, the metastatic tumors were counted, and samples were processed for IHC.

4.5.5 Isolation of Bone Marrow Cells

Mouse bone marrow (BM) cells were isolated as described previously in Chapter 2.¹⁵² C57Bl/6 mice were sacrificed and the hind limbs were removed using aseptic technique, leaving the femur and tibia intact. The excess muscle was removed from the bones with a razor blade. The bones were then cut at the joints and the bone marrow flushed with sterile DPBS (calcium and magnesium free) using a 1 ml syringe with a 27-gauge needle. Bone marrow cells were centrifuged at 300 x g and re-suspended in MACS buffer prior to MDSC isolation.

4.5.6 Isolation of Lymph Node Cells

C57Bl/6 mice were sacrificed and the inguinal, axillary, cervical, and mesenteric lymph nodes were harvested using aseptic technique. Lymph nodes were then pressed through a 70 µm cell strainer to rupture the capsule and then flushed through using sterile PBS to generate single cell suspensions. Isolated cells were centrifuged at 300 × g for 10 minutes and then re-suspended in either MACS buffer (Miltenyi Biotech) for T cell isolation or PBS for analysis by flow cytometry.

4.5.7 Isolation of Spleen Cells

C57Bl/6 mice were sacrificed and the spleens harvested using aseptic technique. Spleens were finely cut and pressed through a 70 µm cell strainer with repeated flushes of sterile PBS to capture both the red and white pulp in single cell suspensions. Red blood cells (RBCs) were then separated and discarded from the rest of the contents through density gradient centrifugation using Histopaque-1077 (Sigma-Aldrich) at room temperature. Any excess RBCs were lysed using RBC lysis buffer (Roche). The remaining cells were re-suspended in PBS for analysis by flow cytometry.

4.5.8 Isolation of Lung Cells

C57Bl/6 mice were euthanized and lungs were removed and rinsed in PBS. Per mouse, lungs were minced in RPMI and subsequently incubated in digestion buffer containing 250 units of collagenase type IV and 200 units of Type IV DNase I in 8 mL of RPMI. Lungs were incubated in digestion buffer for 1 hour at 37 °C with gentle shaking. The digestion was quenched by adding FBS to a final concentration of 5%. The lungs were subsequently filtered through a 70 µm cell strainer and rinsed in an additional 5 ml of RPMI with 5% FBS. Cells were centrifuged at 300 x g for 10 minutes, re-suspended in 2 ml of ACK red blood cell lysis buffer and allowed to incubate for 10 minutes at 4 C. Cells were again centrifuged at 300 x g for 10 minutes and washed in PBS. Cells were counted and re-suspended in PBS at 1×10^7 cells/ml prior to proceeding to flow cytometry.

4.5.9 Orthotopic Melanoma Survival Study

C57Bl/6 mice were inoculated with 5×10^4 B16F10 melanoma cells injected intradermally into the flank. Once the tumors became palpable, ~10 days following tumor cell inoculation, mice were treated every 48 hours with HDL NPs (100 µl, 1 µM). Survival of HDL NP and PBS treated mice was recorded. The study was terminated at Day 40, one week following the death of the final PBS-treated control mouse.

4.5.10 Lethal Irradiation and Bone Marrow Transplant

C57Bl/6 mice were treated with two doses of 500 rads of whole body irradiation separated by a two-hour break. Six hours following the final dose of radiation mice, were transplanted with 1×10^6 bone marrow cells from SR-B^{-/-} mice. Mice were monitored for 1 month, allowing time for reconstitution of the immune system, at which point mice were subjected to the melanoma lung colonization experiment, as described previously.

4.5.11 MTS Assay

B16F10 cells were plated in 96-well plates at a concentration of 20,000 cells/ml (2,000 cells/well) in 100 μ l of DMEM, 10% FBS. Cells were allowed 24 hours to adhere to the dish at which point fresh media was added containing 50 nM HDL NP or natural human HDL (hHDL) (MyBiosource) and allowed to incubate for 24 or 48 hours. Then, the media was aspirated and the cells were washed with PBS. 80 μ l of fresh serum free DMEM was added, as well as 20 μ l of [3-(4,5-dimethylthiazol-2-yl)-5-(3-carboxymethoxyphenyl)-2-(4-sulfophenyl)-2H-tetrazolium] (MTS) (Promega). A baseline absorbance was measured at 490 nm on a Synergy 2 plate reader (Biotek) and the cells incubated for 1 hour, at which point a second absorbance measurement was taken. Normalized metabolic activity was calculated by subtracting the baseline reading and normalizing to untreated control.

4.5.12 Flow Cytometry

Isolated cells were washed with PBS and stained with 0.25 μ l of LIVE/DEAD Fixable Aqua Dead Cell Stain (Thermo Fisher Scientific) in 500 μ l of PBS for 20 min at room temperature in the dark. After washing in FACS buffer, cells were blocked with anti-CD16/CD32 (BD Biosciences) for 10 min and then stained in 100 μ l of Ab mixture in FACS buffer (as detailed in Table 3.1) for 30 min at 4°C in the dark. Cells were then washed in FACS buffer and fixed in 4% paraformaldehyde. Samples were run on an LSRII flow cytometer (BD Biosciences). Compensation on samples collected by the LSRII was performed in FlowJo or FCS Express post-collection.

4.5.13 MDSC HDL NP Treatment and Toxicity Analysis

Bone marrow of mice with B16F10 metastatic melanoma tumors established over the course of two weeks was isolated as outlined above and Myeloid Derived Suppressor Cells (MDSC) were

separated using magnetic activated cell sorting (MACS) MDSC isolation kit (Miltenyi Biotech). Cells were plated in a 24-well plate at 1×10^6 cells/well. Cells were treated in triplicate with 50 nm HDL NP for either 24 or 48 hours later a separate triplicate. At which point, cells were harvested, washed to clear HDL NP and then either analyzed using flow cytometry for percent live cell analysis or used in MDSC mediated T cell suppression assay.

Gene	Primer
Actb	Fwd: 5'-aagtcagtgtacaggttaagcc-3'
	Rev: 5'-gtccccaacttgagatgtatg-3'
S100A9	Fwd: 5'-gaagaaagagaagagaaatgaagcc-3'
	Rev: 5'-ctttgccatcagcatcatacactcc-3'
Nos2	Fwd: 5'-cacttctgctccaaatccaac-3'
	Rev: 5'-gactgagctgttagagacactt3'
Arg1	IDT Assay ID: Mm.PT.58.8651372
CCL5	IDT Assay ID: Mm.PT.58.43548565
TNF	Fwd: 5'-ctgagtctgcaaagggagag-3'
	Rev: 5'-cctcaggaagaatctggaaag-3'
SR-B1 (Genotyping)	Oimr 7768 5'-atctcagccttaggccctgt-3'
	Oimr 7769 5'-tcaaaccctgtgacaacagc-3'
	Oimr 7770 5'-atagattcgcccttgtgtcc-3'

Table 4.2: List of PCR Primers used in Chapter 4

4.5.14 T Cell Suppression Assay

T cells were gathered from lymph nodes isolates (as described above) employing EasySep Mouse T cell isolation kit (Stemcell). T cells were then stained with CFSE (Thermo Fisher Scientific) as previously described.²²³ T Cells were re-suspended in PBS supplemented with 5% FBS after isolation to a cell concentration of 8×10^6 cells/ml. CFSE was added at a final concentration of 5 μ M for 7 minutes at room temperature in the dark. Cells were then washed 3 times in PBS with 5% FBS. Subsequently, T cells were exposed to the MDSC mediated T cell suppression assay as described previously.²²⁴ Ultimately, T cells were plated in a 96-well plate at

2×10^5 cells/well and co-cultured with MDSC isolated from wild-type or SR-B1^{-/-} mice, at a 2:1, 4:1 and 8:1 ratio of T cells to MDSCs in triplicate. T cells were stimulated using anti-CD3/CD28 activation beads (Invitrogen) and cultured for 48 hours after which they were harvested and analyzed by flow cytometry using FlowJo V10.

4.5.15 Immunohistochemistry

C57Bl/6 mice were sacrificed and the lungs perfused with 10% neutral-buffered formalin, excised and allowed to fix in formalin for up to 48 hours. The lungs were paraffin embedded and sectioned at the Robert H. Lurie Comprehensive Cancer Center Pathology Core. H&E staining was also performed by the Robert H. Lurie Comprehensive Cancer Center Pathology Core. H&E staining was analyzed using light microscopy on a Nikon epifluorescence microscope with SPOT software.

For immune microenvironment staining, five- μ m sections were de-paraffinized in two changes of xylene, 10 minutes each. Sections were hydrated by sequential incubations in ethanol, 100% (2 times), 95%, 70% and 50%, 5 minutes each. Samples were then washed in deionized water and the antigens were retrieved by heating in 1x Target Retrieval Solution, Citrate pH 6 (Dako) for 20 min at 95°C followed by cooling to room temperature. For staining, sections were washed in PBS and blocked in PBS with 1% BSA, 1% donkey serum, and 0.3% triton-x 100 and 0.01% sodium azide for 1 hour at room temperature. Primary antibodies (**Table 4.1**) were diluted in blocking buffer and incubated overnight at 4°C. Samples were washed 3 x 10 minutes in PBS and incubated for 1 hour with fluorophore-conjugated secondary antibodies (**Table 4.1**) in blocking buffer. Slides were then washed three times in PBS with 0.1% tween 20, counterstained with DAPI and mounted in Fluoromount-G (Southern Biotech). Fluorescence was visualized using a Nikon A1R confocal microscope at the Center for Advanced Microscopy at

Northwestern University and image analysis was performed using NIS Elements (Nikon) and ImageJ/Fiji (National Institute of Health).

4.5.16 Lewis Lung Carcinoma Xenograft Model

5×10^5 LLC cells (ATCC) were injected subcutaneously into the flanks of C57Bl/6 mice. The tumors were allowed to develop for 8 days at which point the tumor dimensions were measured using calipers. Tumors were measured and volumes determined using the formula $\text{volume} = [(\text{width}^2 \times \text{length}) \times 0.5]$ with width being the smaller of the two measurements every 48 hours until the study was completed.²²⁵ Following the first tumor size measurement, mice were randomly placed in groups and treated with HDL NPs (5 doses over 10 days, 200 μl , 1 μM HDL NP) or left untreated. Following treatment, mice were sacrificed and the tumors were excised and weighed.

4.5.17 RT-PCR

MDSCs were isolated as detailed above and cultured at a concentration of 1×10^6 cells/ml. MDSCs were treated with HDL NP (50 nM) or left untreated for 48 hours at which point cells were lysed and mRNA was isolated using an RNeasy kit (Qiagen), and 200 ng of RNA was converted to cDNA using iScript cDNA synthesis kit (Bio-Rad). After cDNA synthesis samples were diluted 10 times in nuclease-free water. Quantitative RT-PCR was then used to amplify and measure the cDNA content with PerfeCTa SYBR Green mastermix (Quanta) on a CFX Connect RT-PCR Detection System (Bio-Rad). (For primers see **Table 4.2**).

4.5.18 Statistical Analysis

Data were expressed using \pm standard deviation of at least triplicate experiments. GraphPad Prism version 6 was used to analyze and graph data. Microscopy and flow cytometry were analyzed using ImageJ/Fiji and FlowJo V10 or FCS Express, respectively. P values were

calculated using a two-tailed Student's T-test of unpaired samples and statistics were considered significant if $P \leq 0.05$. * Denotes $P \leq 0.05$, ** $P \leq 0.01$, and *** $P \leq 0.001$.

CHAPTER FIVE:

Concluding Remarks and Future Work

The work presented in this dissertation illustrates multiple breakthroughs, which have led to a remarkable expansion in the understanding of the metastatic microenvironment, exosome mediated signaling during cancer progression and the development of nanotechnologies to inhibit metastasis. Chapter 2 demonstrates that exosomes released from non-metastatic cancer cells can in fact suppress melanoma metastasis by promoting an innate immune cell population called patrolling monocytes. Because of the importance exosomes hold at promoting metastasis, in Chapter 3 we demonstrated that high density lipoprotein nanoparticles (HDL NPs) created in our laboratory can specifically inhibit the uptake of exosomes by cells expressing SR-B1. This is the first example of inhibiting the uptake of exosomes in a targeted manner. In Chapter 4 we went on to further develop the HDL NP platform and discovered that HDL NPs potently inhibit the activity of myeloid derived suppressor cells (MDSCs). Inhibition of MDSCs caused robust T cell activation and significantly reduced melanoma metastasis, tumor growth and increased overall survival in mouse models of melanoma.

The major finding described in Chapter 2 is that exosomes from non-metastatic cells can inhibit metastasis by activating an innate immune cell subtype, patrolling monocytes. There are numerous discoveries in addition to this that are also worth noting. First, this work confirmed what previous studies have demonstrated in that patrolling monocytes control metastasis. Additionally, pigment epithelial derived factor (PEDF) is packaged into the exosomes produced by non-metastatic melanoma cells, which in addition to recruiting patrolling monocytes, can drive the polarization of macrophages to a M1 anti-cancer phenotype. Patrolling monocytes can also engulf tumor cells, as well as recruit NK cells, which assist in the clearance of tumor cells. PEDF positive exosomes can also be isolated from the serum of melanoma patients, and patients with recurrent metastasis have significantly less PEDF in exosomes as compared to patients with

non-recurrent primary melanoma or healthy controls. This observation is significant because it points to the possibility of developing an exosomal PEDF-based prognostic indicator with more exosomal PEDF suggesting a better patient outcome. This work also presents the idea that there may be numerous biomolecules present in the exosomes of non-metastatic cancer cells that activate innate immune responses to prevent metastasis. The identification of these signals may provide novel targets that can be further developed into cancer therapeutics. The Volpert Laboratory is actively studying the interaction of cancer exosomes and immune cells in order to identify novel mechanisms by which these exosomes function.

Chapter 3 details the development of HDL NPs as an SR-B1 targeted inhibitor of exosome uptake. While researchers have previously shown that non-specific depletion of cholesterol in lipid rafts reduced exosome uptake, this is the first study showing that exosome uptake can be inhibited in a targeted manner. HDL NPs binding SR-B1 caused a significant increase in the clustering of the receptors, followed by modulating the flux of free cholesterol and cholesteryl esters through SR-B1. While the cholesterol is effluxed to HDL NPs, there is also competitive inhibition of HDL NPs blocking native HDLs from delivering cholesteryl esters. This leads to the destabilization of lipid rafts, which are necessary for the uptake of exosomes. At this time, the Thaxton Laboratory is investigating the effects of HDL NPs at inhibiting exosome uptake and preventing metastasis in other cancers, including prostate cancer, which aggressively metastasizes to the bone. As intercellular communications mediated by exosomes is a critical component of the progression of numerous cancers and other diseases, inhibiting exosome uptake with HDL NPs may be an effective strategy for treating these diseases.

While testing the effects of HDL NPs in metastasis models, we discovered that HDL NPs have anti-cancer effects independent of exosome uptake, as well. This led us to investigate in more detail in Chapter 4. The focus on Chapter 4 is the discovery that HDL NPs inhibit the ability of MDSCs to suppress T cell function. Importantly, we demonstrate that both monocytic Ly6C⁺ and granulocytic Ly6G⁺ MDSCs express SR-B1 with Ly6C⁺ cells expressing more. This leads to the HDL NP primarily targeting Ly6C⁺ MDSCs. Convincingly, treatment of mice with HDL NPs causes decreased primary tumor growth, reduced metastasis and a significant increase in overall survival. Data collected for this project also demonstrates that HDL NPs function in multiple cancer models including the Lewis lung carcinoma model. Because HDL NPs function primarily by binding to SR-B1 and modulating cholesterol homeostasis, it is likely that the HDL NPs effects at inhibiting MDSCs is due to changes in cellular cholesterol. Cholesterol and lipoproteins is intricately tied with the immune system during tumor progression but the exact relationships remain unclear. The Thaxton Lab is currently testing the extent to which cholesterol plays a role in the function of myeloid cells.

In conclusion, this work demonstrates the importance of the pre-metastatic niche to the formation of metastasis and shows the significant contributions that exosomes make during the metastatic process. Results shown here have broadened our understanding of the role of exosomes by establishing that non-metastatic cells deliver anti-metastatic biomolecular cargo, which also highlights their potential as delivery vehicles. This work goes on to describe the development of synthetic HDL NPs, which can inhibit the delivery of exosomes and their pro-tumorigenic effects suppressing the formation of the pre-metastatic niche. Further utilization of HDL NPs revealed that they can potently inhibit MDSCs leading to a second means by which HDL NPs suppress the formation of microenvironments suitable for tumor progression. Overall,

work presented in this dissertation has made significant advancements for the fields of cancer biology and immunology and lays the groundwork for developing novel therapeutics focused on exosomes and tumor immunity.

References

1. Paget S. The distribution of secondary growths in cancer of the breast. 1889. *Cancer Metastasis Rev.* 1989;8(2):98-101.
2. Tkach M, Thery C. Communication by Extracellular Vesicles: Where We Are and Where We Need to Go. *Cell.* 2016;164(6):1226-1232.
3. Quail DF, Joyce JA. Microenvironmental regulation of tumor progression and metastasis. *Nature medicine.* 2013;19(11):1423-1437.
4. Hanahan D, Weinberg RA. Hallmarks of cancer: the next generation. *Cell.* 2011;144(5):646-674.
5. Chaffer CL, Weinberg RA. A perspective on cancer cell metastasis. *Science.* 2011;331(6024):1559-1564.
6. Iannello A, Thompson TW, Ardolino M, Marcus A, Raulat DH. Immunosurveillance and immunotherapy of tumors by innate immune cells. *Curr Opin Immunol.* 2016;38:52-58.
7. Kaplan RN, Rafii S, Lyden D. Preparing the "soil": the premetastatic niche. *Cancer research.* 2006;66(23):11089-11093.
8. Peinado H, Lavotshkin S, Lyden D. The secreted factors responsible for pre-metastatic niche formation: old sayings and new thoughts. *Seminars in cancer biology.* 2011;21(2):139-146.
9. Kalluri R. The biology and function of fibroblasts in cancer. *Nature reviews Cancer.* 2016;16(9):582-598.
10. Kalluri R, Zeisberg M. Fibroblasts in cancer. *Nature reviews Cancer.* 2006;6(5):392-401.
11. Gascard P, Tlsty TD. Carcinoma-associated fibroblasts: orchestrating the composition of malignancy. *Genes Dev.* 2016;30(9):1002-1019.
12. Nwani NG, Deguiz ML, Jimenez B, et al. Melanoma Cells Block PEDF Production in Fibroblasts to Induce the Tumor-Promoting Phenotype of Cancer-Associated Fibroblasts. *Cancer research.* 2016;76(8):2265-2276.
13. Bergers G, Benjamin LE. Tumorigenesis and the angiogenic switch. *Nature reviews Cancer.* 2003;3(6):401-410.
14. De Palma M, Biziato D, Petrova TV. Microenvironmental regulation of tumour angiogenesis. *Nature reviews Cancer.* 2017;17(8):457-474.
15. Zetter BR. Angiogenesis and tumor metastasis. *Annu Rev Med.* 1998;49:407-424.
16. Mantovani A, Marchesi F, Malesci A, Laghi L, Allavena P. Tumour-associated macrophages as treatment targets in oncology. *Nature Reviews Clinical Oncology.* 2017;14(7):399-416.
17. Peinado H, Zhang H, Matei IR, et al. Pre-metastatic niches: organ-specific homes for metastases. *Nature reviews Cancer.* 2017;17(5):302-317.
18. Noy R, Pollard JW. Tumor-associated macrophages: from mechanisms to therapy. *Immunity.* 2014;41(1):49-61.
19. Martinez-Marin D, Jarvis C, Nelius T, de Riese W, Volpert OV, Filleur S. PEDF increases the tumoricidal activity of macrophages towards prostate cancer cells in vitro. *Plos One.* 2017;12(4):e0174968.

20. Plebanek MP, Angeloni NL, Vinokour E, et al. Pre-metastatic cancer exosomes induce immune surveillance by patrolling monocytes at the metastatic niche. *Nat Commun.* 2017;8.
21. Knaapen AM, Gungor N, Schins RP, Borm PJ, Van Schooten FJ. Neutrophils and respiratory tract DNA damage and mutagenesis: a review. *Mutagenesis.* 2006;21(4):225-236.
22. Houghton AM, Rzymkiewicz DM, Ji H, et al. Neutrophil elastase-mediated degradation of IRS-1 accelerates lung tumor growth. *Nature medicine.* 2010;16(2):219-223.
23. Deryugina EI, Zajac E, Juncker-Jensen A, Kupriyanova TA, Welter L, Quigley JP. Tissue-infiltrating neutrophils constitute the major in vivo source of angiogenesis-inducing MMP-9 in the tumor microenvironment. *Neoplasia.* 2014;16(10):771-788.
24. Pillay J, Tak T, Kamp VM, Koenderman L. Immune suppression by neutrophils and granulocytic myeloid-derived suppressor cells: similarities and differences. *Cell Mol Life Sci.* 2013;70(20):3813-3827.
25. Wculek SK, Malanchi I. Neutrophils support lung colonization of metastasis-initiating breast cancer cells. *Nature.* 2015;528(7582):413-+.
26. Hanna RN, Cekic C, Sag D, et al. Patrolling monocytes control tumor metastasis to the lung. *Science.* 2015;350(6263):985-990.
27. Kubo H, Mensurado S, Goncalves-Sousa N, Serre K, Silva-Santos B. Primary Tumors Limit Metastasis Formation through Induction of IL15-Mediated Cross-Talk between Patrolling Monocytes and NK Cells. *Cancer Immunol Res.* 2017;5(9):812-820.
28. Thomas G, Tacke R, Hedrick CC, Hanna RN. Nonclassical patrolling monocyte function in the vasculature. *Arteriosclerosis, thrombosis, and vascular biology.* 2015;35(6):1306-1316.
29. McArdle S, Chodaczek G, Ray N, Ley K. Intravital live cell triggered imaging system reveals monocyte patrolling and macrophage migration in atherosclerotic arteries. *J Biomed Opt.* 2015;20(2):26005.
30. Auffray C, Fogg D, Garfa M, et al. Monitoring of blood vessels and tissues by a population of monocytes with patrolling behavior. *Science.* 2007;317(5838):666-670.
31. Hanna RN, Shaked I, Hubbeling HG, et al. NR4A1 (Nur77) deletion polarizes macrophages toward an inflammatory phenotype and increases atherosclerosis. *Circulation research.* 2012;110(3):416-427.
32. van Amerongen MJ, Harmsen MC, van Rooijen N, Petersen AH, van Luyn MJ. Macrophage depletion impairs wound healing and increases left ventricular remodeling after myocardial injury in mice. *Am J Pathol.* 2007;170(3):818-829.
33. Hilgendorf I, Gerhardt LM, Tan TC, et al. Ly-6Chigh monocytes depend on Nr4a1 to balance both inflammatory and reparative phases in the infarcted myocardium. *Circulation research.* 2014;114(10):1611-1622.
34. Combadiere C, Potteaux S, Rodero M, et al. Combined inhibition of CCL2, CX3CR1, and CCR5 abrogates Ly6C(hi) and Ly6C(lo) monocytosis and almost abolishes atherosclerosis in hypercholesterolemic mice. *Circulation.* 2008;117(13):1649-1657.

35. Shankaran V, Ikeda H, Bruce AT, et al. IFN γ and lymphocytes prevent primary tumour development and shape tumour immunogenicity. *Nature*. 2001;410(6832):1107-1111.
36. Clifford GM, Polesel J, Rickenbach M, et al. Cancer risk in the Swiss HIV Cohort Study: associations with immunodeficiency, smoking, and highly active antiretroviral therapy. *J Natl Cancer Inst*. 2005;97(6):425-432.
37. Engels EA, Pfeiffer RM, Fraumeni JF, Jr., et al. Spectrum of cancer risk among US solid organ transplant recipients. *JAMA*. 2011;306(17):1891-1901.
38. Schumacher TN, Schreiber RD. Neoantigens in cancer immunotherapy. *Science*. 2015;348(6230):69-74.
39. Smyth MJ, Ngiow SF, Ribas A, Teng MW. Combination cancer immunotherapies tailored to the tumour microenvironment. *Nat Rev Clin Oncol*. 2016;13(3):143-158.
40. Pardoll DM. The blockade of immune checkpoints in cancer immunotherapy. *Nature reviews Cancer*. 2012;12(4):252-264.
41. Ueda H, Howson JM, Esposito L, et al. Association of the T-cell regulatory gene CTLA4 with susceptibility to autoimmune disease. *Nature*. 2003;423(6939):506-511.
42. Eggermont AM, Chiarion-Sileni V, Grob JJ, et al. Prolonged Survival in Stage III Melanoma with Ipilimumab Adjuvant Therapy. *N Engl J Med*. 2016;375(19):1845-1855.
43. Zou W, Wolchok JD, Chen L. PD-L1 (B7-H1) and PD-1 pathway blockade for cancer therapy: Mechanisms, response biomarkers, and combinations. *Science translational medicine*. 2016;8(328):328rv324.
44. Gadiot J, Hooijkaas AI, Kaiser AD, van Tinteren H, van Boven H, Blank C. Overall survival and PD-L1 expression in metastasized malignant melanoma. *Cancer*. 2011;117(10):2192-2201.
45. Sadelain M, Brentjens R, Riviere I. The basic principles of chimeric antigen receptor design. *Cancer Discov*. 2013;3(4):388-398.
46. Schuster SJ, Svoboda J, Chong EA, et al. Chimeric Antigen Receptor T Cells in Refractory B-Cell Lymphomas. *N Engl J Med*. 2017.
47. Hodi FS, O'Day SJ, McDermott DF, et al. Improved survival with ipilimumab in patients with metastatic melanoma. *N Engl J Med*. 2010;363(8):711-723.
48. Michot JM, Bigenwald C, Champiat S, et al. Immune-related adverse events with immune checkpoint blockade: a comprehensive review. *Eur J Cancer*. 2016;54:139-148.
49. Mathivanan S, Ji H, Simpson RJ. Exosomes: extracellular organelles important in intercellular communication. *Journal of proteomics*. 2010;73(10):1907-1920.
50. Fevrier B, Raposo G. Exosomes: endosomal-derived vesicles shipping extracellular messages. *Current opinion in cell biology*. 2004;16(4):415-421.
51. Bissig C, Gruenberg J. ALIX and the multivesicular endosome: ALIX in Wonderland. *Trends in cell biology*. 2014;24(1):19-25.
52. Lotvall J, Valadi H. Cell to cell signalling via exosomes through esRNA. *Cell Adh Migr*. 2007;1(3):156-158.

53. Valadi H, Ekstrom K, Bossios A, Sjostrand M, Lee JJ, Lotvall JO. Exosome-mediated transfer of mRNAs and microRNAs is a novel mechanism of genetic exchange between cells. *Nat Cell Biol.* 2007;9(6):654-659.
54. Skog J, Wurdinger T, van Rijn S, et al. Glioblastoma microvesicles transport RNA and proteins that promote tumour growth and provide diagnostic biomarkers. *Nat Cell Biol.* 2008;10(12):1470-U1209.
55. Alvarez-Erviti L, Seow Y, Yin H, Betts C, Lakhali S, Wood MJ. Delivery of siRNA to the mouse brain by systemic injection of targeted exosomes. *Nat Biotechnol.* 2011;29(4):341-345.
56. Pegtel DM, Cosmopoulos K, Thorley-Lawson DA, et al. Functional delivery of viral miRNAs via exosomes. *Proceedings of the National Academy of Sciences of the United States of America.* 2010;107(14):6328-6333.
57. Vlassov AV, Magdaleno S, Setterquist R, Conrad R. Exosomes: Current knowledge of their composition, biological functions, and diagnostic and therapeutic potentials. *Bba-Gen Subjects.* 2012;1820(7):940-948.
58. Thakur BK, Zhang H, Becker A, et al. Double-stranded DNA in exosomes: a novel biomarker in cancer detection. *Cell Res.* 2014;24(6):766-769.
59. Takahashi A, Okada R, Nagao K, et al. Exosomes maintain cellular homeostasis by excreting harmful DNA from cells. *Nat Commun.* 2017;8:15287.
60. Kalluri R, LeBleu VS. Discovery of Double-Stranded Genomic DNA in Circulating Exosomes. *Cold Spring Harb Symp Quant Biol.* 2016;81:275-280.
61. Kahlert C, Kalluri R. Exosomes in tumor microenvironment influence cancer progression and metastasis. *J Mol Med.* 2013;91(4):431-437.
62. Taylor DD, Gercel-Taylor C. Exosomes/microvesicles: mediators of cancer-associated immunosuppressive microenvironments. *Semin Immunopathol.* 2011;33(5):441-454.
63. Peinado H, Aleckovic M, Lavotshkin S, et al. Melanoma exosomes educate bone marrow progenitor cells toward a pro-metastatic phenotype through MET. *Nature medicine.* 2012;18(6):883-891.
64. Hood JL, San RS, Wickline SA. Exosomes released by melanoma cells prepare sentinel lymph nodes for tumor metastasis. *Cancer research.* 2011;71(11):3792-3801.
65. Hood JL, Pan H, Lanza GM, Wickline SA. Paracrine induction of endothelium by tumor exosomes. *Laboratory investigation; a journal of technical methods and pathology.* 2009;89(11):1317-1328.
66. Liu Y, Gu Y, Han Y, et al. Tumor Exosomal RNAs Promote Lung Pre-metastatic Niche Formation by Activating Alveolar Epithelial TLR3 to Recruit Neutrophils. *Cancer Cell.* 2016;30(2):243-256.
67. Kalluri R. The biology and function of exosomes in cancer. *J Clin Invest.* 2016;126(4):1208-1215.
68. Taylor DD, Gercel-Taylor C. MicroRNA signatures of tumor-derived exosomes as diagnostic biomarkers of ovarian cancer. *Gynecol Oncol.* 2008;110(1):13-21.
69. Thind A, Wilson C. Exosomal miRNAs as cancer biomarkers and therapeutic targets. *Journal of extracellular vesicles.* 2016;5:31292.

70. Li W, Li C, Zhou T, et al. Role of exosomal proteins in cancer diagnosis. *Molecular cancer*. 2017;16(1):145.
71. Melo SA, Luecke LB, Kahlert C, et al. Glypican-1 identifies cancer exosomes and detects early pancreatic cancer. *Nature*. 2015;523(7559):177-182.
72. Amabile N, Rautou PE, Tedgui A, Boulanger CM. Microparticles: key protagonists in cardiovascular disorders. *Semin Thromb Hemost*. 2010;36(8):907-916.
73. Densmore JC, Signorino PR, Ou J, et al. Endothelium-derived microparticles induce endothelial dysfunction and acute lung injury. *Shock*. 2006;26(5):464-471.
74. Jansen F, Yang XY, Franklin BS, et al. High glucose condition increases NADPH oxidase activity in endothelial microparticles that promote vascular inflammation. *Cardiovascular research*. 2013;98(1):94-106.
75. Matsumoto S, Sakata Y, Suna S, et al. Circulating p53-Responsive MicroRNAs Are Predictive Indicators of Heart Failure After Acute Myocardial Infarction Short Communication. *Circulation research*. 2013;113(3):322-326.
76. Rajendran L, Honsho M, Zahn TR, et al. Alzheimer's disease beta-amyloid peptides are released in association with exosomes. *Proceedings of the National Academy of Sciences of the United States of America*. 2006;103(30):11172-11177.
77. Gomes C, Keller S, Altevogt P, Costa J. Evidence for secretion of Cu,Zn superoxide dismutase via exosomes from a cell model of amyotrophic lateral sclerosis. *Neurosci Lett*. 2007;428(1):43-46.
78. Quek C, Hill AF. The role of extracellular vesicles in neurodegenerative diseases. *Biochemical and biophysical research communications*. 2017;483(4):1178-1186.
79. Coleman BM, Hill AF. Extracellular vesicles--Their role in the packaging and spread of misfolded proteins associated with neurodegenerative diseases. *Semin Cell Dev Biol*. 2015;40:89-96.
80. Ellwanger JH, Veit TD, Chies JAB. Exosomes in HIV infection: A review and critical look. *Infect Genet Evol*. 2017;53:146-154.
81. Nanbo A, Kawanishi E, Yoshida R, Yoshiyama H. Exosomes derived from Epstein-Barr virus-infected cells are internalized via caveola-dependent endocytosis and promote phenotypic modulation in target cells. *J Virol*. 2013;87(18):10334-10347.
82. Dreux M, Garaigorta U, Boyd B, et al. Short-range exosomal transfer of viral RNA from infected cells to plasmacytoid dendritic cells triggers innate immunity. *Cell Host Microbe*. 2012;12(4):558-570.
83. Bukong TN, Momen-Heravi F, Kodys K, Bala S, Szabo G. Exosomes from hepatitis C infected patients transmit HCV infection and contain replication competent viral RNA in complex with Ago2-miR122-HSP90. *PLoS Pathog*. 2014;10(10):e1004424.
84. Jang SC, Kim OY, Yoon CM, et al. Bioinspired Exosome-Mimetic Nanovesicles for Targeted Delivery of Chemotherapeutics to Malignant Tumors. *ACS nano*. 2013;7(9):7698-7710.
85. Didiot MC, Hall LM, Coles AH, et al. Exosome-mediated Delivery of Hydrophobically Modified siRNA for Huntingtin mRNA Silencing. *Mol Ther*. 2016;24(10):1836-1847.
86. El Andaloussi S, Lakhali S, Mager I, Wood MJ. Exosomes for targeted siRNA delivery across biological barriers. *Adv Drug Deliv Rev*. 2013;65(3):391-397.

87. Wolfers J, Lozier A, Raposo G, et al. Tumor-derived exosomes are a source of shared tumor rejection antigens for CTL cross-priming. *Nature medicine*. 2001;7(3):297-303.
88. Thery C, Duban L, Segura E, Veron P, Lantz O, Amigorena S. Indirect activation of naive CD4+ T cells by dendritic cell-derived exosomes. *Nat Immunol*. 2002;3(12):1156-1162.
89. Vincent-Schneider H, Stumptner-Cuvelette P, Lankar D, et al. Exosomes bearing HLA-DR1 molecules need dendritic cells to efficiently stimulate specific T cells. *Int Immunol*. 2002;14(7):713-722.
90. Andre F, Chaput N, Scharz NEC, et al. Exosomes as potent cell-free peptide-based vaccine. I. Dendritic cell-derived exosomes transfer functional MHC class I/peptide complexes to dendritic cells. *J Immunol*. 2004;172(4):2126-2136.
91. Chaput N, Scharz NEC, Andre F, et al. Exosomes as potent cell-free peptide-based vaccine. II. Exosomes in CpG adjuvants efficiently prime naive Tc1 lymphocytes leading to tumor rejection. *J Immunol*. 2004;172(4):2137-2146.
92. Aline F, Bout D, Amigorena S, Roingeard P, Dimier-Poisson I. Toxoplasma gondii antigen-pulsed-dendritic cell-derived exosomes induce a protective immune response against T gondii infection. *Infect Immun*. 2004;72(7):4127-4137.
93. Giri PK, Schorey JS. Exosomes Derived from M-Bovis BCG Infected Macrophages Activate Antigen-Specific CD4(+) and CD8(+) T Cells In Vitro and In Vivo. *Plos One*. 2008;3(6).
94. Brill A, Dashevsky O, Rivo J, Gozal Y, Varon D. Platelet-derived microparticles induce angiogenesis and stimulate post-ischemic revascularization. *Cardiovascular research*. 2005;67(1):30-38.
95. Rani S, Ryan AE, Griffin MD, Ritter T. Mesenchymal Stem Cell-derived Extracellular Vesicles: Toward Cell-free Therapeutic Applications. *Mol Ther*. 2015;23(5):812-823.
96. Bruno S, Porta S, Bussolati B. Extracellular vesicles in renal tissue damage and regeneration. *Eur J Pharmacol*. 2016;790:83-91.
97. Zhang B, Wang M, Gong AH, et al. HucMSC-Exosome Mediated-Wnt4 Signaling Is Required for Cutaneous Wound Healing. *Stem cells*. 2015;33(7):2158-2168.
98. Salomon C, Ryan J, Sobrevia L, et al. Exosomal Signaling during Hypoxia Mediates Microvascular Endothelial Cell Migration and Vasculogenesis. *Plos One*. 2013;8(7).
99. Plebanek MP, Mutharasan RK, Volpert O, Matov A, Gatlin JC, Thaxton CS. Nanoparticle Targeting and Cholesterol Flux Through Scavenger Receptor Type B-1 Inhibits Cellular Exosome Uptake. *Sci Rep-Uk*. 2015;5.
100. Rader DJ. High-density lipoproteins and atherosclerosis. *Am J Cardiol*. 2002;90(8A):62i-70i.
101. Rader DJ, Alexander ET, Weibel GL, Billheimer J, Rothblat GH. The role of reverse cholesterol transport in animals and humans and relationship to atherosclerosis. *J Lipid Res*. 2009;50 Suppl:S189-194.
102. Mineo C, Shaul PW. Regulation of signal transduction by HDL. *J Lipid Res*. 2013;54(9):2315-2324.
103. Assanasen C, Mineo C, Seetharam D, et al. Cholesterol binding, efflux, and a PDZ-interacting domain of scavenger receptor-BI mediate HDL-initiated signaling. *J Clin Invest*. 2005;115(4):969-977.

104. Saddar S, Mineo C, Shaul PW. Signaling by the high-affinity HDL receptor scavenger receptor B type I. *Arteriosclerosis, thrombosis, and vascular biology*. 2010;30(2):144-150.
105. Danilo C, Gutierrez-Pajares JL, Mainieri MA, Mercier I, Lisanti MP, Frank PG. Scavenger receptor class B type I regulates cellular cholesterol metabolism and cell signaling associated with breast cancer development. *Breast Cancer Res*. 2013;15(5):R87.
106. Twiddy AL, Cox ME, Wasan KM. Knockdown of scavenger receptor class B type I reduces prostate specific antigen secretion and viability of prostate cancer cells. *Prostate*. 2012;72(9):955-965.
107. Yuan B, Wu C, Wang X, et al. High scavenger receptor class B type I expression is related to tumor aggressiveness and poor prognosis in breast cancer. *Tumour Biol*. 2016;37(3):3581-3588.
108. Sjobahl G, Lauss M, Lovgren K, et al. A molecular taxonomy for urothelial carcinoma. *Clin Cancer Res*. 2012;18(12):3377-3386.
109. Bild AH, Yao G, Chang JT, et al. Oncogenic pathway signatures in human cancers as a guide to targeted therapies. *Nature*. 2006;439(7074):353-357.
110. Wilhelm S, Tavares AJ, Dai Q, et al. Analysis of nanoparticle delivery to tumours. *Nat Rev Mater*. 2016;1(5).
111. Wilczewska AZ, Niemirowicz K, Markiewicz KH, Car H. Nanoparticles as drug delivery systems. *Pharmacol Rep*. 2012;64(5):1020-1037.
112. Cardoso MM, Peca IN, Roque ACA. Antibody-Conjugated Nanoparticles for Therapeutic Applications. *Curr Med Chem*. 2012;19(19):3103-3127.
113. Rader DJ. High-density lipoproteins as an emerging therapeutic target for atherosclerosis. *JAMA*. 2003;290(17):2322-2324.
114. Yu BL, Wang SH, Peng DQ, Zhao SP. HDL and immunomodulation: an emerging role of HDL against atherosclerosis. *Immunol Cell Biol*. 2010;88(3):285-290.
115. De Nardo D, Labzin LI, Kono H, et al. High-density lipoprotein mediates anti-inflammatory reprogramming of macrophages via the transcriptional regulator ATF3. *Nat Immunol*. 2014;15(2):152-160.
116. Shahzad MMK, Mangala LS, Han HD, et al. Targeted Delivery of Small Interfering RNA Using Reconstituted High-Density Lipoprotein Nanoparticles. *Neoplasia*. 2011;13(4):309-U142.
117. Luthi AJ, Zhang H, Kim D, Giljohann DA, Mirkin CA, Thaxton CS. Tailoring of biomimetic high-density lipoprotein nanostructures changes cholesterol binding and efflux. *ACS nano*. 2012;6(1):276-285.
118. Zhang Z, Chen J, Ding L, et al. HDL-mimicking peptide-lipid nanoparticles with improved tumor targeting. *Small*. 2010;6(3):430-437.
119. Thaxton CS, Daniel WL, Giljohann DA, Thomas AD, Mirkin CA. Templated spherical high density lipoprotein nanoparticles. *Journal of the American Chemical Society*. 2009;131(4):1384-1385.
120. Sviridov D, Remaley AT. High-density lipoprotein mimetics: promises and challenges. *Biochem J*. 2015;472(3):249-259.
121. Reddy ST, Navab M, Anantharamaiah GM, Fogelman AM. Apolipoprotein A-I mimetics. *Curr Opin Lipidol*. 2014;25(4):304-308.

122. Yang S, Damiano MG, Zhang H, et al. Biomimetic, synthetic HDL nanostructures for lymphoma. *Proceedings of the National Academy of Sciences of the United States of America*. 2013;110(7):2511-2516.
123. Kowal J, Tkach M, Thery C. Biogenesis and secretion of exosomes. *Curr Opin Cell Biol*. 2014;29:116-125.
124. Colombo M, Raposo G, Thery C. Biogenesis, secretion, and intercellular interactions of exosomes and other extracellular vesicles. *Annu Rev Cell Dev Biol*. 2014;30:255-289.
125. Melo SA, Sugimoto H, O'Connell JT, et al. Cancer exosomes perform cell-independent microRNA biogenesis and promote tumorigenesis. *Cancer Cell*. 2014;26(5):707-721.
126. Al-Nedawi K, Meehan B, Rak J. Microvesicles Messengers and mediators of tumor progression. *Cell Cycle*. 2009;8(13):2014-2018.
127. Sceneay J, Smyth MJ, Moller A. The pre-metastatic niche: finding common ground. *Cancer Metast Rev*. 2013;32(3-4):449-464.
128. Wynn TA, Chawla A, Pollard JW. Macrophage biology in development, homeostasis and disease. *Nature*. 2013;496(7446):445-455.
129. Sica A, Mantovani A. Macrophage plasticity and polarization: in vivo veritas. *J Clin Invest*. 2012;122(3):787-795.
130. Franklin RA, Liao W, Sarkar A, et al. The cellular and molecular origin of tumor-associated macrophages. *Science*. 2014;344(6186):921-925.
131. Carlin LM, Stamatiades EG, Auffray C, et al. Nr4a1-Dependent Ly6C(low) Monocytes Monitor Endothelial Cells and Orchestrate Their Disposal. *Cell*. 2013;153(2):362-375.
132. Cros J, Cagnard N, Woollard K, et al. Human CD14dim monocytes patrol and sense nucleic acids and viruses via TLR7 and TLR8 receptors. *Immunity*. 2010;33(3):375-386.
133. Rodero MP, Poupel L, Loyher PL, et al. Immune surveillance of the lung by migrating tissue monocytes. *eLife*. 2015;4:e07847.
134. Caword SE, Fitchev P, Veliceasa D, Volpert OV. The many facets of PEDF in drug discovery and disease: a diamond in the rough or split personality disorder? *Expert Opin Drug Discov*. 2013;8(7):769-792.
135. Ladhani O, Sanchez-Martinez C, Orgaz JL, Jimenez B, Volpert OV. Pigment Epithelium-Derived Factor Blocks Tumor Extravasation by Suppressing Amoeboid Morphology and Mesenchymal Proteolysis. *Neoplasia*. 2011;13(7):633-U686.
136. Dadras SS, Lin RJ, Razavi G, et al. A novel role for microphthalmia-associated transcription factor-regulated pigment epithelium-derived factor during melanoma progression. *Am J Pathol*. 2015;185(1):252-265.
137. Ho TC, Chen SL, Shih SC, et al. Pigment epithelium-derived factor (PEDF) promotes tumor cell death by inducing macrophage membrane tumor necrosis factor-related apoptosis-inducing ligand (TRAIL). *The Journal of biological chemistry*. 2011;286(41):35943-35954.
138. Costa-Silva B, Aiello NM, Ocean AJ, et al. Pancreatic cancer exosomes initiate pre-metastatic niche formation in the liver. *Nat Cell Biol*. 2015;17(6):816-+.

139. Orgaz JL, Ladhani O, Hoek KS, et al. 'Loss of pigment epithelium-derived factor enables migration, invasion and metastatic spread of human melanoma'. *Oncogene*. 2009;28(47):4147-4161.
140. Steeg PS. Targeting metastasis. *Nature reviews Cancer*. 2016;16(4):201-218.
141. Hendrix MJ, Seftor EA, Hess AR, Seftor RE. Vasculogenic mimicry and tumour-cell plasticity: lessons from melanoma. *Nat Rev Cancer*. 2003;3(6):411-421.
142. Ruf W, Seftor EA, Petrovan RJ, et al. Differential role of tissue factor pathway inhibitors 1 and 2 in melanoma vasculogenic mimicry. *Cancer Res*. 2003;63(17):5381-5389.
143. Takahashi Y, Nishikawa M, Shinotsuka H, et al. Visualization and in vivo tracking of the exosomes of murine melanoma B16-BL6 cells in mice after intravenous injection. *Journal of biotechnology*. 2013;165(2):77-84.
144. Hoshino A, Costa-Silva B, Shen TL, et al. Tumour exosome integrins determine organotropic metastasis. *Nature*. 2015;527(7578):329-+.
145. Imai T, Takahashi Y, Nishikawa M, et al. Macrophage-dependent clearance of systemically administered B16BL6-derived exosomes from the blood circulation in mice. *Journal of extracellular vesicles*. 2015;4:26238.
146. Weisser SB, van Rooijen N, Sly LM. Depletion and reconstitution of macrophages in mice. *Journal of visualized experiments : JoVE*. 2012(66):4105.
147. Malladi S, Macalinao DG, Jin X, et al. Metastatic Latency and Immune Evasion through Autocrine Inhibition of WNT. *Cell*. 2016;165(1):45-60.
148. Zand S, Buzney E, Duncan LM, Dadras SS. Heterogeneity of Metastatic Melanoma: Correlation of MITF With Its Transcriptional Targets MLSN1, PEDF, HMB-45, and MART-1. *Am J Clin Pathol*. 2016;146(3):353-360.
149. Fernandez-Barral A, Orgaz JL, Baquero P, et al. Regulatory and functional connection of microphthalmia-associated transcription factor and anti-metastatic pigment epithelium derived factor in melanoma. *Neoplasia*. 2014;16(6):529-542.
150. Sarkar D, Leung EY, Baguley BC, Finlay GJ, Askarian-Amiri ME. Epigenetic regulation in human melanoma: past and future. *Epigenetics*. 2015;10(2):103-121.
151. Kitamura T, Qian BZ, Pollard JW. Immune cell promotion of metastasis. *Nat Rev Immunol*. 2015;15(2):73-86.
152. Zhang X, Goncalves R, Mosser DM. The isolation and characterization of murine macrophages. *Current protocols in immunology / edited by John E Coligan [et al]*. 2008;Chapter 14:Unit 14 11.
153. Thery C, Amigorena S, Raposo G, Clayton A. Isolation and characterization of exosomes from cell culture supernatants and biological fluids. *Current protocols in cell biology / editorial board, Juan S Bonifacino [et al]*. 2006;Chapter 3:Unit 3 22.
154. Martins VR, Dias MS, Hainaut P. Tumor-cell-derived microvesicles as carriers of molecular information in cancer. *Curr Opin Oncol*. 2013;25(1):66-75.
155. Lee Y, El Andaloussi S, Wood MJ. Exosomes and microvesicles: extracellular vesicles for genetic information transfer and gene therapy. *Human molecular genetics*. 2012;21(R1):R125-134.
156. Lai RC, Chen TS, Lim SK. Mesenchymal stem cell exosome: a novel stem cell-based therapy for cardiovascular disease. *Regenerative medicine*. 2011;6(4):481-492.

157. Sahoo S, Klychko E, Thorne T, et al. Exosomes from human CD34(+) stem cells mediate their proangiogenic paracrine activity. *Circulation research*. 2011;109(7):724-728.
158. Skokos D, Le Panse S, Villa I, et al. Mast cell-dependent B and T lymphocyte activation is mediated by the secretion of immunologically active exosomes. *J Immunol*. 2001;166(2):868-876.
159. Sprent J. Direct stimulation of naive T cells by antigen-presenting cell vesicles. *Blood cells, molecules & diseases*. 2005;35(1):17-20.
160. Ramakrishnaiah V, Thumann C, Fofana I, et al. Exosome-mediated transmission of hepatitis C virus between human hepatoma Huh7.5 cells. *Proceedings of the National Academy of Sciences of the United States of America*. 2013;110(32):13109-13113.
161. Jung T, Castellana D, Klingbeil P, et al. CD44v6 dependence of premetastatic niche preparation by exosomes. *Neoplasia*. 2009;11(10):1093-1105.
162. Yu X, Harris SL, Levine AJ. The regulation of exosome secretion: a novel function of the p53 protein. *Cancer research*. 2006;66(9):4795-4801.
163. Filipazzi P, Burdek M, Villa A, Rivoltini L, Huber V. Recent advances on the role of tumor exosomes in immunosuppression and disease progression. *Seminars in cancer biology*. 2012;22(4):342-349.
164. Ekstrom EJ, Bergenfelz C, von Bulow V, et al. WNT5A induces release of exosomes containing pro-angiogenic and immunosuppressive factors from malignant melanoma cells. *Molecular cancer*. 2014;13:88.
165. Marton A, Vizler C, Kusz E, et al. Melanoma cell-derived exosomes alter macrophage and dendritic cell functions in vitro. *Immunol Lett*. 2012;148(1):34-38.
166. Gupta SK, Bang C, Thum T. Circulating MicroRNAs as Biomarkers and Potential Paracrine Mediators of Cardiovascular Disease. *Circ-Cardiovasc Gene*. 2010;3(5):484-488.
167. Janowska-Wieczorek A, Majka M, Kijowski J, et al. Platelet-derived microparticles bind to hematopoietic stem/progenitor cells and enhance their engraftment. *Blood*. 2001;98(10):3143-3149.
168. Anastasiadou E, Slack FJ. Cancer. Malicious exosomes. *Science*. 2014;346(6216):1459-1460.
169. Simons K, Vaz WL. Model systems, lipid rafts, and cell membranes. *Annual review of biophysics and biomolecular structure*. 2004;33:269-295.
170. Svensson KJ, Christianson HC, Wittrup A, et al. Exosome uptake depends on ERK1/2-heat shock protein 27 signaling and lipid Raft-mediated endocytosis negatively regulated by caveolin-1. *The Journal of biological chemistry*. 2013;288(24):17713-17724.
171. Van Eck M, Pennings M, Hoekstra M, Out R, Van Berkel TJC. Scavenger receptor BI and ATP-binding cassette transporter A1 in reverse cholesterol transport and atherosclerosis. *Curr Opin Lipidol*. 2005;16(3):307-315.
172. Atshaves BP, McIntosh AL, Payne HR, et al. SCP-2/SCP-x gene ablation alters lipid raft domains in primary cultured mouse hepatocytes. *J Lipid Res*. 2007;48(10):2193-2211.

173. Valacchi G, Sticozzi C, Lim Y, Pecorelli A. Scavenger receptor class B type I: a multifunctional receptor. *Annals of the New York Academy of Sciences*. 2011;1229:E1-7.
174. Luthi AJ, Lyssenko NN, Quach D, et al. Robust passive and active efflux of cellular cholesterol to a designer functional mimic of high-density lipoprotein. *J Lipid Res*. 2015.
175. Xiang X, Poliakov A, Liu C, et al. Induction of myeloid-derived suppressor cells by tumor exosomes. *International journal of cancer Journal international du cancer*. 2009;124(11):2621-2633.
176. McMahan KM, Thaxton CS. High-density lipoproteins for the systemic delivery of short interfering RNA. *Expert opinion on drug delivery*. 2014;11(2):231-247.
177. McMahan KM, Mutharasan RK, Tripathy S, et al. Biomimetic high density lipoprotein nanoparticles for nucleic acid delivery. *Nano Lett*. 2011;11(3):1208-1214.
178. Nieland TJ, Penman M, Dori L, Krieger M, Kirchhausen T. Discovery of chemical inhibitors of the selective transfer of lipids mediated by the HDL receptor SR-BI. *Proceedings of the National Academy of Sciences of the United States of America*. 2002;99(24):15422-15427.
179. Neculai D, Schwake M, Ravichandran M, et al. Structure of LIMP-2 provides functional insights with implications for SR-BI and CD36. *Nature*. 2013;504(7478):172-176.
180. Olivo-Marin JC. Extraction of spots in biological images using multiscale products. *Pattern Recogn*. 2002;35(9):1989-1996.
181. Jaqaman K, Loerke D, Mettlen M, et al. Robust single-particle tracking in live-cell time-lapse sequences. *Nat Methods*. 2008;5(8):695-702.
182. Gantman A, Fuhrman B, Aviram M, Hayek T. High glucose stimulates macrophage SR-BI expression and induces a switch in its activity from cholesterol efflux to cholesterol influx. *Biochemical and biophysical research communications*. 2010;391(1):523-528.
183. Matveev S, van der Westhuyzen DR, Smart EJ. Co-expression of scavenger receptor-BI and caveolin-1 is associated with enhanced selective cholesteryl ester uptake in THP-1 macrophages. *J Lipid Res*. 1999;40(9):1647-1654.
184. Canton J, Neculai D, Grinstein S. Scavenger receptors in homeostasis and immunity. *Nature reviews Immunology*. 2013;13(9):621-634.
185. Nerambourg N, Werts MHV, Charlot M, Blanchard-Desce M. Quenching of molecular fluorescence on the surface of monolayer-protected gold nanoparticles investigated using place exchange equilibria. *Langmuir*. 2007;23(10):5563-5570.
186. Huang R, Silva RA, Jerome WG, et al. Apolipoprotein A-I structural organization in high-density lipoproteins isolated from human plasma. *Nature structural & molecular biology*. 2011;18(4):416-422.
187. Tim Hesterberg DSM, Shaun Monaghan, Ashley Clipson, Rachel Epstein, Bruce A. Craig, and George P. McCabe. Bootstrap methods and permutation tests. 2010:1-57.
188. Kalos M, Levine BL, Porter DL, et al. T Cells with Chimeric Antigen Receptors Have Potent Antitumor Effects and Can Establish Memory in Patients with Advanced Leukemia. *Science Translational Medicine*. 2011;3(95).

189. van der Burg SH, Arens R, Ossendorp F, van Hall T, Melief AJM. Vaccines for established cancer: overcoming the challenges posed by immune evasion. *Nat Rev Cancer*. 2016;16(4):219-233.
190. Snyder A, Makarov V, Merghoub T, et al. Genetic Basis for Clinical Response to CTLA-4 Blockade in Melanoma. *New Engl J Med*. 2014;371(23):2189-2199.
191. Ott PA, Hodi FS, Robert C. CTLA-4 and PD-1/PD-L1 Blockade: New Immunotherapeutic Modalities with Durable Clinical Benefit in Melanoma Patients. *Clin Cancer Res*. 2013;19(19):5300-5309.
192. Gabrilovich DI, Nagaraj S. Myeloid-derived suppressor cells as regulators of the immune system. *Nat Rev Immunol*. 2009;9(3):162-174.
193. Kumar V, Patel S, Tcyganov E, Gabrilovich DI. The Nature of Myeloid-Derived Suppressor Cells in the Tumor Microenvironment. *Trends Immunol*. 2016;37(3):208-220.
194. Liu C, Workman CJ, Vignali DAA. Targeting regulatory T cells in tumors. *Febs J*. 2016;283(14):2731-2748.
195. Lewis GF, Rader DJ. New insights into the regulation of HDL metabolism and reverse cholesterol transport. *Circulation Research*. 2005;96(12):1221-1232.
196. Rosenson RS, Brewer HB, Davidson WS, et al. Cholesterol Efflux and Atheroprotection Advancing the Concept of Reverse Cholesterol Transport. *Circulation*. 2012;125(15):1905-1919.
197. Shih AY, Sligar SG, Schulten K. Maturation of high-density lipoproteins. *J R Soc Interface*. 2009;6(39):863-871.
198. Kozarsky KF, Donahee MH, Rigotti A, Iqbal SN, Edelman ER, Krieger M. Overexpression of the HDL receptor SR-BI alters plasma HDL and bile cholesterol levels. *Nature*. 1997;387(6631):414-417.
199. Murphy AJ, Woollard KJ, Suhartoyo A, et al. Neutrophil activation is attenuated by high-density lipoprotein and apolipoprotein A-I in in vitro and in vivo models of inflammation. *Arterioscler Thromb Vasc Biol*. 2011;31(6):1333-1341.
200. Chinetti-Gbaguidi G, Colin S, Staels B. Macrophage subsets in atherosclerosis. *Nat Rev Cardiol*. 2015;12(1):10-17.
201. Tall AR, Yvan-Charvet L. Cholesterol, inflammation and innate immunity. *Nat Rev Immunol*. 2015;15(2):104-116.
202. Yvan-Charvet L, Pagler T, Gautier EL, et al. ATP-binding cassette transporters and HDL suppress hematopoietic stem cell proliferation. *Science*. 2010;328(5986):1689-1693.
203. Tang J, Lobatto ME, Hassing L, et al. Inhibiting macrophage proliferation suppresses atherosclerotic plaque inflammation. *Sci Adv*. 2015;1(3).
204. Zamanian-Daryoush M, Lindner D, Tallant TC, et al. The cardioprotective protein apolipoprotein A1 promotes potent anti-tumorigenic effects. *J Biol Chem*. 2013;288(29):21237-21252.
205. Su F, Kozak KR, Imaizumi S, et al. Apolipoprotein A-I (apoA-I) and apoA-I mimetic peptides inhibit tumor development in a mouse model of ovarian cancer. *Proc Natl Acad Sci U S A*. 2010;107(46):19997-20002.
206. Chandler PD, Song Y, Lin J, et al. Lipid biomarkers and long-term risk of cancer in the Women's Health Study. *Am J Clin Nutr*. 2016;103(6):1397-1407.

207. Angeloni NL, McMahon KM, Swaminathan S, et al. Pathways for Modulating Exosome Lipids Identified By High-Density Lipoprotein-Like Nanoparticle Binding to Scavenger Receptor Type B-1. *Sci Rep-Uk*. 2016;6.
208. McMahon KM, Scielzo C, Angeloni NL, et al. Synthetic high-density lipoproteins as targeted monotherapy for chronic lymphocytic leukemia. *Oncotarget*. 2017;8(7):11219-11227.
209. Mieszawska AJ, Mulder WJ, Fayad ZA, Cormode DP. Multifunctional gold nanoparticles for diagnosis and therapy of disease. *Mol Pharm*. 2013;10(3):831-847.
210. Rigotti A, Trigatti B, Babitt J, Penman M, Xu SH, Krieger M. Scavenger receptor BI - a cell surface receptor for high density lipoprotein. *Curr Opin Lipidol*. 1997;8(3):181-188.
211. Acton S, Rigotti A, Landschulz KT, Xu SZ, Hobbs HH, Krieger M. Identification of scavenger receptor SR-BI as a high density lipoprotein receptor. *Science*. 1996;271(5248):518-520.
212. Mooberry LK, Sabnis NA, Panchoo M, Nagarajan B, Lacko AG. Targeting the SR-B1 Receptor as a Gateway for Cancer Therapy and Imaging. *Frontiers in Pharmacology*. 2016;7.
213. Hanson EM, Clements VK, Sinha P, Ilkovitch D, Ostrand-Rosenberg S. Myeloid-derived suppressor cells down-regulate L-selectin expression on CD4+ and CD8+ T cells. *J Immunol*. 2009;183(2):937-944.
214. Yesilaltay A, Dokshin GA, Busso D, et al. Excess cholesterol induces mouse egg activation and may cause female infertility. *Proceedings of the National Academy of Sciences of the United States of America*. 2014;111(46):E4972-E4980.
215. Jani JP, Specht S, Stemmler N, et al. Metastasis of B16F10 mouse melanoma inhibited by lovastatin, an inhibitor of cholesterol biosynthesis. *Invasion Metastasis*. 1993;13(6):314-324.
216. Nagaraj S, Gabrilovich DI. Regulation of suppressive function of myeloid-derived suppressor cells by CD4+ T cells. *Semin Cancer Biol*. 2012;22(4):282-288.
217. Sica A, Strauss L. Energy metabolism drives myeloid-derived suppressor cell differentiation and functions in pathology. *J Leukocyte Biol*. 2017;102(2):325-334.
218. Tani S, Nagao K, Anazawa T, et al. Association of Leukocyte Subtype Counts With Coronary Atherosclerotic Regression Following Pravastatin Treatment. *Am J Cardiol*. 2009;104(4):464-469.
219. Ji A, Meyer JM, Cai L, et al. Scavenger receptor SR-BI in macrophage lipid metabolism. *Atherosclerosis*. 2011;217(1):106-112.
220. Dominguez GA, Condamine T, Mony S, et al. Selective Targeting of Myeloid-Derived Suppressor Cells in Cancer Patients Using DS-8273a, an Agonistic TRAIL-R2 Antibody. *Clin Cancer Res*. 2017;23(12):2942-2950.
221. Kim K, Skora AD, Li Z, et al. Eradication of metastatic mouse cancers resistant to immune checkpoint blockade by suppression of myeloid-derived cells. *Proc Natl Acad Sci U S A*. 2014;111(32):11774-11779.
222. Gabrilovich DI, Ostrand-Rosenberg S, Bronte V. Coordinated regulation of myeloid cells by tumours. *Nat Rev Immunol*. 2012;12(4):253-268.

223. Quah BJ, Warren HS, Parish CR. Monitoring lymphocyte proliferation in vitro and in vivo with the intracellular fluorescent dye carboxyfluorescein diacetate succinimidyl ester. *Nat Protoc.* 2007;2(9):2049-2056.
224. Lechner MG, Liebertz DJ, Epstein AL. Characterization of cytokine-induced myeloid-derived suppressor cells from normal human peripheral blood mononuclear cells. *J Immunol.* 2010;185(4):2273-2284.
225. McMahon KM, Plebanek MP, Thaxton CS. Properties of Native High-Density Lipoproteins Inspire Synthesis of Actively Targeted In Vivo siRNA Delivery Vehicles. *Advanced Functional Materials.* 2016;26(43):7824-7835.

Michael P. Plebanek

m-plebanek@northwestern.edu

Curriculum Vitae

Education:

Northwestern University, Driskill Graduate Program in Life Sciences, Chicago, IL

- PhD. Thesis Advisors: C. Shad Thaxton and Olga Volpert
- Thesis focused on translation immunology in cancer. I study the role of cancer exosomes on immune cells in tumorigenesis and tumor metastasis and develop nanotechnologies to treat cancer

Purdue University, College of Pharmacy, West Lafayette, IN

- Bachelor of Science
- Major: Pharmaceutical Sciences specializing in Medicinal Chemistry and Molecular Pharmacology
- Minor: Biological Sciences, Chemistry
- Research Advisor: Laurie Parker, PhD.
- Research focused on the development of biosensors to detect kinase activity in tumor cells

Laboratory Experience:

- September 2011 to Present- Worked with Dr. C. Shad Thaxton and Dr. Olga Volpert in the Department of Urology on the study of exosomes and design exosomes mimetics for the treatments of metastatic melanoma.
- December 2008 to June 2011-Worked with Dr. Laurie Parker in the Department of Medicinal Chemistry and Molecular Pharmacology on the design of peptide biosensors for the detection of kinase activity.

Publications:

- **Plebanek MP**, Bhaumik D, Bryce PJ, Thaxton CS, Scavenger Receptor Type B1 and Lipoprotein Nanoparticles Inhibit Myeloid Derived Suppressor Cells, Molecular Cancer Therapeutics. 2017 Dec 27
- **Plebanek MP**, Angeloni NL, Vinokour E, Li J, Henkin A, Martinez-Marin D, Filleur S, Bhowmick R, Henkin J, Miller SD, Ifergan I, Lee Y, Osman I, Thaxton CS, Volpert OV, Pre-metastatic Cancer Exosomes Induce Immune Surveillance by Patrolling Monocytes at the Metastatic Niche. Nature Communications. 2017 Nov 6;8(1)
- McMahon KM, **Plebanek MP**, Thaxton CS, Single-Strand RNAs Self-Assemble with Lipids and Nanoparticles Enabling Targeted siRNA Delivery. Advanced Functional Materials. 2016 Nov 15;26(43)
- Angeloni NL, McMahon KM, Swaminathan S, **Plebanek MP**, Osman I, Volpert OV, Thaxton CS, Pathways for Modulating Exosome Lipids Identified By High-Density Lipoprotein-Like Nanoparticle Binding to Scavenger Receptor Type B-1. Scientific Reports. 2016 Mar 11;6:22915.

- **Plebanek MP**, Mutharasan RK, Volpert O, Matov A, Gatlin JC, Thaxton CS, Nanoparticle Targeting and Cholesterol Flux Through Scavenger Receptor Type B-1 Inhibits Cellular Exosome Uptake. Scientific Reports. 2015 Oct 29;5:15724.
- Rink JS, **Plebanek MP**, Tripathy S, Thaxton CS, Update on current and potential nanoparticle cancer therapies. Current Opinions in Oncology. 2013 Nov; 25(6): 646-51.
- Placzek EA, **Plebanek MP**, Lipchik AM, Kidd SR, Parker LL, A peptide biosensor for detecting intracellular Abl kinase activity using matrix-assisted laser desorption/ionization time-of-flight mass spectrometry. Analytical Biochemistry, 2010 Feb; 397(1): 73-78.

Research Presentations:

- May 2017-Oral Presentation- Pre-metastatic cancer exosomes induce immune surveillance by patrolling monocytes presented at International Society for Extracellular Vesicles Annual Meeting, Toronto, Canada
- May 2016- Oral presentation- High-density lipoprotein-like nanoparticles target SR-B1 and inhibit melanoma cell-derived exosome uptake to block the pre-metastatic niche, presented at International Society for Extracellular Vesicles Annual Meeting, Rotterdam, Netherlands
- June 2015- Oral presentation- High-Density Lipoprotein-Like Nanoparticles Inhibit Melanoma Cell-Derived Exosome Uptake by Targeting SR-B1 and Modulating Cholesterol Flux, presented at TechConnect World Innovation Conference, Washington D.C.
- April 2015- Poster presentation- High-Density Lipoprotein-Like Nanoparticles Target SR-B1 and Inhibit the Cellular Uptake of Melanoma-Cell Derived Exosomes, presented at The American Association for Cancer Research Annual Meeting, Philadelphia, Pennsylvania
- April 2014 –Oral presentation-The Development of Exosomes as a Therapy to Treat Metastatic Melanoma, presented at The International Society for Extracellular Vesicles Annual Meeting, Rotterdam, Netherlands
- April 2014 –Poster presentation- A prevention of exosome uptake by high-density lipoprotein mimetic gold nanoparticles, presented at The International Society for Extracellular Vesicles Annual Meeting, Rotterdam, Netherlands
- December 2012 –Poster Presentation- Exosomes from a Non Metastatic Source Actively Block Melanoma Metastasis, presented at the Driskill Graduate Program Poster symposium, Chicago, Illinois
- October 2012 – Poster Presentation- Exosomes from a Non Metastatic Source Actively Block Melanoma Metastasis, presented at Exosomes and Microvesicles Research Conference, Orlando, FL
- April 2011 - Poster Presentation- A Mass Spectrometry Method to Determine the Optimal Substrate for Syk Kinase, presented at Human Chronic Disease Research Poster Symposium, Purdue University, West Lafayette, IN
- March 2011- Poster Presentation- A Mass Spectrometry Method to Determine the Optimal Substrate for Syk Kinase, presented at US HUPO poster symposium, Raleigh, NC

Fellowships:

- June 1, 2017- May 31, 2018- NIH NIDDK Urology Training Program- 5T32DK062716-12
- September 2014- August 2015- Fishel Fellowship for Cancer Research presented by the Robert H. Lurie Comprehensive Cancer Center

- May-August 2010 - Purdue University Dean's Undergraduate Summer Research Program
- May 2009- May 2010 - NIH Cancer Prevention Internship Program at Purdue University

Scholarships and Awards:

- 2015- Northwestern University Conference Travel Grant Recipient
- 2014-Katten Muchin Rosenman Travel Scholarship Recipient
- 2014- Northwestern University Conference Travel Grant Recipient
- 2010-2011- Charles V. and Madonna D. Dienhart Flemming Scholarship Recipient
- 2009-2010- Lilly BPS Merit Scholarship Recipient
- 2007-2011-Purdue University Dean's List

Professional Memberships:

- 2016- International Society for Extracellular Vesicles
- 2015- American Association for Cancer Research
- 2011-2012- United States Human Proteomics Organization (US-HUPO) Student Member
- 2009 – 2011- American Chemical Society Student Affiliate

Teaching Activities:

- December 2012 – August 2013- Designed and instructed a nanotechnology course for high school teachers through the Northwestern School of Education
- August 2010 – May 2011 - Organic Chemistry Laboratory Teaching Assistant